Gausemycins A,B – cyclic lipoglycopeptides from *Streptomyces sp.*

Anton P. Tyurin,[†,1] Vera A. Alferova,[†,‡,1] Alexander S. Paramonov,[‡,1] Maxim V. Shuvalov,[†,§] Gulnara Kh. Kudryakova,[†] Eugene A. Rogozhin,[†,‡] Alexander Ya. Zherebker,[∥] Vladimir A. Brylev,[‡] Alexey A. Chistov,[‡] Anna A. Baranova,[†] Mikhail V. Birykov,[†,□] Igor A. Ivanov,[‡] Igor A. Prokhorenko,[†,‡] Natalia E. Grammatikova,[†] Tatyana V. Kravchenko,[†] Elena B. Isakova,[†] Elena P. Mirchink,[†] Elena G. Gladkikh,[†] Elena V. Svirshchevskaya,[‡] Andrey V. Mardanov,[⊥] Aleksey V. Beletsky,[⊥] Milita V. Kocharovskaya,[‡] Valeriya V. Kulyaeva,[†] Alexander S. Shashkov,[◊] Dmitry E. Tsvetkov,[◊] Nikolay E. Nifantiev,[◊] Alexander S. Apt,[▽] Konstantin B. Majorov,[▽] Svetlana S. Efimova,[△] Nikolai V. Ravin,[⊥] Evgeny N. Nikolaev,[∥] Olga S. Ostroumova,[△] Genrikh S. Katrukha,[†] Olda A. Lapchinskaya,[†] Olga A. Dontsova,[‡,§,∥] Stanislav S. Terekhov,[*,‡,§] Ilya A. Osterman,[§,∥] Zakhar O. Shenkarev,[*,‡,○] Vladimir A. Korshun[*,†,‡]

[†]Gause Institute of New Antibiotics, B. Pirogovskaya 11, 119021 Moscow, Russia

[‡]Shemyakin-Ovchinnikov Institute of Bioorganic Chemistry, Miklukho-Maklaya 16/10, 117997 Moscow, Russia

[§]Department of Chemistry, Lomonosov Moscow State University, 1-3 Leninskie Gory, 119992 Moscow, Russia

[□]Department of Biology, Lomonosov Moscow State University, 1-3 Leninskie Gory, 119992 Moscow, Russia

[∥]Skolkovo Institute of Science and Technology, 3 Nobel street, Skolkovo, 143026 Moscow Region, Russia

[⊥]Institute of Bioengineering, Research Center of Biotechnology, 119071 Moscow, Russia

[◊]Zelinsky Institute of Organic Chemistry, Leninsky Prospect 47, 119991 Moscow, Russia

[△]Institute of Cytology of the Russian Academy of Sciences, 194064 St. Petersburg, Russia

[▽]Central Tuberculosis Research Institute, Yauzskaya alley 2, 107564 Moscow, Russia

[○]Moscow Institute of Physics and Technology, Institutsky lane 9, Dolgoprydny, 141700 Moscow region, Russia

[1] Equal contribution

KEYWORDS Antibiotics, peptides, lipoglycopeptides, structure elucidation, antibacterial activity

ABSTRACT: We report a novel family of natural lipoglycopeptides produced by *Streptomyces* sp. INA-Ac-5812. Two major components of the mixture, named gausemycins A and B, were isolated, and their structures were elucidated. The compounds are cyclic peptides with a unique peptide core and several remarkable structural features, including unusual positions of D-amino acids, lack of the Ca^{2+}-binding Asp-X-Asp-Gly (DXDG) motif, tyrosine glycosylation with arabinose, presence of 2-amino-4-hydroxy-4-phenylbutyric acid (Ahpb) and chlorinated kynurenine (ClKyn), N-acylation of the ornithine side chain. These major components of the peptide antibiotic family have pronounced activity against Gram-positive bacteria. The mechanism of action of gausemycins was explored by a number of methods, showing significant differences compared to glycopeptides and related lipopeptides. Gausemycins exhibit only slight Ca^{2+}-dependence of antimicrobial activity and induce no pore formation at low concentrations. Moreover, there is no detectable accumulation of cell wall biosynthesis precursors under treatment with gausemycins.

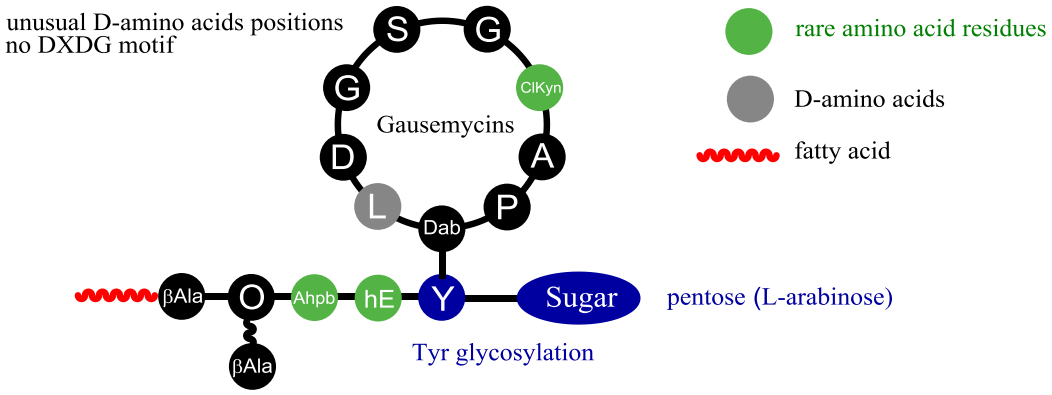

INTRODUCTION

Antibiotic discoveries of the 1940s–1960s 'golden era' introduced most known classes of these natural products. Antibiotics led to a revolution in medicine, curing the most lethal diseases of that time. However, emergence and rapid development of microbial resistance to the treatment required and still requires constant introduction of new active compounds.[1] Nowadays, discovery of novel molecular scaffolds has slowed down significantly, and new antibiotics are developed mainly by modification of existing ones. At present, we are facing the 'resistance era',[2] where novel chemotypes with original mechanisms of action will be of key importance.[3]

Peptide antibiotics are widely used to treat life-threatening infections. Natural glycopeptide antibiotics of the vancomycin-teicoplanin family have been in clinical use for many years.[3] Spurred by the emergence of vancomycin-resistant strains, new semi-synthetic analogues of the vancomycin-teicoplanin family (oritavancin, televancin, cefilavancin) have reached the market.[4] A number of cyclopeptide antibiotics (daptomycin, colistin) are used as last resort drugs against severe infectious diseases.

There are four vastly structurally diverse families of compounds that are usually referred to as lipoglycopeptides – teicoplanin,[5] ramoplanin,[6] hassalidins[7] and occidiofungins[8] (Figure 1A). Moreover, these groups of antibiotics exhibit essentially different spectra of biological activity: ramoplanin and teicoplanin have pronounced antibacterial activity, whereas hassalidins and occidofungins are antifungal compounds. In this paper we report discovery of gausemycins – lipoglycopeptides, whose peptide core differs entirely from the aforementioned scaffolds, but somewhat resembles that of cyclic lipopeptides. The closest structurally related compounds are depsipeptides (daptomycin,[9] taromycins,[10,11] and cadasides[12]) and cyclopeptides (amphomycin,[13,14] rumycins,[15] and malacidins[16]) (Figure 1B).

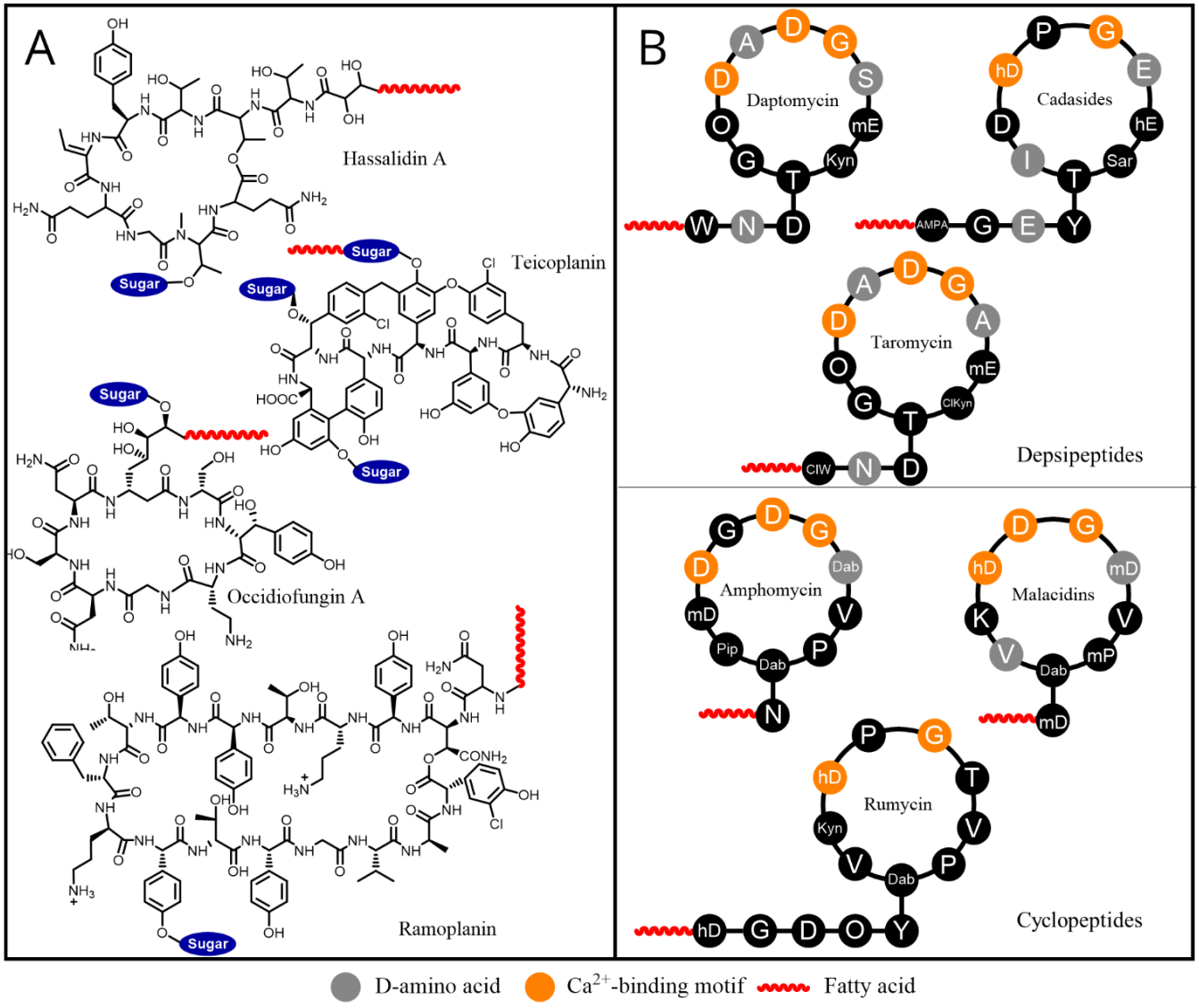

Figure 1. Structures of some natural peptide antibiotics: A) natural peptide antibiotics, combining a fatty acid tail and carbohydrate moiety in their structures; B) natural calcium-dependent cyclic lipopeptides: daptomycin,[9] amphomycin (discovery,[13] structure[14]), malacidins,[16] cadasides,[12] taromycin[10] and rumycin.[15] Kyn, kynurenine; hE, hydroxy-glutamic acid; hD, hydroxyaspartic acid; AMPA, 3-amino-2-methylpropionic acid; ClKyn, Cl-kynurenine; ClW, Cl-tryptophan; Dab, 2,3-diaminobutyric acid; mE, methylglutamic acid; mD, methylaspartic acid; mP, methylproline.

Historically, lipopeptides are the last discovered chemical class of antibiotics. The first-in-class approved drug was daptomycin in 2003.[17] However, other compounds, formally belonging to lipopeptides (e.g. surfactins, echinocandins, streptogramins, arylomycins, enopeptins, globomycins, etc.), are very different both from structural and biological points of view. The recent report of the peptide antibiotic teixobactin[18] also claims to be the discovery of a new (latest) class of antibiotics[19] due to its unique mechanism of action and structural peculiarity. Extremely high chemical diversity of peptide-based active compounds leads to plethora of structurally different antibiotic families. Whether it is a new class of antibiotics rather depends on how they are defined.

Earlier we reported on the production of a complex mixture of antibiotic peptides by an actinomycete strain initially referred to as *Streptomyces roseoflavus* INA-Ac-5812.[20,21] Now we have isolated two major individual components, termed gausemycins A and B, determined their structures and examined the spectrum of their biological activity. These compounds possess several unique structural features indicating that they constitute a new class of antibiotics.

RESULTS AND DISCUSSION

Isolation and Structural Elucidation. The gausemycin antibiotic complex was found in fermentation broth of *Streptomyces sp.* INA-Ac-5812. According to genetic characteristics, the strain is close to *Streptomyces kanamyceticus* (Figure S1). These compounds were at first referred to as INA-5812.[20] Initially, gausemycins were characterized as intrinsically fluorescent peptides with a broad spectrum of antibiotic activity. Crude extracts were separated from the antifungal fraction containing irumamycin/venturicidin-type polyketide macrolides[22] and purified by solid-phase extraction on LPS-500-H resin followed by reversed-phase chromatography on C18 column yielding gausemycin concentrate.

Hydrolysis of the antibiotic concentrate showed that the blue fluorescence of the studied peptides originates entirely from a chlorinated amino acid – 4-chloro-L-kynurenine (ClKyn).[23] The latter has previously been found in only one antibiotic family – taromycins A,B.[10,11]

Preliminary LCMS analysis showed that the gausemycin antibiotic complex contains more than 30 similar lipoglycopeptides and lipopeptides (Figures S2–S4). Concentrate fractionation with HILIC HPLC (see Suppl. S5) afforded two individual substances, named gausemycins A and B. It is worth noting that gausemycins exhibited a strong tendency to form associates in a polar solvent, thus, chromatographic purity was not sufficient to ensure homogeneity of the compounds. Chromatographically pure samples of gausemycin B, obtained using reverse-phase HPLC, exhibited up to 40% percent of a homologous component in MS spectra (+14 Da). Therefore, all fractions and isolated compounds were monitored using LCMS.

Gausemycins A, B were obtained as white solids and, using ESI HRMS, were determined to have exact masses of 1845.788 Da and 1916.826 Da,[20] corresponding to molecular compositions $C_{84}H_{116}ClN_{17}O_{28}$ and $C_{87}H_{121}ClN_{18}O_{29}$, respectively. Structures of gausemycins A, B (Figure 2) were determined from NMR spectroscopy data measured in DMSO-d_6 at 30 and 45°C (Suppl. S8-S17) and supported by MS/MS experiments for gausemycin B (Suppl. S6).

Elucidated structures are consistent with previously reported amino acid composition of gausemycin A.[20] In this work we additionally performed Marfey's derivatization of peptide hydrolysis products and established absolute configurations of most amino acid residues. 2-Amino-4-hydroxy-4-phenylbutyric acid (Ahpb3) and hydroxyglutamic acid (hGlu4) degraded under acidic hydrolysis conditions (6M HCl, 110°C, 120 h), other amino acids produced normal derivatization products (Table S7). The D-configuration was identified only for Leu7 residue. The L-configuration of ClKyn12 was reported earlier.[23] The L-configuration of arabinose moiety was identified by mild acidic hydrolysis (2M TFA, 50°C, 6 h) of gausemycin A and subsequent comparison of the isolated material's optical rotation with D- and L-arabinose.

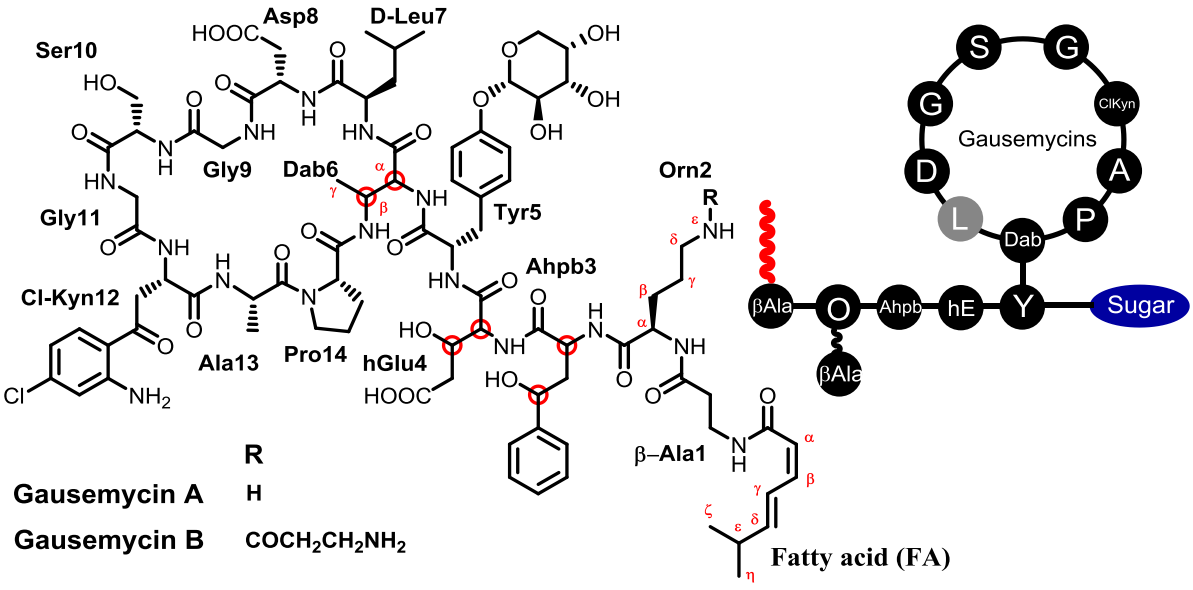

Figure 2. Structures of gausemycins A,B. Red circles indicate the six chiral centers, whose configuration was examined using NMR study and biosynthetic gene cluster analysis.

The characteristic pattern of signals in 2D TOCSY, NOESY and natural abundance ^{15}N-HSQC spectra (Figure 3A) confirmed the presence of a peptide fragment in gausemycins A and B. Spin systems of individual residues and the corresponding residue types were identified in the 2D TOCSY, COSY and natural abundance ^{13}C-HSQC spectra (Suppl. S11). Information from ^{13}C-HMBC spectrum was also used.

Two sets of NMR signals with an intensity ratio of ~2:1 were observed in the spectra of gausemycins (Figure 3A–C and Suppl. S8–S16, the atom names for the minor form are designated by an apostrophe and highlighted red). This, together with exchange cross-peaks observed in the 2D NOESY spectra (mixing time τ_m = 200–400 ms) (Figure S13), revealed conformational heterogeneity of gausemycin A in solution. The exchange process between the two structural forms goes with characteristic time of about 0.1 s.

The sequential connections between individual spin-systems were established *via* HNi-1–HNi, HCαi-1–HNi and/or HCβi-1–HNi cross-peaks observed in the NOESY spectra. Some interresidual connections were additionally supported by cross-peaks in the ^{13}C-HMBC spectra. The observation of the additional side chain HNγ signal in the region of amide protons revealed the presence of 2,3-diaminobutyric acid residue (2,3-Dab or Dab). The characteristic NOE contacts between Dab6 and Pro14 side chains (Figure S14) showed the macrocyclic structure in the polypeptide fragment of gausemycin A. The 9-membered cycle (Dab6–Pro14) is linked by bond between side chain amide group of Dab6 and Pro14 carbonyl (Figure 2). The *N*-terminal part (from β-alanine 1 (βAla1) to Tyr5) of the polypeptide fragment is linear. The pattern of COSY/TOCSY cross-peaks and data from multiplicity-edited ^{13}C-HSQC spectrum confirmed the β-position of OH-group in hGlu4 residue (Suppl. S15). ^{1}H and ^{15}N chemical shift difference of backbone and side chain amide groups between two conformational isoforms of gausemycin A was increased toward Pro14 (Figure 3B). Therefore, the corresponding exchange process could be caused by *trans-cis* isomerization of the Ala13–Pro14 peptide bond. Indeed, the observed differences in the ^{13}Cβ and ^{13}Cγ chemical shifts (Figure 3C) revealed a *trans*-configuration in the major form and a *cis*-configuration in the minor form of gausemycin A.[24]

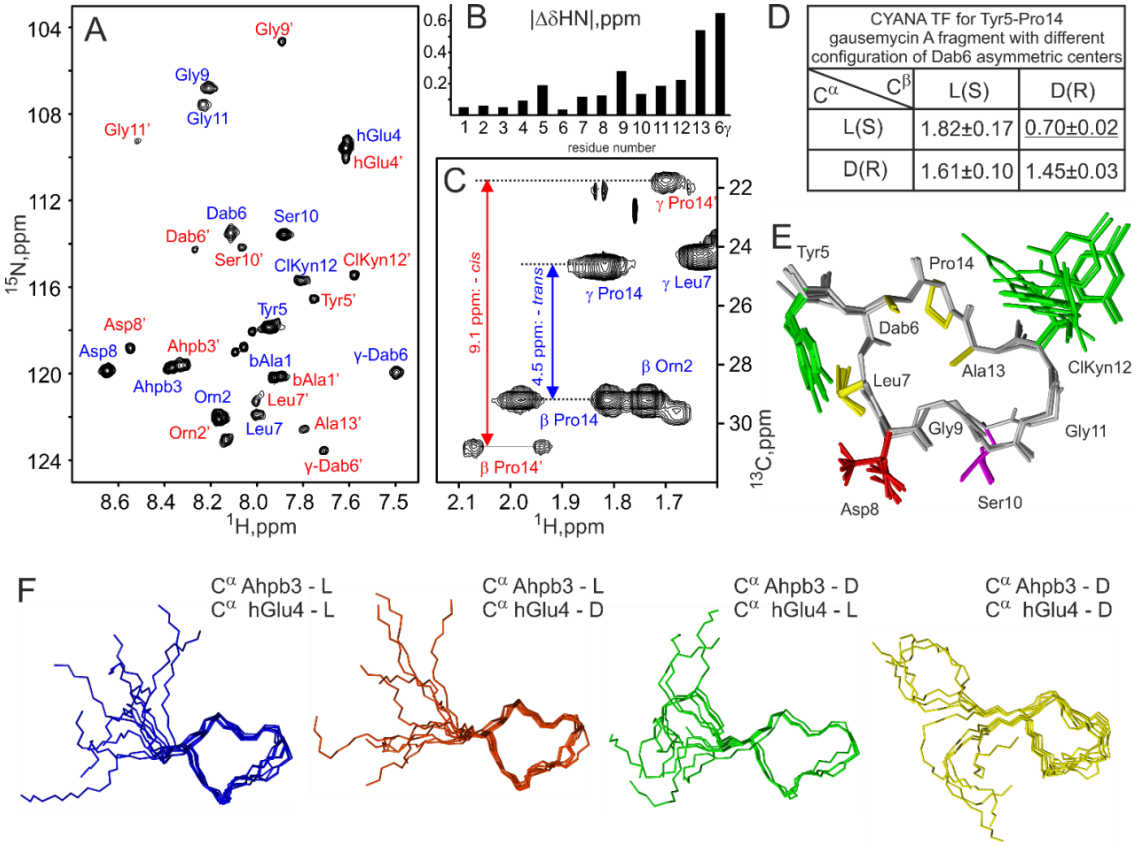

Figure 3. NMR study of gausemycin A. (A) ^{15}N-HSQC spectrum of gausemycin A in DMSO-d_6 (45°C, 800 MHz, natural abundance). Signals of the major and minor forms (Ala13–Pro14 – *trans* and *cis*) are labeled blue and red, respectively. (B) Difference in ^{1}H-^{15}N chemical shifts ($|\Delta\delta HN| = \sqrt{(\Delta\delta H)^2 + (\Delta\delta N/5)^2}$) of gausemycin A amide groups between the major and minor forms. (C) A fragment of natural abundance ^{13}C-HSQC spectrum. Difference in ^{13}C chemical shifts for $C\beta H_2$ and $C\gamma H_2$ groups of Pro14 confirms the assignment of the major and minor forms to the *trans* and *cis* isomers of the Ala13–Pro14 peptide bond, respectively. (D) Calculation of the spatial structure of the Tyr5-Pro14 fragment of the major gausemycin form with four possible absolute configurations of Dab6 residue. Lower values of the CYANA target function (mean ± s.d.) indicate that the L/R (Cα/Cβ) configuration better corresponds to the NMR data. (E) Set of the best 10 structures of the Tyr5–Pro14 gausemycin A fragment with the L/R configuration of the Dab6 residue. Only heavy atoms are shown. Aromatic, hydrophobic, negatively charged, and polar side chains are shown in green, yellow, red, and magenta, respectively. The α-arabinose group attached to Tyr5 was omitted from calculations. (F) Backbone representation of the sets of full-length gausemycin A structures (major form) calculated with different absolute configurations of Cα atoms in Ahpb3 and hGlu4 residues. Ten best structures are shown in each case. The fatty acid group is omitted.

The *N*-terminal fatty-acid group was identified using 2D COSY, TOCSY and ^{13}C-HMBC spectra. The signals of fatty acids appeared as one set, indicating that the conformational exchange process does not affect this part of the molecule. Vicinal proton-proton scalar couplings ^{3}J ^{1}HCα–^{1}HCβ (11.4 Hz) and ^{1}HCγ–^{1}HCδ (15.6 Hz) revealed that the corresponding double bonds in the fatty acid moiety have *cis*- and *trans*- configurations, respectively (Figure 2). The ^{1}HCβ-^{1}HCγ ^{3}J coupling constants have an amplitude of 11.0 Hz, which probably corresponds to the *trans*-configuration of this partially double bond.[25] The whole fatty acid residue forms a large conjugated system, which tends to be planar. This system also contains two other partially double bonds (the NH-C′ peptide bond and the bond between C′ and Cα atoms). The low intensity of the NOESY cross-peak observed between the ^{1}HN signal of bAla1 and ^{1}HCα of the fatty acid was consistent only with a *trans-cis* or *cis-trans* configuration of these bonds. The analysis of molecular models *in vacuo* revealed that these configurations are both possible, but Van der Waals atom repulsion could lead to a non-planar geometry at the C′-Cα bond.

Signals corresponding to the sugar group were observed in NMR spectra. NOESY correlations between ^{1}HCα, ^{1}HCγ and ^{1}HCε (Figure S16), along with large vicinal coupling constants ^{3}J ^{1}HCα–^{1}HCβ (6.8 Hz) and ^{1}HCβ–^{1}HCγ (8.4 Hz) suggested axial position of HCα, HCβ, HCγ and, therefore, a α-glycoside bond. Small vicinal proton coupling constants ^{3}J ^{1}HCγ–^{1}HCδ (3.5 Hz) and ^{1}HCδ–^{1}HCε (1.7 Hz, 3.0 Hz), as well as NOESY cross-peak between ^{1}HCδ and ^{1}HCε, corroborated an equatorial position of HCδ. Signal assignment, vicinal *J*-couplings and optical rotation data allowed to identify this sugar as α-L-arabinopyranose. Strong ^{13}C-NMBC and NOESY cross-peaks observed between ^{1}HCα of α-arabinose and ^{13}Cζ or ^{1}HCδ signals of Tyr5 (Figure S16) revealed attachment of arabinose to the *para* position of the tyrosine ring.

The same set of NMR spectra was obtained for gausemycin B. The fatty acid and sugar groups and main chain of the peptide fragment in gausemycin B were identical to those observed in gausemycin A. A similar conformational exchange process associated with *trans-cis* isomerization of the Ala13–Pro14 peptide bond was also observed. The only significant differences found in gausemycin B NMR spectra were the changes in the Orn2 spin-system and the presence of an additional spin-system corresponding to β-alanine residue attached to the Orn2 side chain (bAla[Orn2]). ^{13}C-HMBC and NOESY cross-peaks observed between ^{13}C′ and ^{1}HCβ signals of bAla[Orn2] residue and side-chain ^{1}HCδ and ^{1}HNε signals of Orn2 (Figure S17) confirmed peptide bond formation between side chain HNε amide group of Orn2 and the carbonyl group of bAla[Orn2]. This was in agreement with the results of mass-spectrometry analysis, which reports 71.04 Da mass difference between gausemycins A and B.

The configuration of six stereocenters in gausemycin remains undetermined (two centers at Cα and Cγ atoms of Ahpb3, two centers at Cα and Cβ of hGlu4, and two centers at Cα and Cβ of Dab6, Figure 2, red circles). In an attempt to derive these configurations from NMR data, we performed several cycles of calculation of the spatial structure of gausemycin A in the CYANA 3.98 program.[26] The chirality of the corresponding centers was varied and the calculated sets of structures were compared by value of the CYANA target function, which is the measure of compliance of NMR data with the calculated structures.

To diminish the influence of conformational exchange, we derived interproton distance restraints from NOESY spectra measured with short mixing times (50 and 100 ms) at 30°C. Dihedral angle restraints were derived from amplitudes of $^{3}J_{HH}$ couplings. Due to limitations in sensitivity, the calculations were performed only for the major form of gausemycin A (Ala13–Pro14 – *trans*). The fatty acid and sugar groups were omitted from the calculations as they did not show NOE contacts with the rest of the molecule (except for the contacts with ^{1}HN of bAla1 and ^{1}HCδ of Tyr5, Figure S16).

The variation in the configurations of the six asymmetric centers led to 64 possible variants. To simplify this task, we ran the calculations in a stepwise manner. In the first stage, we calculated the structures of the macrocycle fragment (Tyr5–Pro14) with four possible configurations of the Dab6 residue (Table S18 and S19). Best fit to the experimental NMR data was observed in the case of the L/R configuration of Cα/Cβ atoms (Figure 3D). The resulting set of 10 structures with the L/R configuration is shown in Figure 3E.

After that, we calculated the structures of the full molecule, varying the configurations of the asymmetric centers in Ahpb3 and hGlu4 residues, but fixing the L/R configuration for Dab6 (Tables S20 and S21). However, due to high mobility of the *N*-terminal fragment, the obtained NOE and ^{3}J coupling data were insufficient to discriminate between different Ahpb3 and hGlu4 configurations. To illustrate this, we calculated the structures of the full-length gausemycin A peptide fragment with different chiralities of Cα atoms in Ahpb3 and hGlu4 residues (configurations of Ahpb3 Cγ and hGlu4 Cβ were fixed to R). Analysis of the resulting structural ensembles (Figure 3F) revealed that uncertainties introduced into the peptide structure by unknown chirality and increased mobility of the *N*-terminal fragment are comparable.

Thus, gausemycins were found to be macrocyclic peptides containing 14 amino acids, including non-proteinogenic and D-configured residues. Some structural motifs in the gausemycin molecules are very rare for biologically active natural products. Glycosylation of tyrosine residue is quite uncommon for natural peptides,[27,28] and there are no examples of glycosylation with pentose. Arabinose itself is an unusual fragment for natural glycopeptides and it is mostly found as *O*-hydroxyproline derivatives. Thus, tyrosine glycosylation with arabinose in gausemycins is a unique structural feature among natural products. While kynurenine is a quite common metabolite of tryptophan found in natural products, its chlorinated analogue, was previously found in the only one family of antibiotics – taromycins.[10,11] β-Hydroxyglutamic acid (hGlu4, Figure 2) rarely occurs in natural peptides as several diastereomers.[29–33] 3-Amino-4-hydroxy-4-phenylbutyric acid (Ahpb3) and N$^{\varepsilon}$-(β-alaninoyl)ornithine (Orn2) (Figure 2) have never been encountered in natural peptides before.

Gausemycin biosynthetic gene cluster. Inspired by the striking structural novelty of gausemycins, we decided to look into the biosynthesis of these compounds. Genome mining revealed a large (68 ORFs) NRPS biosynthetic gene cluster (BGC) that we called the Gau BGC (Figure 4).

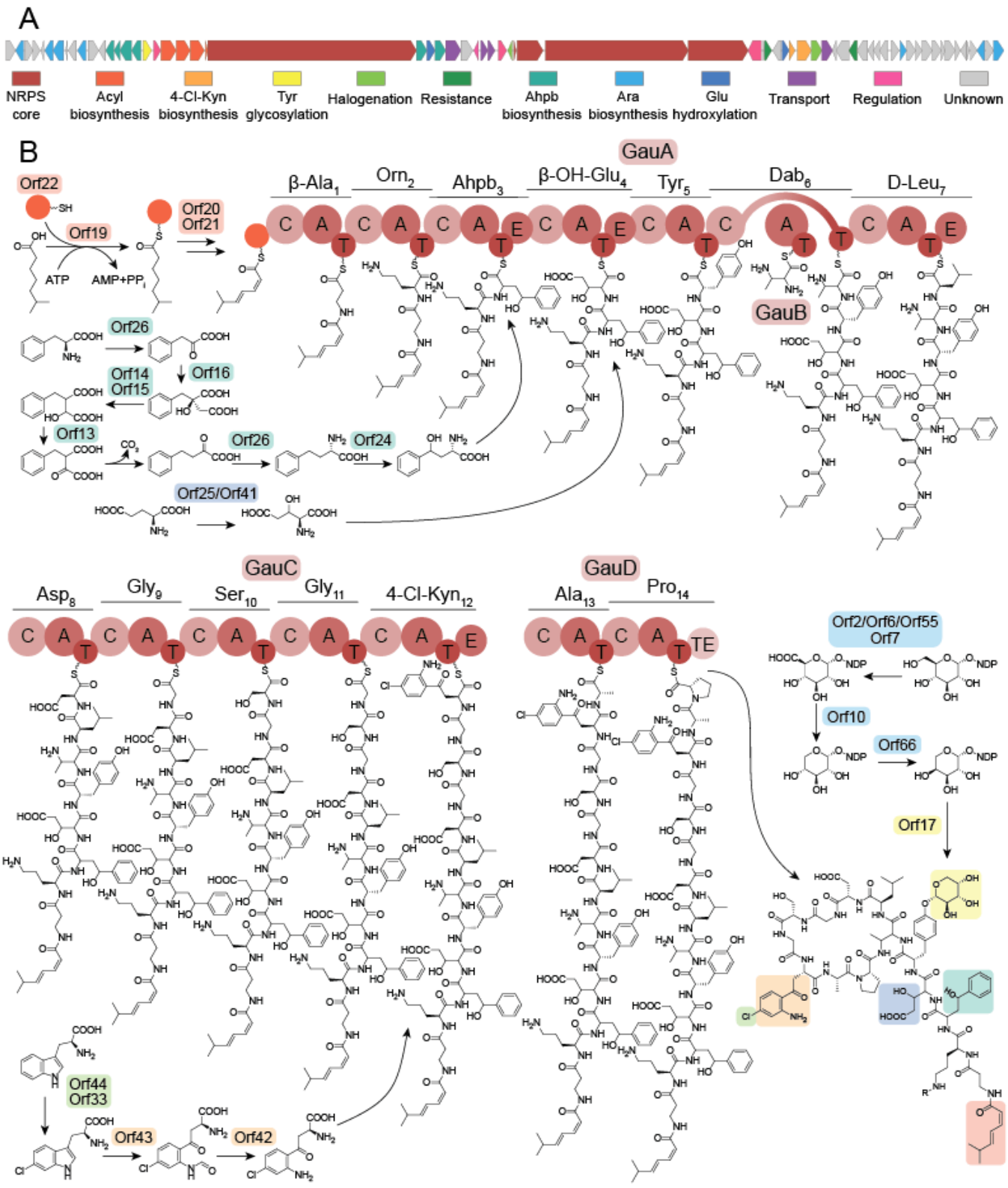

Figure 4. A) A fragment of predicted Gau BGC (Orf1–Orf62) with some of the proposed functions; B) The modular architecture of the gausemycin NRPS assembly line and proposed biosynthesis of gausemycin A. A, adenylation domain; C, condensation domain; E, epimerization domain; T, thiolation domain; TE thioesterase domain. The biosynthetic pathways of unusual amino acids and modifications are predicted based on protein homology. They may take place before or post-NRPS assembly. NDP indicates that the nucleotide could not be specified.

We analyzed the general architecture and similarity of proteins in the Gau cluster comparing it with known Gau-related BGCs (Tables S22, S23). Four core NRPS genes of the gausemycin BGC contain 14 modules responsible for the introduction of β-Ala1-Orn2-Ahpb3-hGlu4-Tyr5-D-Leu7 (*gauA*), Dab6 (*gauB*); Asp8-Gly9-Ser10-Gly11-ClKyn12 (*gauC*), and Ala13-Pro14 (*gauD*) amino acids (Table S24). BGCs of related cyclic lipopeptides malacidin[16], friulimicin[34], and laspartomycin[35] contain NRPS (MlcK, PstB, and LpmB, respectively) similar to GauA. In addition, all of them have special module interacting in *trans* with the corresponding A-T didomains (MlcA, PstA, LpmA, and GauB) incorporating 2,3-diaminobutyric acid residue involved in the macrolactam formation. The biosynthesis of 2,3-Dab is encoded in the genome outside of the Gau BGC. Nonetheless, these ORFs are similar to genes providing 2,3-Dab biosynthesis in related malacidin, friulimicin, and laspartomycin BGCs (Table S25).

In contrast to other cyclic lipopeptides, GauA has an especially high number of modules defining the unique peptidyl linker placed between the *N*-terminal fatty acid tail and macrolactam ring (Figure 4). This linker contains five residues of non-proteinogenic or modified amino acids. At the same time, related malacidin, friulimicin, and laspartomycin have one-amino acid linker, while the more distant daptomycin-like antibiotics have three N-terminal residues after fatty acid tail. The only similar compounds with a five-amino acid linker are rumycins, reported in a patent literature[15] with no biosynthetic origin mentioned. Hence, we consider this feature essential for the biologic activity of gausemycins, allowing us to place them in a distinct subtype of lipopeptide antibiotics.

The next NRPS, GauC, contains a unique combination of modules encoding the DGSG-ClKyn peptide sequence. This fragment is highly different from related KhDDGmD, mDDGDG-Dab, GDGDG-dThr, and Orn-DADGS sequences of malacidin, friulimicin, laspartomycin, and daptomycin-like antibiotics, respectively (see caption to Figure 1 for definition of nonstandard amino acids). Hence, this sequence stands apart from the classic DXDG motif of Ca^{2+} dependent lipopeptides. The last module in the GauC protein, integrating 4-Cl-kynurenine residue, contains the epimerization domain, thus suggesting the D-configuration for this amino acid. Nonetheless, we detected no trace of a Marfey's derivative corresponding to D-configured 4-Cl-Kyn in LCMS spectra of hydrolyzed gausemycins, neither for individual components nor for the case of antibiotic concentrate. While the epimerization domain provides a mixture of configurations, we can propose that the downstream C domain is $^{L}C_{L}$-catalyst[36] and selectively reacts with chains ended by L-configured chlorinated kynurenine. Furthermore, the epimerization domain located in the terminal module of the GauC protein could be inactive, like previously reported for comB and StaB NRPS from complestatin and A47934 BGC, respectively.[37]

The last NRPS, GauD, encodes the AP fragment, which is similar to terminal VmP, VP, IP sequences in related malacidin, friulimicin, rumycin and laspartomycin. This conservation emphasizes the structural significance of the terminal proline in macrolactam-containing lipopeptides, probably providing conformation optimal for the cycle closure.

Biosynthesis of 4-Cl-Kyn from L-Trp was recently reported in detail.[38] The Gau cluster does not contain the full quartet of enzymes described previously for the BGC of the daptomycin-like antibiotic taromycin. However, it contains three key enzymes essential for L-Trp conversion to 4-Cl-Kyn, resembling tryptophan-2,3-dioxygenase, flavin-dependent halogenase, and the flavin reductase (Orf 43, 44, and 33, respectively, protein identity of 50%, 79%, and 59%). The final step of 4-Cl-Kyn biosynthesis in the taromycin quartet is catalyzed by kynurenine formamidase. However, this is not the rate-limiting step[38] and, in the case of gausemycins, it could be spontaneous or catalyzed by a non-specific hydrolase, for example by adjacent putative alpha/beta hydrolase (Orf42).

GauA mediates the incorporation of unusual aromatic amino acid 2-Amino-4-hydroxy-4-phenylbutyric acid (Ahpb3), which was not described in natural peptides. Ahpb3 was not chlorinated in any of the resulting structures, including those minor components that were detected by mass spectra. This distinguishes Gau from the taromycin BGC, encoding incorporation of two chlorinated amino acids, 6-Cl-Trp and 4-Cl-Kyn, both originating from L-Trp. Hence, we consider Ahpb not a product of tryptophan modification. We suggest that Ahpb biosynthesis originates from phenylalanine and includes biosynthesis of homophenylalanine, described earlier[39]. The genes presumably involved in biosynthesis of homophenylalanine (Figure 4) exhibit high similarity to previously reported enzymes (Table S23, Orf13-Orf16). Orf13-Orf16 and Orf26 are highly similar to the respective proteins in *Salinispora pacifica* strain DPJ-0016 lomaiviticin BGC[40] (67–54% protein identity). Although their role in lomaiviticin biosynthesis is not clear, we suggest that they are responsible for Ahpb biosynthesis, and putative tyrosine aminotransferase Orf26 is involved in the process. The final step of the proposed Ahpb biosynthesis is homophenylalanine hydroxylation provided by the respective oxygenase. This step could be mediated by the putative cytochrome P450 monooxygenase Orf24, similar to Tlo29 and Tlo23 (34% and 32% protein identity, respectively) of the related telomycin BGC. Tlo29 and Tlo23 are cytochrome P450 monooxygenases responsible for *(S)-β*-hydroxylation of Pro and Leu, respectively.[41] While tailoring by Tlo29 and Tlo23 is likely to take place post-NRPS assembly, we cannot propose the exact mechanism for gausemycin yet.

To confirm the involvement of phenylalanine as a substrate for the biosynthesis of gausemycins, we fed fluorinated phenylalanine derivatives (2-F-Phe, 4-F-Phe) to *Streptomyces* sp. INA-Ac-5812. Indeed, LC-MS analysis showed that fluorinated Ahpb were incorporated into gausemycin molecules (Figure S26). The incorporation was illustrated by emergence of intense ions with m/z 932.9 and 968.4, corresponding to monofluorinated molecules of gausemycins A and B, respectively. The position of fluorine incorporation was confirmed by MS/MS peptide sequencing. We observed ^{19}F vs. ^{1}H mass increment (18 Da) in the FA-βAla1-Orn2(βAla)-[F]Ahpb3 fragment ion, but not in the subsequent FA-βAla1-Orn2(βAla) fragment (Figure S27).

The Gau BGC contains a number of enzymes involved in rare modifications and tailoring. Orf20 and Orf21 are acyl-CoA dehydrogenases similar to CdeF and CdeG (54% and 54% protein identity, respectively), recently described in cadaside A BGC.[12] Both gausemycins and cadasides have rare unsaturated (2*Z*,4*E*)-fatty acid tails. Another modified amino acid residue in gausemycins is β-OH-Glu4. We suggest that hydroxylation of Glu is mediated by putative dioxygenase Orf25 or Orf41, similar to dioxygenase KtzP (49% and 41% protein identity, respectively) mediating stereospecific synthesis of

erythro-β-hydroxyglutamic acid during kutzneride biosynthesis.[32]

The tailoring step that is proposed to take place after NRPS assembly is Tyr5 glycosylation. The proposed glycosylation includes the biosynthesis of NDP-α-L-arabinopyranose from NDP-α-D-glucose. Nucleotide specificity here could not be specified, and we consider that putative uncharacterized nucleotidyltransferase Orf68 could be involved in the process. We suggest that glycosylation is mediated by the putative glycosyltransferase family 2 protein Orf17. Orf17 is the only glycosyltransferase in the Gau BGC, and it has some similarity (33% protein identity) to HasX glycosyltransferase from the BGC of the lipopeptide hassallidin.[42] Similarly to gausemycin, hassallidin has arabinose glycosylation. While it is impossible to correctly predict all enzymes involved in arabinose biosynthesis, we can speculate that putative dehydrogenases Orf2, Orf6, Orf7, and/or Orf55 mediate primary NDP-α-D-glucose oxidation, Orf10 is a putative decarboxylase, and Orf66 is involved in the epimerization step (Figure 4). While homologs of Orf10, Orf55, and Orf66 are also identified in hassallidin BGC (HasP, HasL, and HasP, respectively), they have only mediocre similarity (23–27%), insufficient to unambiguously propose their function. A number of Orfs could not be characterized precisely solely based on protein homology (especially the Orf46–Orf67 region). However, we suggest that the terminal part of the Gau BGC contains enzymes involved in sugar and fatty acid metabolism that may be responsible for the production of minor gausemycins.

Gausemycin biological activity and mechanism of action. Gausemycins are cyclic lipoglycopeptides, resembling anionic lipopeptides, but with a completely distinct peptide sequence. Moreover, gausemycins do not contain any variation of the Ca^{2+}-binding motif, canonical for calcium-dependent antibiotics.[43] To determine the calcium requirement for antibiotic activity of gausemycins, we measured MICs of gausemycins against a number of strains after addition of 0.45 mM Ca^{2+} (Table S28). Despite the fact that a calcium-dependent mode of action was previously reported for one of the peptide antibiotics isolated from the *Streptomyces roseoflavus* INA-Ac-5812 strain,[21] we did not observe a Ca^{2+} dependence for the antibacterial activity of gausemycin. Under the same conditions, daptomycin activity increased at least 10-fold.[44] This behavior is unique amongst acidic lipopeptides and glycopeptides, including recently discovered malacidins[16] and cadasides.[12]

Gausemycins have pronounced activity against gram-positive bacteria, including methicillin-resistant *Staphylococcus aureus* (MRSA), but were found to be inactive against Gram-negative bacteria and enterococci. Interestingly, gausemycins exhibited no antibacterial activity against both vancomycin-resistant and vancomycin-susceptible *Enterococcus* sp. strains (Table S29). Along with enterococci, *Streptococcus* sp. and *Mycobacterium tuberculosis* species exhibited practically no susceptibility to gausemycins. Thus, gausemycins have a relatively narrow spectrum of activity, which can be advantageous for development of narrow-spectrum therapeutics, regarded as one of the approaches to overcoming the spread of resistance to antibiotics.[45]

To further evaluate clinical prospects of the obtained compounds, we tested the activity of gausemycins against 62 clinical isolates of *Staphylococcus* sp., and, in some cases, we observed MICs significantly lower than those of glycopeptides and even daptomycin (0.125–1.0 μg/mL, Table S30). Thus, we can assume that gausemycins are promising antibacterial agents. Coagulase-negative staphylococci, including methicillin-sensitive (MSSA) and methicillin-resistant strains, are also sensitive to gausemycin. No significant difference in activity of gausemycins A and B against MSSA and MRSA was observed. The cytotoxic activity of gausemycins A and B was assayed on a panel of mammalian cells using the MTT test. The measured IC_{50} values (5–10 μg/mL, Table S31) were significantly higher than the MICs, indicating a relatively large therapeutic index. Taking into account these unique biological features, we decided to compare the activity and mode of action of gausemycins with previously studied antibiotics.

To get a general understanding of the mode of action of gausemycins, we used the BCP (bacterial cytological profiling) approach. This method involves observation of morphological changes in test microorganism under treatment with various antibiotics, visualized using fluorescent staining. Initially, this method was developed for an *Escherichia coli* strain as the test microorganism,[46] but gausemycins were found to be inactive against wild-type *E. coli*, ΔtolC *E. coli* and even the lptD mutant strain with a permeable outer barrier. Therefore, we used a modified approach, using *Bacillus subtilis* as the test microorganism.[47,48] We treated the test strain with 2.5 MICs of gausemycin or various antibiotics, including DNA replication inhibitors (rifampicin and ciprofloxacin), cell wall biosynthesis inhibitors (vancomycin, benzylpenicillin), protein synthesis inhibitor (chloramphenicol), and membrane-active compounds with inhibitory activity on cell wall biosynthesis (daptomycin, nisin), for 2 h. In this experiment, treatment with gausemycin, as well as with membrane-active antibiotics (daptomycin, nisin), led to almost complete cell lysis, with only singular detectable cells with visible membrane disruption (Figure S32).

To directly confirm the inability of gausemycin to inhibit protein synthesis in bacteria, we employed an *in vitro* cell-free translation system based on *E. coli* extract. Investigating influence of gausemycin on the expression of firefly luciferase (Fluc) by monitoring Fluc luminescence (Figure S33) showed no protein synthesis inhibition.

Inhibition of cell wall biosynthesis is one of the most common mechanisms of how peptides kill bacterial cells (Figure 5). The cell wall biosynthesis process involves several essential steps, which are targeted by antibiotic peptides, and therefore the molecular targets of different peptides in the cell wall are quite diverse. For example, friulimicins sequester lipid-carrier undecaprenyl phosphate (C55-P), and bacitracin inhibits peptidoglycan synthesis by preventing undecaprenyl pyrophosphate dephosphorylation (Figure 5A). Many lipopeptide antibiotics target cell wall biosynthesis precursors, especially Lipid II (Figure 5B).[49,50] Even in this molecule, antibiotics have various binding sites. Glycopeptides, such as vancomycin bind with the D-Ala-D-Ala fragment of the pentapeptide moiety, while ramoplanin, teixobactin and nisin interact with the diphosphate fragment. In addition, semisynthetic derivatives of glycopeptides (e.g. oritavancin) are assumed to have a secondary site at the bridging segments of peptidoglycan.[51]

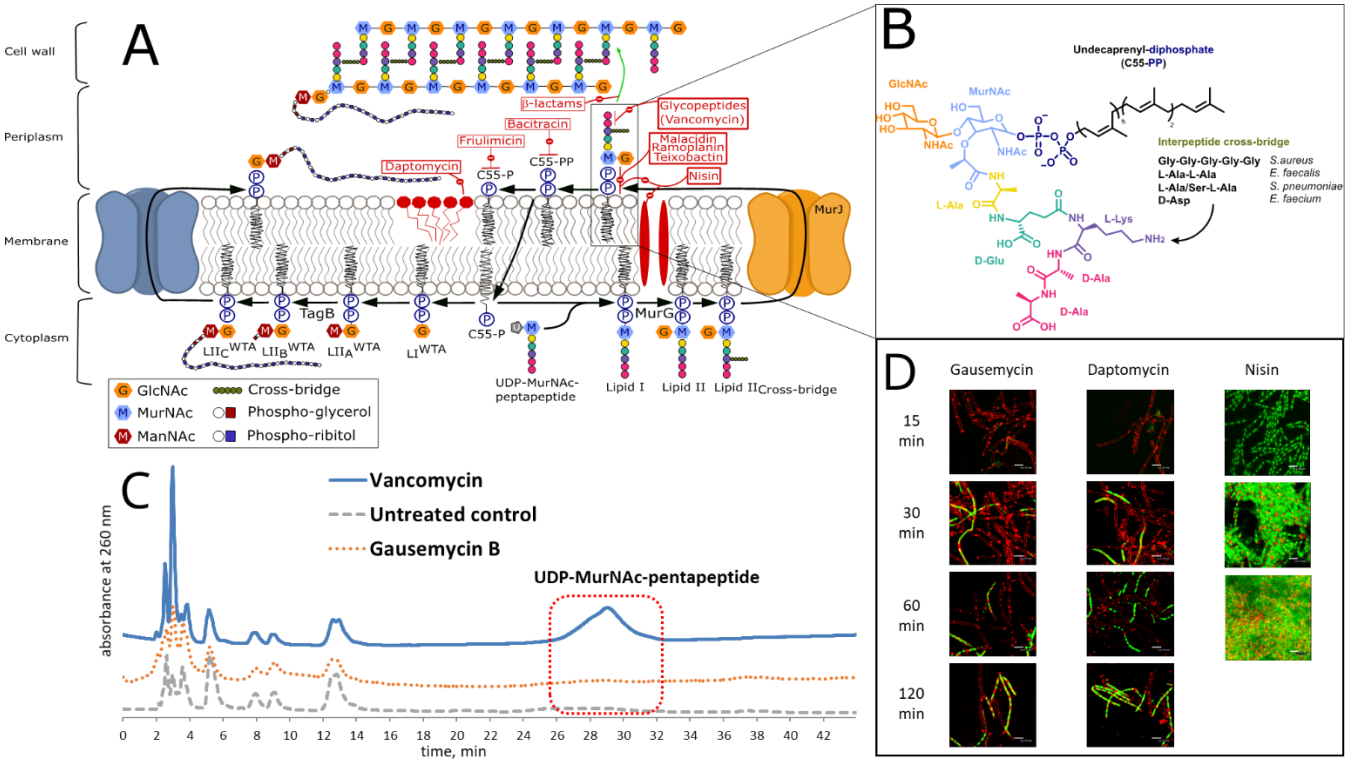

Figure 5. A) Schematic diagram showing modes of action of some cell wall biosynthesis inhibitors. B) Structure of lipid II and its variations. C) Comparison with cell wall biosynthesis inhibitor vancomycin, exposing MRSA to gausemycin does not result in accumulation of cell wall intermediate UDP-MurNAc-pentapeptide. The UDP-MurNAc-pentapeptide peak ($[M+H]^+ = 1150.4$) has retention time 29 min on HPLC profile. D) *B. subtilis* cells under treatment with 1 MIC of gausemycin, daptomycin and nisin, stained with FM 4-64 (red) and SYTOX Green (green).

Generally, the inhibition of the cell wall biosynthesis leads to accumulation of the cell wall precursor molecules. For example, the accumulation of UDP-*N*-AcMur-PP was previously described for the peptide antibiotics targeting cell wall biosynthesis, including vancomycin,[52] laspartomycin,[53] ramoplanin,[52] friulimicin,[14] teixobactin,[18] malacidins[16] and cadasides.[12] The only related compound causing no observable UDP-*N*-AcMur-PP accumulation in treated cells is daptomycin.[16,53] The UDP-*N*-AcMur-PP accumulation assay indicates that gausemycin B has no effect on cell wall biosynthesis precursor pool in contrast to vancomycin (Figure 5C).

On the basis of these findings we deduced, that gausemycins have similar mode of action with membrane-active compounds like daptomycin. To confirm this proposal, we used a modified BCP approach. *B.subtilis* cells were treated with lower antibiotic concentration (1 MIC) and visualized after various treatment periods (Figure 5D). Here we used SYTOX Green dye, staining nucleic acids, but incapable of passing through intact membrane, and FM 4-64, staining membranes with red. Rate of membrane permeabilization under treatment with gausemycin was similar to that in case of daptomycin, whereas nisin, which not only sequester Lipid II molecules, but also forms multimeric transmembrane pores in complex with Lipid II,[54,55] caused more rapid membrane damage, leading to complete cell lysis in 60 min after treatment. Thus, daptomycin was found the most similar to gausemycins among membrane-active compounds.

Daptomycin, isolated in 1985 and used in clinical practice since 2003,[17] is one of the most studied lipopeptide antibiotics. Nonetheless, there is still room for study in this field, new data and models of daptomycin mode of action are reported regularly.[56] Before recent discoveries[57] it was assumed that the cytotoxic effect of daptomycin is caused by membrane depolarization due to its pore-forming activity, but later it was found not to be the primary mode of action. Despite its obvious membrane activity, daptomycin seems to disrupt cell wall biosynthesis by dislocation of membrane-associated enzymes involved in this process, such as MurG, TagB and others (Figure 5A).[57] According to the latest findings,[58] daptomycin (in presence of Ca^{2+} ions) forms a tripartite complex with the anionic lipid phosphatidylglycerol (PG) and bactoprenyl-coupled cell wall precursors ($C_{55}P$, $C_{55}PP$, or lipid II), and these complexes trigger the delocalization of the cell wall biosynthetic machinery. This model explains the narrow spectrum of activity of daptomycin by the requirement for simultaneous presence of a high PG level and a specific cell wall precursor in susceptible microorganisms. Thus, daptomycin has a distinct mode of action, leading to inhibition of cell wall biosynthesis.[59] Taking into account similar bacterial cytological profiles, we assumed that gausemycins have a mode of action similar to that of daptomycin.

Model membrane systems have proved useful for studies of membrane-active peptides,[60–63] therefore, we decided to study the effects of gausemycin B on ion permeability in planar lipid bilayers composed of DOPE/DOPG (1:1) and DOPC/DOPG (1:1). The addition of gausemycin to the *cis*-side of the membrane resulted in step-like current fluctuations (Figure 6AB) corresponding to the opening and closure of individual channels in both lipid systems. The quasi-Ohmic and symmetrical

current–voltage curves (Figure 6E) revealed absence of a voltage-dependent incorporation of the peptide into membrane hydrophobic interior. Most probably, gausemycin binds to the lipid bilayer and freely diffuses through it, forming symmetric pores without noticeable rectification. Phosphatidylethanolamine (PE) lipids induce a negative curvature strain in the bilayer, which usually stabilizes the surface-bound state of membrane-active peptides and impairs their transition into the transmembrane state and channel formation.[64] The similarity of the single-channel properties and threshold concentrations in the DOPE/DOPG and DOPC/DOPG membranes (Figure 6CD, Suppl. S34) indicates an absence of energyc penalty for transition of the gausemycin molecule from the surface-bound to the transmembrane (or equivalent) state. This is also consistent with free diffusion of gausemycin through the lipid bilayer.

Similar relatively narrow conductance levels were observed in both lipid systems (Figure 6CD, Suppl. S34). The close similarity of unit conductance indicates that gausemycin channels have a well-defined structure. This channel likely represents a definite oligomer of the antibiotic molecules (dimer, trimer, tetramer, etc) or a mixed gausemycin/DOPG aggregate. The observed conductance level (~15 pS in 0.1 M KCl) corresponds to a very narrow pore with a diameter ~3Å (for the calculation, the equivalent cylinder model with a membrane thickness of 5 nm was used, access resistance was accounted for).[65] The comparison with the characteristic radii of the most common cations and anions indicates that gausemycin pores might be permeable for partially dehydrated monovalent cations H^+, Li^+, Na^+, K^+ and, probably, for dehydrated divalent cations Be^{2+}, Ca^{2+}, Mn^{2+}. We note that additional experiments are needed to study the selectivity of gausemycin channels. The length of the *N*-terminal fatty-acid tail in gausemycin is about 0.8 nm, while the overall length of the antibiotic molecule, depending from the conformation of the β-Ala1–Tyr5 fragment, is in the range of 2.2–4.0 nm (Figure 3F). Thus, the two gausemycin molecules are long enough to completely span two opposite lipid monolayers and form a transmembrane pore.

A significant fraction of the anionic component (DOPG) made the properties of the used lipid systems similar to those of bacterial membranes. The comparison of threshold concentrations in the model membranes (Suppl. S34) with the typical concentration range of antibiotic activity (Suppl. S28–S30) revealed that gausemycin B damages membrane integrity and forms ion channels only at concentrations of 10×MIC and higher. Likely, similarly to daptomycin, gausemycin specifically interacts with some molecular target in the membranes of susceptible microorganisms, and this interaction significantly increase its pore-forming activity (decrease the threshold concentration by an order of magnitude). A similar mechanism was previously reported for nisin, which forms pores in model lipid bilayers at micromolar concentrations, while interaction with lipid II shifts the range of its activity to nanomolar scale.[66] The fact that treatment with 2.5 MICs resulted in almost complete lysis of *Bacillus subtilis* cells (Figure S29) indicates that accumulation of bound gausemycin molecules induces a strain in the lipid bilayer, which ultimately leads to membrane rupture or micellization.

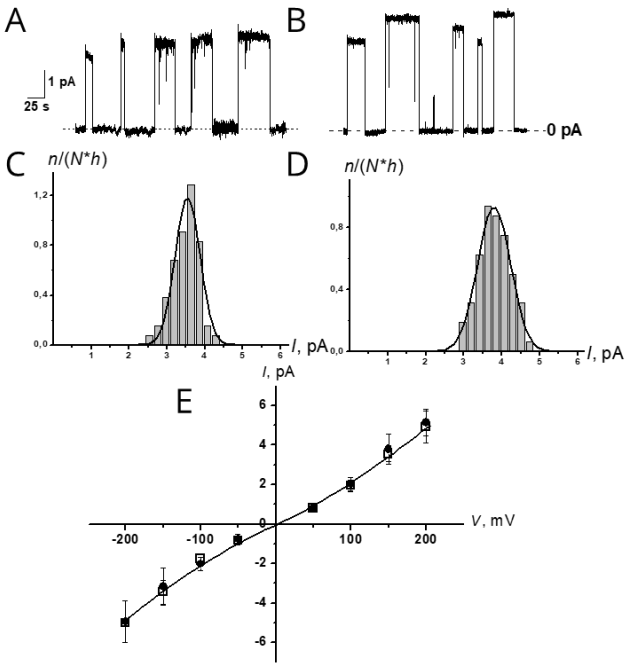

Figure 6. Current fluctuations (A,B) and current-transition histograms (C,D) of single channels induced by gausemycin B in lipid bilayers composed of DOPE/DOPG (1:1) (A,C) and DOPC/DOPG (1:1) (B,D) and bathed in 0.1 M KCl (pH 7.4). The transmembrane voltage was 150 mV. (E) I–V curves of single gausemycin channels in the DOPE/DOPG (●) and DOPC/DOPG (□) membranes.

Despite the observed similarity, gausemycins have a different spectrum of activity compared to daptomycin. Daptomycin exhibits comparable MICs against staphylococci and enterococci, and the formation of the drug-PG-C_{55}P lipid tripartite complex seems to be of crucial importance,[58] while gausemycins are inactive against PG-rich daptomycin-susceptible enterococci. A narrow spectrum of activity is quite unusual for membrane-disrupting compounds, which frequently have low selectivity. Thus, the selectivity of gausemycins confirms the presence of specific molecular target(s) in the membranes of susceptible Gram-positive bacteria, and these targets are probably different from those of daptomycin (PG and C_{55}P, C_{55}PP, or lipid II).

The death of susceptible cells under gausemycin action can be a result of pore formation and rapid membrane permeabilization,[21] or it can be a result of blockade of some process essential for bacterium survival. Cell wall biosynthesis is one of such processes.[55] The absence of UDP-*N*-AcMur-PP accumulation clearly indicates that gausemycins are not sequester lipid peptidoglycan precursors. This fact does not necessarily mean that cell wall biosynthesis is not affected by gausemycins: they can inhibit PBPs and/or affect cell wall biosynthesis indirectly, for example, by dislocating the involved proteins (like daptomycin). Nonetheless, the lack of differences in MRSA and MSSA susceptibility indicates that PBP-binding activity has to involve a mode of action distinct from than that of β-lactams. These data hint at a novel mechanism of antimicrobial action for gausemycin-type lipopeptides, to be thoroughly studied further.

SUMMARY AND CONCLUSIONS

Gausemycins show a vivid structural difference compared to main types of glycolipopeptides, but somewhat resemble cyclic lipopeptides (e.g. daptomycin, rumycin, etc.). Gausemycins have unique structural features: rare and unprecedented natural peptide amino acids (chlorinated kynurenine, 2-amino-4-hydroxy-4-phenybutyric acid), glycosylation of tyrosine with arabinose, N-acylation of ornithine side chain, a five-amino acid exocyclic fragment. Described unique biosynthetic gene cluster architecture leads to these extremely unusual chemical structures, but the exact mode of action of the involved enzymes is yet to be discovered.

Gausemycins exhibit potent activity against Gram-positive bacteria, including clinical isolates of resistant pathogens. Nonetheless, gausemycins are rather selective antibiotics, and the spectrum of activity of these compounds distinguishes them from any known analogues. Moreover, a number of assays show that the molecular target of gausemycins differs from those of cell wall biosynthesis inhibitors, DNA replication inhibitors, and protein synthesis inhibitors. The channel-forming activity and bacteria cell lysis observed under treatment with high peptide concentration suggest the presence of an additional, less efficient and nonspecific membrane-mediated mechanism of action of gausemycins.

Exceptional structural novelty of gausemycins, along with the apparently original mode of action, allows considering them a new class of peptide antibiotics. Discovery of these antibiotics is promising for the development of novel antibacterial agents, both natural and semi-synthetic.

EXPERIMENTAL SECTION

Instrumentation. NMR experiments were carried out on Avance-III-800 spectrometer (Bruker) equipped with 5 mm triple-resonance (^{1}H, ^{13}C, ^{15}N) CryoProbe.

Routine ESI LCMS mass spectra were acquired using Agilent 6340 Ion Trap equipped with an electrospray ionization source (ESI) ("Agilent Technologies") coupled to an Agilent 1100 HPLC system (G1379A degasser, G1312A binary gradient pump, G1367B high performance autosampler, G1316A column thermostat and G1314A variable wavelength detector) ("Agilent Technologies") equipped with a YMC-Triart C18 (YMC) (50×2.1 mm, 1.9 μm particle size) column, maintained at 30°C.

For time-of-flight detection HPLC system (Agilent-1260 Infinity (USA)) consisting of binary pump, thermostat, photometric detector VWD, and the mass spectrometer Agilent 6520 Accurate-Mass quadrupole time-of-flight (Q-TOF) (USA) were used.

HRMS MS/MS fragmentation of gausemycins (Table S5) was performed on FTICR MS Bruker Apex Ultra with harmonized cell equipped with a 7 T superconducting magnet and electrospray ion source (ESI).

Medium-pressure fractionation was performed using Interchim Puriflash 4250. Semipreparative and preparative HPLC was performed using Knauer HPLC system equipped with K-2501 detector with manual fractions collection. Lyophilization was performed using FreeZone 1 Liter Benchtop Freezy Dry Systems. Evaporation under reduced pressure was performed with Labconco Acid-Resistant CentriVap Centrifugal Vacuum Concentrator and Heidolph Hei-VAP Precision rotary evaporator. For cultivation incubator shaker New Brunswick Innova® 40/40R was used.

Current measurements for model membrane experiments were carried out using the Axopatch 200B amplifier (AutoMate Scientific Inc., Berkeley, CA, USA) in the voltage-clamp mode. Data were digitized by Digidata 1440A and analyzed using pClamp 10 (AutoMate Scientific Inc., Berkeley, CA, USA) and Origin 8.0 (OriginLab Corporation, Northampton, MA, USA). Data acquisition was performed with a 5 kHz sampling frequency and low-pass filtering at 1 kHz. The current tracks were processed through an 8-pole Bessel 100 Hz filter.

Chemicals. o-Fluoro-DL-phenylalanine and p-Fluoro-DL-phenylalanine, L-FDAA (Marfey's reagent, N-(2,4-dinitro-5-fluorophenyl)-L-valinamide) were supplied by Sigma-Aldrich. Reagents for model membrane study: synthetic 1,2-dioleoyl-sn-glycero-3-phosphoethanolamine (DOPE), 1,2-dioleoyl-sn-glycero-3-phospho-(1′-rac-glycerol) (DOPG), 1,2-dioleoyl-sn-glycero-3-phosphocholine (DOPC), KCl, HEPES, DMSO, KOH, 3-(4,5-dimethyl-2-thiazolyl)-2,5-diphenyl-2*H*-tetrazolium bromide (MTT) were purchased from Sigma-Aldrich.

Solvents: methanol (MeOH, "Chimmed") acetonitrile (HPLC grade ("Panreac"), ULC/MS grade acetonitrile ("Biosolve"), trifluoroacetic acid (TFA, "Sigma-Aldrich"); formic acid (HCO_2H, "Honeywell"). Deionized water for HPLC was produced by a Milli-Q water purifier (Milli-Q®Plus "Millipore").

HPLC eluents. Eluent A (20mM BisTris in 50% EtOH, pH 6.9), eluent B (20 mM BisTris, pH 6.9, 50% EtOH + 1M LiCl); eluent C (0.1% TFA, 25% PrOH, 74.9% CH_3CN (v/v)); eluent D (0.1 % TFA in H_2O (v/v)); eluent E (0.1 % TFA in CH_3CN (v/v)), eluent F (0.1 $AcONH_4$/TFA buffer, pH 3.0).

Cultivation and extraction. *Streptomyces* sp. INA-Ac-5812 was cultured as described previously.[20] Gausemycins were isolated from fermentation broth of Streptomyces sp. INA-Ac-5812 by the combination of several chromatographic approaches (Figure S5).

For antibiotic concentrate production, fermentation broth of Streptomyces sp. INA-Ac-5812 was acidified to pH 4 and extracted with butanol. Mycelium was extracted with ethanol under ultrasonic dispersion. Crude extracts were washed with ethyl acetate to separate antifungal fraction (containing irumamycin and related compounds).[22] Resulting mixtures were subjected to sorption on LPS-500-H resin in order to set apart low molecular weight impurities and after that, additional stage preparative reversed-phase C18 HPLC was applied, yielding mixture of gausemycins A and B fraction without hydrophobic impurities.

Solid-phase sorption on LPS-500-H. Preparative solid-phase extraction was performed on cartridges, filled with LPS-500-H sorbent. Step elution with 0%, 10%, 20%, 30%, 40%, 50%, 100% of acetonitrile in water was used.

Ion-exchange HPLC. Analytical ion-exchange HPLC was performed on Ultropac Column TSK DEAE-5PW (7.5×75 mm). Preparative ion-exchange HPLC was performed on BIO-RAD analytical grade macroporous anion resin AG MP-1, 200–400 mesh, styrene type, strong quaternary ammonium. Ion-exchange HPLC was performed on DEAE resin (0–25% buffer B in buffer A).

Reversed-phase separation. Analytical C18 HPLC was performed on Sunfire column (C_{18}; 5 μm, 4.6×250 mm), injection

volume was 20 μL. Components were eluted as follows: linear gradient of eluent C in eluent D 36→42% for 25 min, 42→64% for 5 min, 64→35% for 5 min. Flow rate was 1 mL/min. For preparative C18 HPLC ZORBAX SB-C18 (250×21.2 mm, 7 μm) column was used. Injection volume was 2000 μL, flow rate 20 mL/min. Column was eluted with 33% of eluent E in eluent D for 30 min, 50% of eluent E in eluent D for 10 min.

HILIC HPLC. Analytical HILIC HPLC was performed on Waters Spherisorb Silica column (unmodified silica; 5 μm, 4.6×250 mm), injection volume was 10 μL. Components were eluted as follows: linear gradient of eluent D in eluent C 5→17% for 20 min, flow rate was 1 mL/min. For preparative HILIC HPLC VDSpher PUR 100 SIL (250×10 mm, 5 μm) column with unmodified silica was used. Injection volume was 500 μL, flow rate 4 mL/min. Column was eluted with 4% of eluent D in eluent C.

LCMS control method. Fractions compositions and purity of isolated compounds was monitored using LCMS at all stages, while gausemycins exhibited tendency to form complexes with other mixture components, undetectable with HPLC. LCMS was performed as follows: eluent A was triple-distilled water with LC/MS grade formic acid (0.1%, v/v, Honeywell), eluent B was ULC/MS grade acetonitrile with the same acid additive. The column was eluted at a flow rate of 0.35 mL/min: 0–10 min 100:0→0:100 (A:B, v/v); 10–12 min 0:100→100:0 (A:B, v/v). Detection wavelength was 205 nm. The conditions of electrospray ionization (ESI) source in positive ion mode were as follows: temperature, 335°C; nebulizer pressure, 30 psi (N_2); drying gas flow rate, 10 L/min (N_2); capillary voltage, 3500 V. Acquisition parameters were as follows: MS scan range, m/z 50–2200 Da (8100 Da/sec); target mass tune, 800 Da. Samples were taken from solution in 200 μL of MeOH (HPLC grade). Injection volume was 3 μL. Chemstation (rev. B.01.03 SR1), 6300 series TrapControl (v 6.2) and Data Analysis (v. 3.4) software was used for data acquisition and qualitative analyses.

Structure elucidation and analysis. Gausemycins were obtained as white solids, their structure was elucidated using NMR data (chemical shifts are presented in Table S8). Physico-chemical characteristics of obtained compounds are listed below:

Gausemycin A: colorless amorphous powder; $[\alpha]^{22}_D$ -6.9 (c 0.3, MeOH); UV (MeOH) λ_{max} (log ε) 203 (4.7), 229 (4.5), 262 (4.4), 363 (3.7) nm IR ν_{max} 3330, 3070, 2960, 2930, 1660, 1540, 1450, 1200, 1180, 1070 cm^{-1}; HRESIMS m/z 1845.788[20] (calcd for $C_{84}H_{116}ClN_{17}O_{28}$, M^+ 1845.786).

Gausemycin B: colorless amorphous powder; $[\alpha]^{25}_D$ = -9.7 (c 0.4, MeOH); UV (MeOH) λ_{max} (log ε) 204 (4.7), 229 (4.5), 262 (4.4), 363 (3.7) nm; IR ν_{max} 3330, 3070, 2960, 2930, 1660, 1540, 1450, 1230, 1200, 1180, 1070 cm^{-1}; HRESIMS m/z 959.41873 (z=2) (calcd for $C_{87}H_{121}ClN_{18}O_{29}$, $[M+2H]^{2+}$ 959.41905).

Deglycosylation of gausemycin A. Sample of gausemycin A (2.05 mg) was dissolved in 50% methanol in water (1 mL) with 2 M trifluoroacetic acid. Reaction was performed in a sealed vial at 50°C, 6 h. The residue obtained after evaporation of reaction mass *in vacuo* was dissolved in water (1 mL) and transferred to the top of the column (0.5×2.5 cm) with octadecyl silica and eluted by water. Obtained fractions controlled by TLC (ethyl acetate–isopropanol–water, 5:3:1). Fractions containing arabinose (R_f = 0.42) were collected and lyophilized. Dried material (0.11 mg) was dissolved in water (2 mL) and optical rotation was measured after 1 h as well as for authentic samples of D- and L-arabinose. Isolated arabinose (α= + 0.0131°) showed similar result with L-arabinose (α= + 0.0142°)

NMR experiments. NMR samples of gausemycins A and B contained about 8 mM of the compounds in DMSO-d_6. Spectra were measured at 30 and 45°C. The following 2D NMR spectra were measured using standard gradient-enhanced pulse sequences: DQF-COSY, TOCSY (τ_m = 80 ms), NOESY (τ_m = 50, 100, 200, 300 and 400 ms), ^{15}N-HSQC, ^{13}C-HSQC, ^{13}C-HMBC. The ^{1}H chemical shifts were referenced to the residual CD_2H signals of DMSO-d_5 at 2.50 ppm. Chemical shifts of ^{13}C and ^{15}N were referenced indirectly relative to tetramethylsilane (TMS) and liquid NH_3. The structures of non-proteinogenic amino acid residues with different configurations of chiral centers and N-terminal fatty acid group were created in the Avogadro program (version 1.2.0). The geometry of these residues was optimized by energy minimization in Avogadro and transferred to the library of CYANA[26] program. Spatial structure calculations were performed in CYANA (version 3.98.5). ^{1}H-^{1}H spin-spin coupling constants were measured in the DQF-COSY spectrum using the ACME program.[67] The MOLMOL program[68] was used for visual analysis of the structures and figure drawings.

Genome sequencing, annotation and analysis. Genomic DNA was isolated from *Streptomyces* sp. strain INA-Ac-5812 using the PowerSoil DNA isolation kit (Mo Bio Laboratories Inc., Carlsbad, CA). The sequencing library for Illumina sequencing was prepared using the NEBNext Ultra II DNA Library Prep Kit (New England Biolabs, USA) following the manufacturer's instructions. The sequencing of this library on the Illumina HiSeq-2500 platform using HiSeq Rapid Run v2 sequencing reagents generated 9,239,432 single-end reads with an average length of 250 nt (2.3 Gbp in total). Primer sequences were removed from the Illumina reads using Cutadapt v.1.17[69] with the default settings, and low quality read ends were trimmed using Sickle v.1.33 (option q = 30) (https://github.com/najoshi/sickle). For Nanopore sequencing the library was prepared using the 1D ligation sequencing kit (SQK-LSK108, Oxford Nanopore, UK). Sequencing of this library in an R9.4 flow cell (FLO-MIN106) using MinION device yielded 275632 reads with a total length of 1,1 Gbp. Hybrid assembly of Illumina and Nanopore reads was performed using Unicycler v. 0.4.8.[70] A single circular contig of 8,957,687 bp was obtained. Gene search and annotation were performed using the RAST server,[71] followed by manual correction. The genome of *Streptomyces* sp. INA-Ac-5812 was analyzed with antiSMASH[72] to identify potential biosynthetic gene clusters and annotate amino acid substrate specificities of their adenylation domains. Homologous gene clusters were identified with MultiGeneBlast[73] using MIBiG database.[74] Putative functions of tailoring enzymes were assigned according to the predicted function of the closest characterized relative identified by Blast search[75] in NCBI.

***In vitro* antibacterial testing.** Strains obtained from The State Research Center for Antibiotics. *In vitro* antimicrobial activity of 5812 was determined by the broth microdilution method as suggested by the CLSI guidelines document M100-S25 (CLSI M100 S25 Performance Standards for Antimicrobial Susceptibility Testing; Twenty-Fifth Informational Supplement, January 2015). The bacterial inoculums suspensions were standard-

ized by based on the 0.5 McFarland (by DEN-1 McFarland Densitometer). Series of dilutions in the Müller-Hinton broth was carried out in 96-well microtiter plates, the final volume per well was 50 μL. The sensitivity to the sample evaluated after 18 h of growth at 37°C. The MICs was defined as the lowest concentration of sample inhibiting visible growth of a microorganism.

MICs against *M. tuberculosis* strain H37Rv from the collection of the Central Institute for Tuberculosis (Moscow, Russia), were evaluated as previously described.[76]

MTT test. Cells COLO357, J774, EL-4, Colon26, HT-29 were grown in DMEM medium supplemented with 10% fetal calf serum (FCS), pen-strep-glut (all from PanEco, Moscow, Russian Federation). All cell lines used were routinely tested for mycoplasma. Adherent cells were detached using 0.05% trypsin-EDTA (PanEco, Moscow), counted and sub-cultured. Cytotoxic effect of the gausemycins was estimated by a standard 3-(4,5-dimethyl-2-thiazolyl)-2,5-diphenyl-2H-tetrazolium bromide (MTT, Sigma) test as described earlier.[77] All the compounds were dissolved in DMSO to 20 mM concentration and stored at -20 °C until the assay. Before the assay all the compounds were dissolved in culture medium to 200 μM of which 25 μL were transferred to the wells containing 100 μL of culture medium. The compounds were titrated from 20 μM to 0.1 nM with 1 to 5 dilutions. Cells were adjusted to 104 cells/mL, and 100 μL were added to all wells. Non-treated cells served as controls. Plates were incubated for 72 h. For the last 4 h, 5 mg/mL of MTT were added in the amount of 10 μL to each well. After the incubation, culture medium was removed and 100 μL of DMSO were added to each well. Plates were incubated at shaking for 15 min to dissolve the formed formazan product. Optical density was read on spectrophotometer Titertek (UK) at 540 nm. Results were analyzed by Excel package (Microsoft). Cytotoxic concentration giving 50% of the maximal toxic effect (IC50) was calculated from the titration curves. The inhibition of proliferation (inhibition index, II) was calculated as [1 - (ODexperiment/ODcontrol)], where OD was MTT optical density.

Determination of absolute configuration of gausemycins by chiral derivatization. Chiral derivatization of gausemycins hydrolysate was performed according to known procedure.[23,78] 0.6 mg of gausemycin samples (gausemycin B, gausemycin concentrate) were hydrolyzed in 1 mL of 6 M HCl at 115°C for 6 days. After drying *in vacuo*, the resulting hydrolysate was suspended in H_2O. This solution was divided into two aliquots. To each aliquot of the gausemycins hydrolysate and to aliquot (25 μL) of a 50 mM solution (1.25 μM) of each amino acid standard (D, L or DL mixture) was added 10 μL of a 1 M $NaHCO_3$ solution (10 μM). A 1% (w/v) acetone solution (50 μL) of L-FDAA (0.5 mg, 1.8 μM) was added, the molar ration of FDAA to amino acid 1.4:1. The reaction mixtures were mixed and heated for 60 min at 40°C. After cooling to room temperature, the reactions were quenched by addition of of 1 M HCl (10 μL) and dried *in vacuo*. Each residue was then dissolved in DMSO (0.25 mL). A 1:7 dilutions of these were made and 20 μL of sample of each was analyzed with HPLC and LCMS. HPLC analysis was performed on Sunfire column (C_{18}; 5 μm, 4.6×250 mm) with linear gradient 10→50% of acetonitrile in buffer F for 90 min, flow rate was 1 mL/min. Unreacted Marfey's reagent and its hydrolysis product were used as internal standards for retention time correction. The resulting rt comparison for standard amino acids and hydrolysis products are presented in Table S7. Accuracy of peak assignment in hydrolysate HPLC was corroborated by LCMS experiments.

Chemical supplementation (feeding) experiment. The strain *Streptomyces* sp. INA-Ac-5812 was grown in the incubator shaker for 7 days at 28ºC (in autoclaved 250 mL Erlenmeyer flasks containing 50 mL medium) using a nutrient medium of the following composition, %: soy flour, 3.0; glucose, 3.0; NaCl, 0.3; $CaCO_3$, 0.3. After 18 and 40 h of cultivation, fluorinated phenylalanine analogues (*o*-fluoro-DL-phenylalanine and *p*-fluoro-DL-phenylalanine) in the form of water suspension were added to the producing strain to a final concentration 2 mM. The cultures were further incubated for 4 days before extraction and further analysis by LC-MS and MS^n experiments (using TOF instrument, see Figures S26, S27). All experiments were repeated independently with three replicates for each compound. In parallel, culture of *Streptomyces* sp. INA-Ac-5812 was grown as a control.

UDP-*N*-acetylmuramic acid pentapeptide accumulation in *S. aureus*. UDP-MurNAc-PP accumulation was measured in *S. aureus* as previously described[79] with slight modifications. Mid-log phase *S. aureus* ATCC 29213 (OD_{600} = 0.5) pretreated with chloramphenicol (130 μg/mL) was split into 10-mL aliquots and exposed to 10×MIC test antibiotic (10 μg/mL gausemycin B, 10 μg/mL vancomycin). After 1 h incubation at 37°C, 240 rpm, cells were pelleted and extracted with boiling water. Soluble extracts were lyophilized, resuspended in water (150 μL) and a 20 μL aliquot was analyzed on the Waters Sunfire C18 5 μm 4.6×250 mm column with isocratic elution (1.0 mL/min, 50 mM sodium phosphate buffer, pH 5.0) at 25°C and UV-detection (absorbance at 260 nm). The results reported are representative of two independent experiments. Identity and purity of the UDP-MurNAc-PP sample were confirmed by mass spectrometry. Peak at 29 min was collected and analyzed by ESI-HRMS.

Bacterial cytological profiling. *B. subtilis* cells were grown in Luria Bertani (LB) medium at 37°C until the optical density at 600 nm (OD_{600}) was ~0.20. Cells were then left untreated or treated with test substances, as described previously.[46,48] After fixed exposure time, cells were stained with FM 4-64 (1 μg/mL) to visualize cell membranes; DAPI (1 μg/mL) to visualize DNA, and SYTOX Green (1 μg/mL), a vital stain which is normally excluded from cells with an intact membrane but brightly stains cells that are lysed.[46]

Registration of the transmembrane currents through planar lipid bilayers. Virtually solvent-free planar lipid bilayers were prepared according to a monolayer-opposition technique.[80] The aperture was pretreated with hexadecane. The lipid bilayers were made from the equimolar mixtures of DOPE/DOPG (50/50 mol%) and DOPC/DOPG (50/50 mol%). Solutions of 0.1 M KCl were buffered using 5 mM HEPES at pH 7.4. After the membrane was completely formed and stabilized, gausemycin B from a stock solution (5 mg/mL in DMSO) were added to cis-compartment to obtain the final concentrations of 50–150 μg/mL. Ag/AgCl electrodes with agarose/2 M KCl bridges were used to apply a transmembrane voltage (V) and measure the transmembrane current. "Positive voltage" refers to the case in which the cis-side compartment was positive with respect to the trans-side. Single-channel conductance (G) was defined as the ratio between the current flowing through a single pore (I) and transmembrane potential (V). The dwell time (τ) of the channels was determined using

pClamp 10. The total numbers of events used for the channel conductance fluctuation and dwell time analysis were 30–40. The characteristic parameters of channel-forming activity of gausemycin were averaged from 4 bilayers of certain composition (mean ± sd). All experiments were performed at room temperature. Current transition histograms were constructed for tested voltages. A ratio n/(N·h) was set as the histogram ordinate, where n is the number of current fluctuations corresponding to a particular current level; N is the total number of fluctuations; h is the bin size. The total number of events used for the analysis was in the range of 50÷150.

ASSOCIATED CONTENT

Supporting Information. Phylogenetic analysis of a producing strain; LCMS analysis of normal-phase HPTLC fractions; LCMS analysis of ion-exchange fractions; LCMS analysis of C18-HPLC fractions; supplemental discussion of isolation of gausemycins A,B; HRMS fragmentation of individual gausemycin B; chemical shifts of gausemycin A and B; 2D NOESY, ^{13}C-NMBC, ^{13}C-HMBC, TOCSY experiments; Marfey's derivatization of gausemycin hydrolysate; CYANA structure calculations; homologous NRPS clusters; biosynthetic gene cluster analysis; adenylation domains in gausemycin BGC; comparison of putative Dab-encoding proteins; feeding/chemical complementation experiment, biological activity of gausemycins; activity; supplemental discussion of model membrane conductivity experiments.

AUTHOR INFORMATION

Corresponding Authors

Stanislav S. Terekhov – Shemyakin-Ovchinnikov Institute of Bioorganic Chemistry, Miklukho-Maklaya 16/10, 117997 Moscow, Russia; Department of Chemistry, Lomonosov Moscow State University, 1-3 Leninskie Gory, 119992 Moscow, Russia; orcid.org/0000-0003-2220-0452; E-mail: sterekhoff@gmail.com

Zakhar O. Shenkarev – Shemyakin-Ovchinnikov Institute of Bioorganic Chemistry, Miklukho-Maklaya 16/10, 117997 Moscow, Russia; Moscow Institute of Physics and Technology, Institutsky lane 9, Dolgoprydny, 141700 Moscow region, Russia, Russia; orcid.org/0000-0003-1383-3522; E-mail: zakharshenkarev@yandex.ru

Vladimir A. Korshun – Gause Institute of New Antibiotics, Bolshaya Pirogovskaya 11, 119021 Moscow, Russia; Shemyakin-Ovchinnikov Institute of Bioorganic Chemistry, Miklukho-Maklaya 16/10, 117997 Moscow, Russia; orcid.org/0000-0001-9436-6561; E-mail: v-korshun@yandex.ru

Author Contributions

A.P.T., V.A.A., O.A.D., and V.A.K. – conceptualization; O.A.L. discovered a producing strain; G.S.K. and N.E.N. started chemical studies of secondary metabolites, E.G.G. and O.A.L. performed cultivation of a producing strain; A.V.M., A.V.B., N.V.R., and I.A.O. performed sequencing of a producing strain; V.A.A., A.A.B., and I.A.I. performed biosynthesis study using chemical supplementation; V.A.A., M.V.B., S.S.T., and I.A.O. identified and analyzed the biosynthetic cluster and the pathway of biosynthesis; A.P.T., V.A.A., G.Kh.K., E.A.R., V.A.B., A.A.B., I.A.P., T.V.K., V.V.K., and D.T.T. developed approaches to isolation of compounds; A.Y.Z., A.A.C., M.V.B., I.A.I., and E.N.N. performed MS studies; A.S.P., M.V.S., M.V.K., A.S.S., N.E.N., and Z.O.S. performed NMR and structural studies; A.P.T., V.A.A., A.A.C., and T.V.K. performed analysis of configurations of amino acids and arabinose; S.S.E. and O.S.O. performed membrane studies in model bilayers; A.P.T. and T.V.K. performed UPD-MurNAc-PP accumulation experiment; A.P.T., N.E.G., E.B.I., E.P.M., E.V.S., A.S.A., K.B.M., S.S.T., and I.A.O. performed susceptibility and biological activity studies; A.P.T., V.A.A., A.S.P., M.V.S., S.S.T., Z.O.S., and V.A.K. wrote the paper.

Funding Sources

The research was supported in part by the budget funding of the topic 006 "Isolation and physico-chemical characterization of microbially produced antibiotic compounds" at the Gause Institute of New Antibiotics and RFBR (project № 20-33-70215). NMR studies were supported by RSF (project № 19-74-30014). Genome sequencing and mechanistic studies were supported in part by RFBR (project № 20-54-53014). The FTICR MS study was supported by RSF (project № 21-47-04405).

ABBREVIATIONS

BGC, biosynthetic gene cluster; COSY, ^{1}H-^{1}H correlation spectroscopy; DEAE, diethylaminoethyl (resin); DMSO, dimethyl sulfoxide; DOPE, 1,2-dioleoyl-*sn*-glycero-3-phosphoethanolamine; DOPG, 1,2-dioleoyl-*sn*-glycero-3-phospho-rac-(1-glycerol) sodium salt; ESI HRMS, electrospray ionization high resolution mass spectrometry; HEPES, 4-(2-hydroxyethyl)-1-piperazineethanesulfonic acid; HILIC, hydrophilic interaction liquid chromatography; HMBC, heteronuclear multiple bond correlation; HPLC, high-performance liquid chromatography; HSQC, heteronuclear single quantum coherence; MIC, minimum inhibitory concentration; MRSA, methicillin-resistant *Staphylococcus aureus*; MSSA, methicillin-susceptible *Staphylococcus aureus*; MTT, 3-(4,5-dimethylthiazol-2-yl)-2,5-diphenyltetrazolium bromide; NMR, nuclear magnetic resonance, NOESY, nuclear Overhauser effect spectroscopy; NRPS, non-ribosomal peptide synthetase; PBP, penicillin-binding proteins; PG, phosphatidylglycerol; TFA, trifluoroacetic acid; TLC, thin layer chromatography; TOCSY, total correlated spectroscopy; UDP-N-AcMur-PP, undecaprenyl-phosphate-N-acetylmuramate diphosphate; Q-TOF, quadrupole time-of-flight.

REFERENCES

(1) Tacconelli, E.; Carrara, E.; Savoldi, A.; Harbarth, S.; Mendelson, M.; Monnet, D. L.; Pulcini, C.; Kahlmeter, G.; Kluytmans, J.; Carmeli, Y.; Ouellette, M.; Outterson, K.; Patel, J.; Cavaleri, M.; Cox, E. M.; Houchens, C. R.; Grayson, M. L.; Hansen, P.; Singh, N.; Theuretzbacher, U.; Magrini, N.; Aboderin, A. O.; Al-Abri, S. S.; Awang Jalil, N.; Benzonana, N.; Bhattacharya, S.; Brink, A. J.; Burkert, F. R.; Cars, O.; Cornaglia, G.; Dyar, O. J.; Friedrich, A. W.; Gales, A. C.; Gandra, S.; Giske, C. G.; Goff, D. A.; Goossens, H.; Gottlieb, T.; Guzman Blanco, M.; Hryniewicz, W.; Kattula, D.; Jinks, T.; Kanj, S. S.; Kerr, L.; Kieny, M.-P.; Kim, Y. S.; Kozlov, R. S.; Labarca, J.; Laxminarayan, R.; Leder, K.; Leibovici, L.; Levy-Hara, G.; Littman, J.; Malhotra-Kumar, S.; Manchanda, V.; Moja, L.; Ndoye, B.; Pan, A.; Paterson, D. L.; Paul, M.; Qiu, H.; Ramon-Pardo, P.; Rodríguez-Baño, J.; Sanguinetti, M.; Sengupta, S.; Sharland, M.; Si-Mehand, M.; Silver, L. L.; Song, W.; Steinbakk, M.; Thomsen, J.; Thwaites, G. E.; van der Meer, J. W.; Van Kinh, N.; Vega, S.; Villegas, M. V.; Wechsler-Fördös, A.; Wertheim, H. F. L.; Wesangula, E.; Woodford, N.; Yilmaz, F. O.; Zorzet, A. Discovery, research, and development of new antibiotics: the WHO priority list of antibiotic-resistant bacteria and tuberculosis. *Lancet Inf. Dis.* **2018**, *18* (3), 318–327. https://doi.org/10.1016/S1473-3099(17)30753-3

(2) Wencewicz, T. A. New antibiotics from nature's chemical inventory. *Bioorg. Med. Chem.* **2016**, *24* (24), 6227–6252. https://doi.org/10.1016/j.bmc.2016.09.014

(3) Luther, A.; Bisang, C.; Obrecht, D. Advances in macrocyclic peptide-based antibiotics. *Bioorg. Med. Chem.* **2018**, *26* (10), 2850–2858. https://doi.org/10.1016/j.bmc.2017.08.006

(4) Blaskovich, M. A. T.; Hansford, K. A.; Butler, M. S.; Jia, Z.; Mark, A. E.; Cooper, M. A. Developments in glycopeptide antibiotics. *ACS Infect. Dis.* **2018**, *4* (5), 715–735. https://doi.org/10.1021/acsinfecdis.7b00258

(5) Somma, S.; Gastaldo, L.; Corti, A. Teicoplanin, a new antibiotic from *Actinoplanes teichomyceticus* nov. sp. *Antimicrob. Agents Chemother.* **1984**, *26* (6), 917–923. https://doi.org/10.1128/aac.26.6.917

(6) Ciabatti, R.; Kettenring, J. K.; Winters, G.; Tuan, G.; Zerilli, L.; Cavalleri, B. Ramoplanin (A-16686), a new glycolipodepsipeptide antibiotic. III. Structure elucidation. *J. Antibiot.* **1989**, *42* (2), 254–267. https://doi.org/10.7164/antibiotics.42.254

(7) Neuhof, T.; Schmieder, P.; Preussel, K.; Dieckmann, R.; Pham, H.; Bartl, F.; von Döhren, H. Hassallidin A, a glycosylated lipopeptide with antifungal activity from the cyanobacterium *Hassallia* sp. *J. Nat. Prod.* **2005**, *68* (5), 695–700. https://doi.org/10.1021/np049671r

(8) Lu, S.-E.; Novak, J.; Austin, F. W.; Gu, G.; Ellis, D.; Kirk, M.; Wilson-Stanford, S.; Tonelli, M.; Smith, L. Occidiofungin, a unique antifungal glycopeptide produced by a strain of *Burkholderia contaminans*. *Biochemistry* **2009**, *48* (35), 8312–8321. https://doi.org/10.1021/bi900814c

(9) Debono, M.; Barnhart, M.; Carrell, C. B.; Hoffmann, J. A.; Occolowitz, J. L.; Abbott, B. J.; Fukuda, D. S.; Hamill, R. L.; Biemann, K.; Herlihy, W. C. A21978C, a complex of new acidic peptide antibiotics. Isolation, chemistry, and mass spectral structure elucidation. *J. Antibiot.* **1987**, *40* (6), 761–777. https://doi.org/10.7164/antibiotics.40.761

(10) Yamanaka, K.; Reynolds, K. A.; Kersten, R. D.; Ryan, K. S.; Gonzalez, D. J.; Nizet, V.; Dorrestein, P. C.; Moore, B. S. Direct cloning and refactoring of a silent lipopeptide biosynthetic gene cluster yields the antibiotic taromycin A. *Proc. Natl. Acad. Sci. USA* **2014**, *111* (5), 1957–1962. https://doi.org/10.1073/pnas.1319584111

(11) Reynolds, K. A.; Luhavaya, H.; Li, J.; Dahesh, S.; Nizet, V.; Yamanaka, K.; Moore, B. S. Isolation and structure elucidation of lipopeptide antibiotic taromycin B from the activated taromycin biosynthetic gene cluster. *J. Antibiot.* **2018**, *71* (2), 333–338. https://doi.org/10.1038/ja.2017.146

(12) Wu, C.; Shang, Z.; Lemetre, C.; Ternei, M. A.; Brady, S. F. Cadasides, calcium-dependent acidic lipopeptides from the soil metagenome that are active against multidrug-resistant bacteria. *J. Am. Chem. Soc.* **2019**, *141* (9), 3910–3919. https://doi.org/10.1021/jacs.8b12087

(13) Heinemann, B.; Kaplan, M. A.; Muir, R. D.; Hooper, I. R. Amphomycin, a new antibiotic. *Antibiot. Chemother. (Northfield)* **1953**, *3* (12), 1239–1242

(14) Vértesy, L.; Ehlers, E.; Kogler, H.; Kurz, M.; Meiwes, J.; Seibert, G.; Vogel, M.; Hammann, P. Friulimicins: novel lipopeptide antibiotics with peptidoglycan synthesis inhibiting activity from *Actinoplanes friuliensis* sp. nov. II. Isolation and structural characterization. *J. Antibiot.* **2000**, *53* (8), 816–827. https://doi.org/10.7164/antibiotics.53.816

(15) Borg, M.; Neary, J. M.; Wrigley, S. K.; Jim, J. M.; Smith, C. P. Cyclic lipopeptides. Pat. WO2007072082A1, 2007

(16) Hover, B. M.; Kim, S.-H.; Katz, M.; Charlop-Powers, Z.; Owen, J. G.; Ternei, M. A.; Maniko, J.; Estrela, A. B.; Molina, H.; Park, S.; Perlin, D. S.; Brady, S. F. Culture-independent discovery of the malacidins as calcium-dependent antibiotics with activity against multidrug-resistant Gram-positive pathogens. *Nat. Microbiol.* **2018**, *3* (4), 415–422. https://doi.org/10.1038/s41564-018-0110-1

(17) Eisenstein, B. I.; Oleson, F. B., Jr; Baltz, R. H. Daptomycin: from the mountain to the clinic, with essential help from Francis Tally, MD. *Clin. Inf. Dis.* **2010**, *50* (Suppl. 1), S10–S15. https://doi.org/10.1086/647938

(18) Ling, L. L.; Schneider, T.; Peoples, A. J.; Spoering, A. L.; Engels, I.; Conlon, B. P.; Mueller, A.; Schaberle, T. F.; Hughes, D. E.; Epstein, S.; Jones, M.; Lazarides, L.; Steadman, V. A.; Cohen, D. R.; Felix, C. R.; Fetterman, K. A.; Millett, W. P.; Nitti, A. G.; Zullo, A. M.; Chen, C.; Lewis, K. A new antibiotic kills pathogens without detectable resistance. *Nature* **2015**, *517* (7535), 455–459. https://doi.org/10.1038/nature14098

(19) Piddock, L. J. V. Teixobactin, the first of a new class of antibiotics discovered by iChip technology? *J. Antimicrob. Chemother.* **2015**, *70* (10), 2679–2680. https://doi.org/10.1093/jac/dkv175

(20) Lapchinskaya, O. A.; Katrukha, G. S.; Gladkikh, E. G.; Kulyaeva, V. V.; Coodan, P. V.; Topolyan, A. P.; Alferova, V. A.; Pogozheva, V. V.; Sukonnikov, M. A.; Rogozhin, E. A.; Prokhorenko, I. A.; Brylev, V. A.; Korolev, A. M.; Slyundina, M. S.; Borisov, R. S.; Serebryakova, M. V.; Shuvalov, M. V.; Ksenofontov, A. L.; Stoyanova, L. G.; Osterman, I. A.; Formanovsky, A. A.; Tashlitsky, V. N.; Baratova, L. A.; Timofeeva, A. V.; Tyurin, A. P. Investigation of the complex antibiotic INA-5812. *Russ. J. Bioorg. Chem.* **2016**, *42* (6), 664–671. https://doi.org/10.1134/S1068162016060078

(21) Vasilchenko, A. S.; Julian, W. T.; Lapchinskaya, O. A.; Katrukha, G. S.; Sadykova, V. S.; Rogozhin, E. A. A novel peptide antibiotic produced by *Streptomyces roseoflavus* strain INA-Ac-5812 with directed activity against Gram-positive bacteria. *Front. Microbiol.* **2020**, *11*, 556063. https://doi.org/10.3389/fmicb.2020.556063

(22) Alferova, V. A.; Shuvalov, M. V.; Novikov, R. A.; Trenin, A. S.; Dezhenkova, L. G.; Gladkikh, E. G.; Lapchinskaya, O. A.; Kulyaeva, V. V.; Bychkova, O. P.; Mirchink, E. P.; Solyev, P. N.; Kudryakova, G. Kh.; Korshun, V. A.; Tyurin, A. P. Structure-activity studies of irumamycin type macrolides from *Streptomyces* sp. INA-Ac-5812. *Tetrahedron Lett.* **2019**, *60* (21), 1448–1451. https://doi.org/10.1016/j.tetlet.2019.04.051

(23) Alferova, V. A.; Shuvalov, M. V.; Suchkova, T. A.; Proskurin, G. V.; Aparin, I. O.; Rogozhin, E. A.; Novikov, R. A.; Solyev, P. N.; Chistov, A. A.; Ustinov, A. V.; Tyurin, A. P.; Korshun, V. A. 4-Chloro-L-kynurenine as fluorescent amino acid in natural peptides. *Amino Acids* **2018**, *50* (12), 1697–1705. https://doi.org/10.1007/s00726-018-2642-3

(24) Schubert, M.; Labudde, D.; Oschkinat, H.; Schmieder, P. A software tool for the prediction of Xaa-Pro peptide bond conformations in proteins based on ^{13}C chemical shift statistics. *J. Biomol. NMR* **2002**, *24* (2), 149–154. https://doi.org/10.1023/A:1020997118364

(25) Schrumpf, G.; Becher, G.; Lüttke, W. The ^{1}H NMR spectrum of [1-^{13}C]butadiene-1,3. *J. Magn. Res.* **1973**, *10* (1), 90–94. https://doi.org/10.1016/0022-2364(73)90239-4

(26) Güntert, P.; Buchner, L. Combined automated NOE assignment and structure calculation with CYANA. *J. Biomol. NMR* **2015**, *62* (4), 453–471. https://doi.org/10.1007/s10858-015-9924-9

(27) Lafite, P.; Daniellou, R. Rare and unusual glycosylation of peptides and proteins. *Nat. Prod. Rep.* **2012**, *29* (7), 729–738. https://doi.org/10.1039/C2NP20030A

(28) Dutta, D.; Mandal, C.; Mandal, C. Unusual glycosylation of proteins: beyond the universal sequon and other amino acids. *BBA Gen. Subj.* **2017**, *1861* (12), 3096–3108. https://doi.org/10.1016/j.bbagen.2017.08.025

(29) Shoji, J.; Sakazaki, R. A new peptide antibiotic complex S-520. III Isolation of L-*threo*-β-hydroxyglutamic acid from

the hydrolysate. *J. Antiobiot.* **1970**, *23* (8), 418–419. https://doi.org/10.7164/antibiotics.23.418

(30) von Nussbaum, F.; Anlauf, S.; Freiberg, C.; Benet-Buchholz, J.; Schamberger, J.; Henkel, T.; Schiffer, G.; Häbich, D. Total synthesis and initial structure–activity relationships of longicatenamycin A. *ChemMedChem* **2008**, *3* (4), 619–626. https://doi.org/10.1002/cmdc.200700297

(31) Broberg, A.; Menkis, A.; Vasiliauskas, R. Kutznerides 1–4, depsipeptides from the *Actinomycete Kutzneria* sp. 744 inhabiting mycorrhizal roots of *Picea abies* seedlings. *J. Nat. Prod.* **2006**, *69* (1), 97–102. https://doi.org/10.1021/np050378g

(32) Strieker, M.; Nolan, E. M.; Walsh, C. T.; Marahiel, M. A. Stereospecific synthesis of *threo*- and *erythro*-*β*-hydroxyglutamic acid during kutzneride biosynthesis. *J. Am. Chem. Soc.* **2009**, *131* (37), 13523–13530. https://doi.org/10.1021/ja9054417

(33) Schleifer, K. H.; Plapp, R.; Kandler, O. Identification of *threo*-3-hydroxyglutamic acid in the cell wall of *Microbacterium lacticum*. *Biochem. Biophys. Res. Commun.* **1967**, *28* (4), 566–570. https://doi.org/10.1016/0006-291X(67)90351-8

(34) Müller, C.; Nolden, S.; Gebhardt, P.; Heinzelmann, E.; Lange, C.; Puk, O.; Welzel, K.; Wohlleben, W.; Schwartz, D. Sequencing and analysis of the biosynthetic gene cluster of the lipopeptide antibiotic friulimicin in *Actinoplanes friuliensis*. *Antimicrob. Agents Chemother.* **2007**, *51* (3), 1028–1037. https://doi.org/10.1128/AAC.00942-06

(35) Wang, Y.; Chen, Y.; Shen, Q.; Yin, X. Molecular cloning and identification of the laspartomycin biosynthetic gene cluster from *Streptomyces viridochromogenes*. *Gene* **2011**, *483* (1), 11–21. https://doi.org/10.1016/j.gene.2011.05.005

(36) Rausch, C.; Hoof, I.; Weber, T.; Wohlleben, W.; Huson, D. H. Phylogenetic analysis of condensation domains in NRPS sheds light on their functional evolution. *BMC Evolut. Biol.* **2007**, *7*, 78. https://doi.org/10.1186/1471-2148-7-78

(37) Sosio, M.; Stinchi, S.; Beltrametti, F.; Lazzarini, A.; Donadio, S. The gene cluster for the biosynthesis of the glycopeptide antibiotic A40926 by *Nonomuraea* species. *Chem. Biol.* **2003**, *10* (6), 541–549. https://doi.org/10.1016/S1074-5521(03)00120-0

(38) Luhavaya, H.; Sigrist, R.; Chekan, J. R.; McKinnie, S. M. K.; Moore, B. S. Biosynthesis of L-4-chlorokynurenine, an antidepressant prodrug and a non-proteinogenic amino acid found in lipopeptide antibiotics. *Angew. Chem. Int. Ed.* **2019**, *58* (25), 8394–8399. https://doi.org/10.1002/anie.201901571

(39) Koketsu, K.; Mitsuhashi, S.; Tabata, K. Identification of homophenylalanine biosynthetic genes from the cyanobacterium *Nostoc punctiforme* PCC73102 and application to its microbial production by *Escherichia coli*. *Appl. Environ. Microbiol.* **2013**, *79* (7), 2201–2208. https://doi.org/10.1128/AEM.03596-12

(40) Janso, J. E.; Haltli, B. A.; Eustáquio, A. S.; Kulowski, K.; Waldman, A. J.; Zha, L.; Nakamura, H.; Bernan, V. S.; He, H.; Carter, G. T.; Koehn, F. E.; Balskus, E. P. Discovery of the lomaiviticin biosynthetic gene cluster in *Salinispora pacifica*. *Tetrahedron* **2014**, *70* (27), 4156–4164. https://doi.org/10.1016/j.tet.2014.03.009

(41) Fu, C.; Keller, L.; Bauer, A.; Brönstrup, M.; Froidbise, A.; Hammann, P.; Herrmann, J.; Mondesert, G.; Kurz, M.; Schiell, M.; Schummer, D.; Toti, L.; Wink, J.; Müller, R. Biosynthetic studies of telomycin reveal new lipopeptides with enhanced activity. *J. Am. Chem. Soc.* **2015**, *137* (24), 7692–7705. https://doi.org/10.1021/jacs.5b01794

(42) Vestola, J.; Shishido, T. K.; Jokela, J.; Fewer, D. P.; Aitio, O.; Permi, P.; Wahlsten, M.; Wang, H.; Rouhiainen, L.; Sivonen, K. Hassallidins, antifungal glycolipopeptides, are widespread among cyanobacteria and are the end-product of a nonribosomal pathway. *Proc. Natl. Acad. Sci. USA* **2014**, *111* (18), E1909–E1917. https://doi.org/10.1073/pnas.1320913111

(43) Strieker, M.; Marahiel, M. A. The structural diversity of acidic lipopeptide antibiotics. *ChemBioChem* **2009**, *10* (4), 607–616. https://doi.org/10.1002/cbic.200800546

(44) Hanberger, H.; Nilsson, L. E.; Maller, R.; Isaksson, B. Pharmacodynamics of daptomycin and vancomycin on *Enterococcus faecalis* and *Staphylococcus aureus* demonstrated by studies of initial killing and postantibiotic effect and influence of Ca^{2+} and albumin on these drugs. *Antimicrob. Agents Chemother.* **1991**, *35* (9), 1710–1716. https://doi.org/10.1128/AAC.35.9.1710

(45) Melander, R. J.; Zurawski, D. V.; Melander, C. Narrow-spectrum antibacterial agents. *Med. Chem. Commun.* **2018**, *9* (1), 12–21. https://doi.org/10.1039/C7MD00528H

(46) Nonejuie, P.; Burkart, M.; Pogliano, K.; Pogliano, J. Bacterial cytological profiling rapidly identifies the cellular pathways targeted by antibacterial molecules. *Proc. Natl. Acad. Sci.* **2013**, *110* (40), 16169–16174. https://doi.org/10.1073/pnas.1311066110

(47) Lamsa, A.; Liu, W.-T.; Dorrestein, P. C.; Pogliano, K. The *Bacillus subtilis* cannibalism toxin SDP collapses the proton motive force and induces autolysis. *Mol. Microbiol.* **2012**, *84* (3), 486–500. https://doi.org/10.1111/j.1365-2958.2012.08038.x

(48) Mohammad, H.; Younis, W.; Ezzat, H. G.; Peters, C. E.; AbdelKhalek, A.; Cooper, B.; Pogliano, K.; Pogliano, J.; Mayhoub, A. S.; Seleem, M. N. Bacteriological profiling of diphenylureas as a novel class of antibiotics against methicillin-resistant *Staphylococcus aureus*. *PLoS One* **2017**, *12* (8), e0182821. https://doi.org/10.1371/journal.pone.0182821

(49) Grein, F.; Schneider, T.; Sahl, H.-G. Docking on lipid II –a widespread mechanism for potent bactericidal activities of antibiotic peptides. *J. Mol. Biol.* **2019**, *431* (18), 3520–3530. https://doi.org/10.1016/j.jmb.2019.05.014

(50) Breukink, E.; de Kruijff, B. Lipid II as a target for antibiotics. *Nat. Rev. Drug Discov.* **2006**, *5* (4), 321–332. https://doi.org/10.1038/nrd2004

(51) Zhanel, G. G.; Schweizer, F.; Karlowsky, J. A. Oritavancin: mechanism of action. *Clin. Inf. Dis.* **2012**, *54* (Suppl. 3), S214–S219. https://doi.org/10.1093/cid/cir920

(52) Billot-Klein, D.; Shlaes, D.; Bryant, D.; Bell, D.; Legrand, R.; Gutmann, L.; van Heijenoort, J. Presence of UDP-N-acetylmuramyl-hexapeptides and -heptapeptides in enterococci and staphylococci after treatment with ramoplanin, tunicamycin, or vancomycin. *J. Bacteriol.* **1997**, *179* (15), 4684–4688. https://doi.org/10.1128/JB.179.15.4684-4688.1997

(53) Kleijn, L. H. J.; Oppedijk, S. F.; 't Hart, P.; van Harten, R. M.; Martin-Visscher, L. A.; Kemmink, J.; Breukink, E.; Martin, N. I. Total synthesis of laspartomycin C and characterization of its antibacterial mechanism of action. *J. Med. Chem.* **2016**, *59* (7), 3569–3574. https://doi.org/10.1021/acs.jmedchem.6b00219

(54) Hasper, H. E.; de Kruijff, B.; Breukink, E. Assembly and stability of nisin–lipid II pores. *Biochemistry* **2004**, *43* (36), 11567–11575. https://doi.org/10.1021/bi049476b

(55) Hasper, H. E.; Kramer, N. E.; Smith, J. L.; Hillman, J. D.; Zachariah, C.; Kuipers, O. P.; de Kruijff, B.; Breukink, E. An alternative bactericidal mechanism of action for lantibiotic peptides that target lipid II. *Science* **2006**, *313* (5793), 1636–1637. https://doi.org/10.1126/science.1129818

(56) Gray, D. A.; Wenzel, M. More than a pore: a current perspective on the *in vivo* mode of action of the lipopeptide

antibiotic daptomycin. *Antibiotics* **2020**, *9* (1), 17. https://doi.org/10.3390/antibiotics9010017

(57) Müller, A.; Wenzel, M.; Strahl, H.; Grein, F.; Saaki, T. N. V.; Kohl, B.; Siersma, T.; Bandow, J. E.; Sahl, H.-G.; Schneider, T.; Hamoen, L. W. Daptomycin inhibits cell envelope synthesis by interfering with fluid membrane microdomains. *Proc. Natl. Acad. Sci. USA* **2016**, *113* (45), E7077–E7086. https://doi.org/10.1073/pnas.1611173113

(58) Grein, F.; Müller, A.; Scherer, K. M.; Liu, X.; Ludwig, K. C.; Klöckner, A.; Strach, M.; Sahl, H.-G.; Kubitscheck, U.; Schneider, T. Ca^{2+}-Daptomycin targets cell wall biosynthesis by forming a tripartite complex with undecaprenyl-coupled intermediates and membrane lipids. *Nat. Commun.* **2020**, *11* (1), 1455. https://doi.org/10.1038/s41467-020-15257-1

(59) Wood, T. M.; Martin, N. I. The calcium-dependent lipopeptide antibiotics: structure, mechanism, & medicinal chemistry. *Med. Chem. Commun.* **2019**, *10* (5), 634–646. https://doi.org/10.1039/C9MD00126C

(60) Chugunov, A.; Pyrkova, D.; Nolde, D.; Polyansky, A.; Pentkovsky, V.; Efremov, R. Lipid-II forms potential "landing terrain" for lantibiotics in simulated bacterial membrane. *Sci. Rep.* **2013**, *3* (1), 1678. https://doi.org/10.1038/srep01678

(61) Balleza, D.; Mescola, A.; Alessandrini, A. Model lipid systems and their use to evaluate the phase state of biomembranes, their mechanical properties and the effect of non-conventional antibiotics: the case of daptomycin. *Eur. Biophys. J.* **2020**, *49* (5), 401–408. https://doi.org/10.1007/s00249-020-01445-w

(62) Seydlová, G.; Sokol, A.; Lišková, P.; Konopásek, I.; Fišer, R. Daptomycin pore formation and stoichiometry depend on membrane potential of target membrane. *Antimicrob. Agents Chemother.* **2019**, *63* (1), e01589-18. https://doi.org/10.1128/AAC.01589-18

(63) Hollmann, A.; Martinez, M.; Maturana, P.; Semorile, L. C.; Maffia, P. C. Antimicrobial peptides: interaction with model and biological mem-branes and synergism with chemical antibiotics. *Front. Chem.* **2018**, *6*, 204. https://doi.org/10.3389/fchem.2018.00204

(64) Lee, M.-T.; Hung, W.-C.; Chen, F.-Y.; Huang, H. W. Many-body effect of antimicrobial peptides: on the correlation between lipid's spontaneous curvature and pore formation. *Biophys. J.* **2005**, *89* (6), 4006–4016. https://doi.org/10.1529/biophysj.105.068080

(65) Sansom, M. S. P. The biophysics of peptide models of ion channels. *Progr. Biophys. Mol. Biol.* **1991**, *55*, 139–235. https://doi.org/10.1016/0079-6107(91)90004-C

(66) Breukink, E. Use of the cell wall precursor lipid II by a pore-forming peptide antibiotic. *Science* **1999**, *286* (5448), 2361–2364. https://doi.org/10.1126/science.286.5448.2361

(67) Delaglio, F.; Wu, Z.; Bax, A. Measurement of homonuclear proton couplings from regular 2D COSY spectra. *J. Magn. Res.* **2001**, *149* (2), 276–281. https://doi.org/10.1006/jmre.2001.2297

(68) Koradi, R.; Billeter, M.; Wüthrich, K. MOLMOL: A program for display and analysis of macromolecular structures. *J. Mol. Graph.* **1996**, *14* (1), 51–55. https://doi.org/10.1016/0263-7855(96)00009-4

(69) Martin, M. Cutadapt removes adapter sequences from high-throughput sequencing reads. *EMBnet J.* **2011**, *17* (1), 10. https://doi.org/10.14806/ej.17.1.200

(70) Wick, R. R.; Judd, L. M.; Gorrie, C. L.; Holt, K. E. Unicycler: resolving bacterial genome assemblies from short and long sequencing reads. *PLoS Comput. Biol.* **2017**, *13* (6), e1005595. https://doi.org/10.1371/journal.pcbi.1005595

(71) Aziz, R. K.; Bartels, D.; Best, A. A.; DeJongh, M.; Disz, T.; Edwards, R. A.; Formsma, K.; Gerdes, S.; Glass, E. M.; Kubal, M.; Meyer, F.; Olsen, G. J.; Olson, R.; Osterman, A. L.; Overbeek, R. A.; McNeil, L. K.; Paarmann, D.; Paczian, T.; Parrello, B.; Pusch, G. D.; Reich, C.; Stevens, R.; Vassieva, O.; Vonstein, V.; Wilke, A.; Zagnitko, O. The RAST server: rapid annotations using subsystems technology. *BMC Genomics* **2008**, *9* (1), 75. https://doi.org/10.1186/1471-2164-9-75

(72) Blin, K.; Shaw, S.; Steinke, K.; Villebro, R.; Ziemert, N.; Lee, S. Y.; Medema, M. H.; Weber, T. antiSMASH 5.0: updates to the secondary metabolite genome mining pipeline. *Nucleic Acids Res.* **2019**, *47* (W1), W81–W87. https://doi.org/10.1093/nar/gkz310

(73) Medema, M. H.; Takano, E.; Breitling, R. Detecting sequence homology at the gene cluster level with MultiGeneBlast. *Mol. Biol. Evol.* **2013**, *30* (5), 1218–1223. https://doi.org/10.1093/molbev/mst025

(74) Kautsar, S. A.; Blin, K.; Shaw, S.; Navarro-Muñoz, J. C.; Terlouw, B. R.; van der Hooft, J. J. J.; van Santen, J. A.; Tracanna, V.; Suarez Duran, H. G.; Pascal Andreu, V.; Selem-Mojica, N.; Alanjary, M.; Robinson, S. L.; Lund, G.; Epstein, S. C.; Sisto, A. C.; Charkoudian, L. K.; Collemare, J.; Linington, R. G.; Weber, T.; Medema, M. H. MIBiG 2.0: a repository for biosynthetic gene clusters of known function. *Nucleic Acids Res.* **2020**, *48* (D1), D454–D458. https://doi.org/10.1093/nar/gkz882

(75) Altschul, S. F.; Gish, W.; Miller, W.; Myers, E. W.; Lipman, D. J. Basic local alignment search tool. *J. Mol. Biol.* **1990**, *215* (3), 403–410. https://doi.org/10.1016/S0022-2836(05)80360-2

(76) Majorov, K. B.; Nikonenko, B. V.; Ivanov, P. Yu.; Telegina, L. N.; Apt, A. S.; Velezheva, V. S. Structural modifications of 3-triazeneindoles and their increased activity against *Mycobacterium tuberculosis*. *Antibiotics* **2020**, *9* (6), 356. https://doi.org/10.3390/antibiotics9060356

(77) Mosmann, T. Rapid colorimetric assay for cellular growth and survival: application to proliferation and cytotoxicity assays. *J. Immunol. Meth.* **1983**, *65* (1/2), 55–63. https://doi.org/10.1016/0022-1759(83)90303-4

(78) Bhushan, R.; Brückner, H. Marfey's reagent for chiral amino acid analysis: A review. *Amino Acids* **2004**, *27* (3), 231–247. https://doi.org/10.1007/s00726-004-0118-0

(79) Schneider, T.; Gries, K.; Josten, M.; Wiedemann, I.; Pelzer, S.; Labischinski, H.; Sahl, H.-G. The lipopeptide antibiotic friulimicin B inhibits cell wall biosynthesis through complex formation with bactoprenol phosphate. *Antimicrob. Agents Chemother.* **2009**, *53* (4), 1610–1618. https://doi.org/10.1128/AAC.01040-08

(80) Montal, M.; Mueller, P. Formation of bimolecular membranes from lipid monolayers and a study of their electrical properties. *Proc. Natl. Acad. Sci. USA* **1972**, *69* (12), 3561–3566. https://doi.org/10.1073/pnas.69.12.3561

Supporting Information

Gausemycins A,B – cyclic lipoglycopeptides from *Streptomyces sp.*

Table of Contents:

Figure S1. Phylogenetic tree analysis *of Streptomyces* sp. INA-Ac-5812

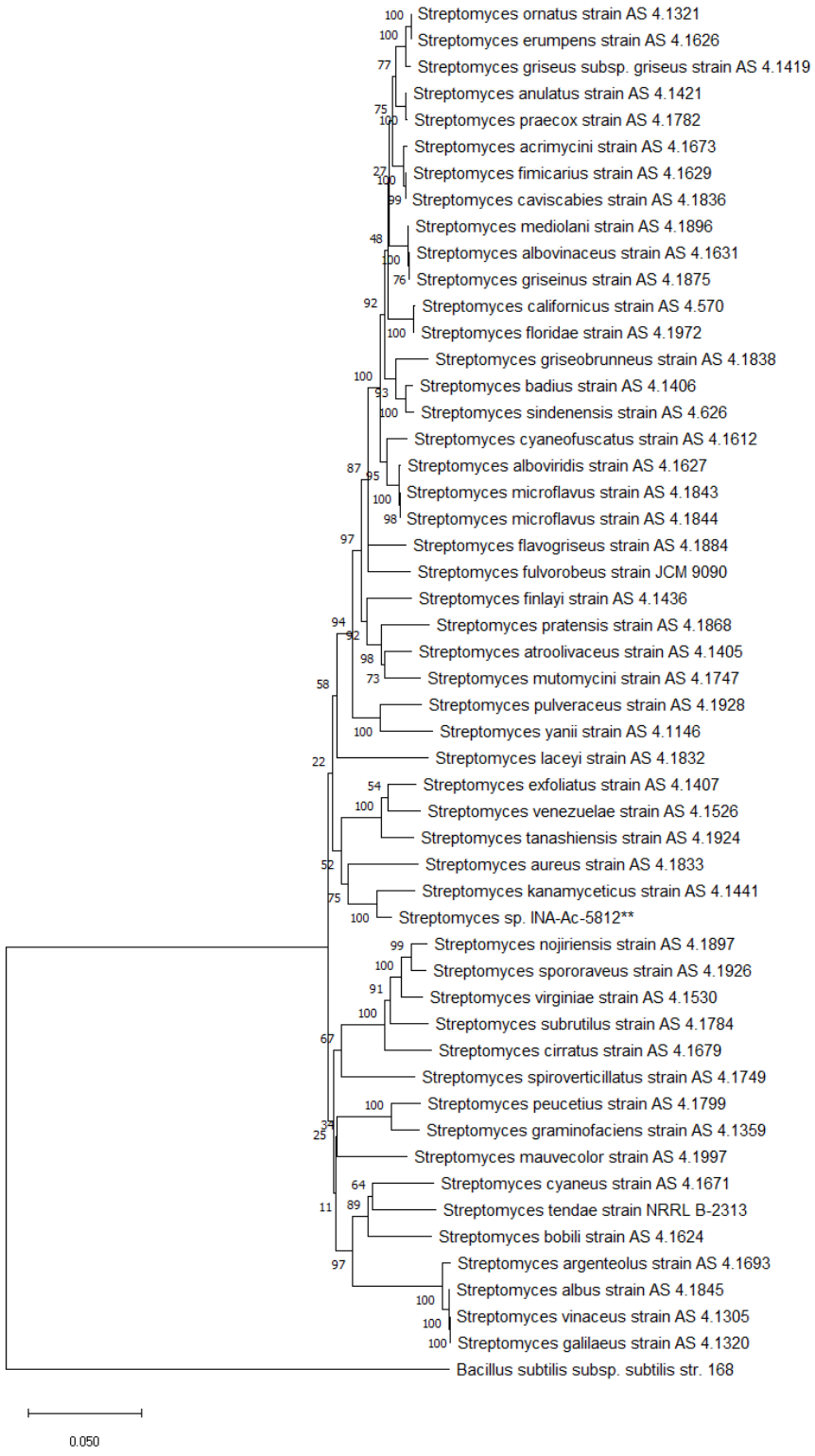

Back to Contents

The evolutionary history was inferred using the Neighbor-Joining method.[1] The optimal tree with the sum of branch length = 1.17934836 is shown. The percentage of replicate trees in which the associated taxa clustered together in the bootstrap test (500 replicates) are shown next to the branches.[2] The tree is drawn to scale, with branch lengths in the same units as those of the evolutionary distances used to infer the phylogenetic tree. The evolutionary distances were computed using the Maximum Composite Likelihood method[3] and are in the units of the number of base substitutions per site. This analysis involved 52 nucleotide sequences. All ambiguous positions were removed for each sequence pair (pairwise deletion option). There were a total of 6490 positions in the final dataset. Evolutionary analyses were conducted in MEGA X.[4]

Back to Contents

Figure S2. LCMS analysis of normal-phase HPTLC fractions

The antibiotic concentrate analyzed on HPTLC plates 10x20 cm (unmodified silica) and eluted with 1-propanol–water (7:2). The resulting fractions were washed of silica with 50% ethanol and analyzed via LCMS (ESI Ion Trap, method described in Experimental Section). The resulting spectra contained massed of doubly protonated ions of antibiotic components. For convenience, masses of the components were rounded to the whole numbers. Masses correspond to unprotonated molecules.

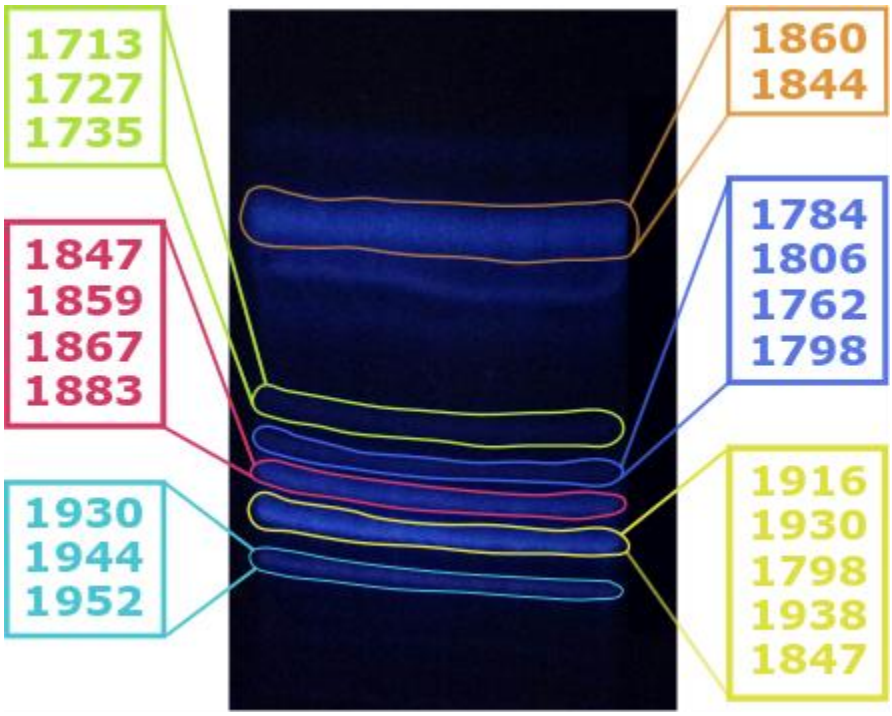

Back to Contents

Figure S3. LCMS analysis of ion-exchange fractions

Preparative ion exchange chromatography was performed on BIO-RAD analytical grade macroporous anion resin AG MP-1, 200–400 mesh, styrene type, strong quaternary ammonium, (0-25% buffer B (20 mM BisTris, pH 6.9, 50% EtOH + 1M LiCl) in buffer A (20mM BisTris in 50% EtOH, pH 6.9). Four collected fractions were analyzed by LCMS. The resulting spectra contained massed of doubly protonated ions of antibiotic components. For convenience, masses of the components were rounded to the whole numbers. Masses correspond to non-protonated molecules.

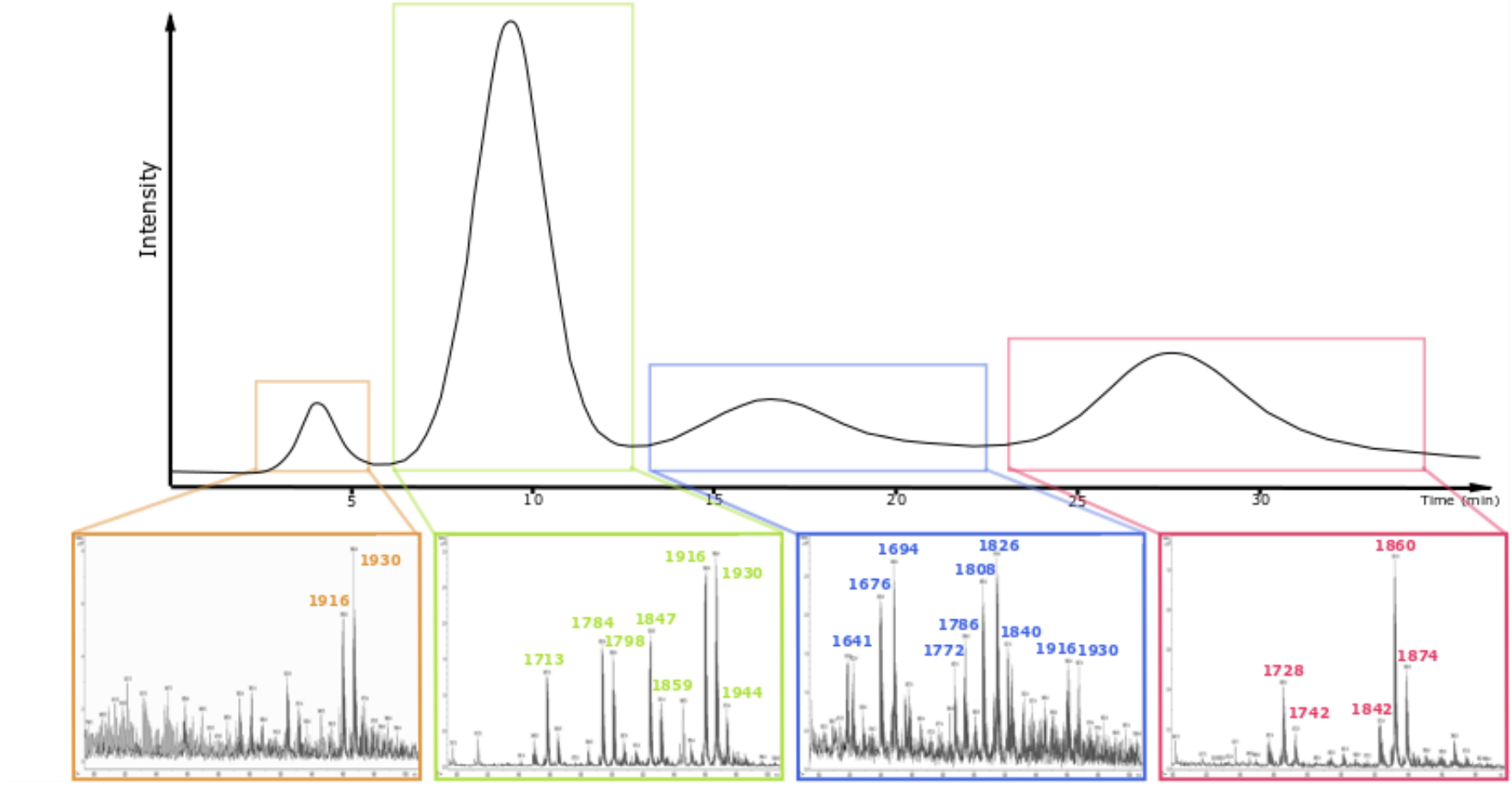

Back to Contents

Figure S4. LCMS analysis of C18-HPLC fractions

Antibiotic concentrate was analyzed by reversed-phase analytical method. Analytical C18 HPLC was performed on Sunfire column (C18; 5 µm, 4.6×250 mm), injection volume was 20 µL. Components were eluted as follows: linear gradient of eluent C (0.1% TFA, 25% PrOH, 74.9% CH_3CN (v/v)) in eluent D (0.1 % TFA in H_2O (v/v)) 36→42% for 25 min, 42→64% for 5 min, 64→35% for 5 min. Flow rate was 1 mL/min.. It was analyzed by LCMS (ESI, Ion Trap). The resulting spectra contained massed of doubly protonated ions of antibiotic components. For convenience, masses of the components were rounded to the whole numbers. Masses correspond to non-protonated molecules.

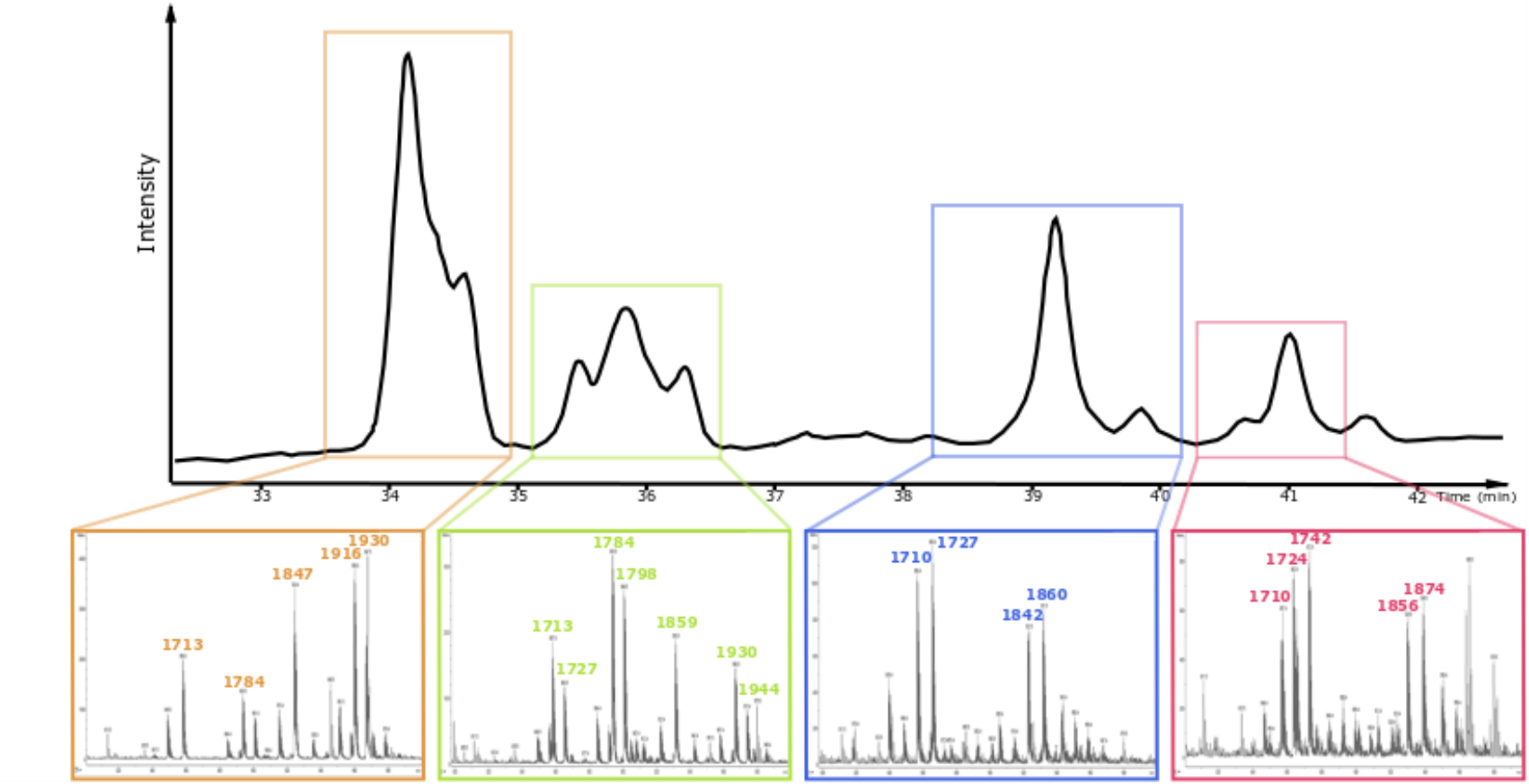

Back to Contents

Supplement S5. Gausemycins isolation scheme

Separation of closely related peptides and isolation of individual components proved to be quite challenging task. First purification scheme of gausemycins included initial liquid-liquid extraction of fermentation broth with butanol. After solvent evaporation, extract was treated with EtOAc to remove macrolide antifungal fraction. Low-weight impurities were removed with Sephadex G15 and high-weight hydrophobic impurities were removed with reversed-phase chromatography (C18), yielding antibiotic concentrate (Figure S5-1).

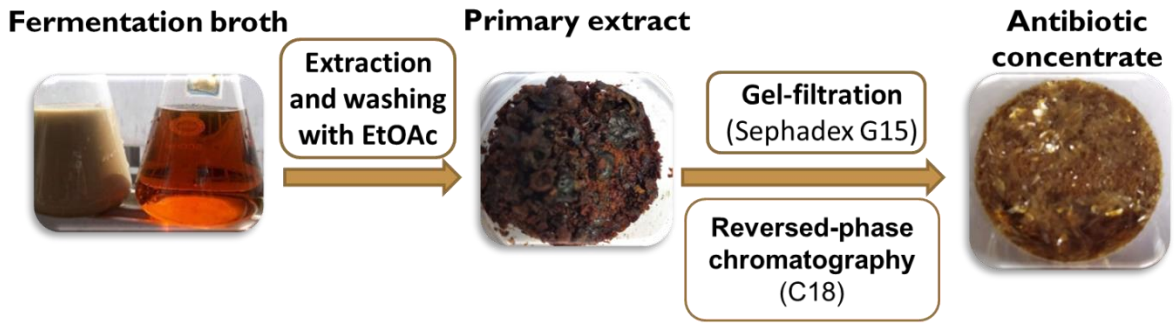

Figure S5-1. Initial gausemycins isolation scheme

This mixture was separated with ion-exchange preparative HPLC (Figure S3), second fraction was collected. This fraction contains first and second groups of peaks on reversed-phase C18 HPLC (see Figure S4). First group of peaks, containing gausemycin B as major compound, was separated with preparative C18 HPLC and then subjected to preparative HILIC HPLC, yielding two individual components – gausemycins A and B. These components were analyzed with analytical rp-HPLC (Figure S5-2). Since there was the only peak on chromatogram the substance was considered to be pure.

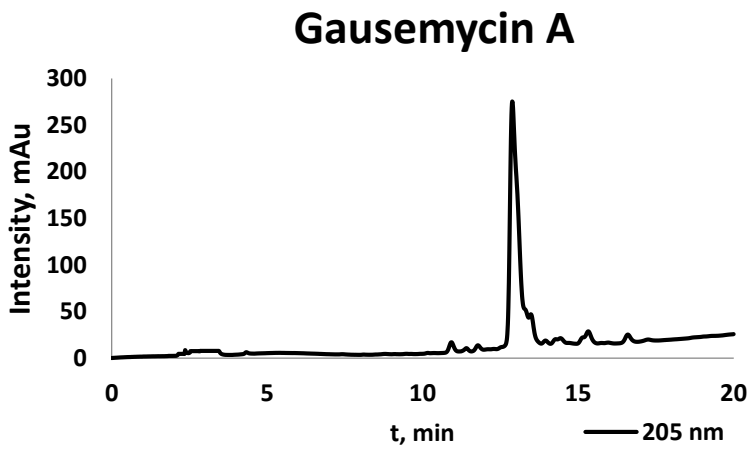

Back to Contents

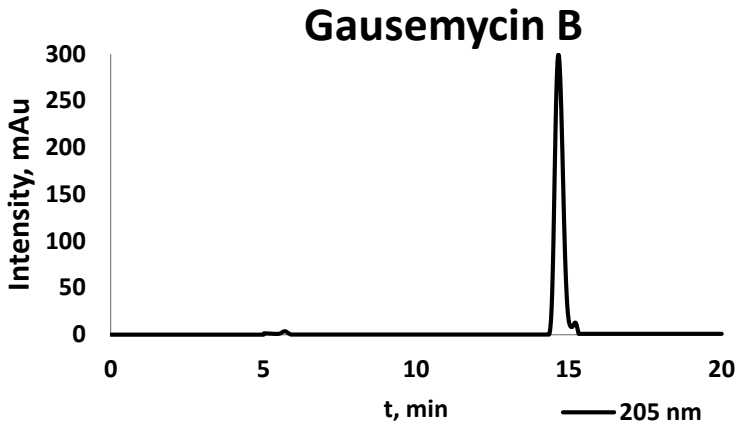

Figure S5-2. rp-HPLC traces of the purified gausemycins A and B

Antimicrobial activities of both components were analyzed and unexpectedly they were less active than after ion exchange chromatography. Mass-spectra revealed an ion with mass 556 Da (Figure S5-3).

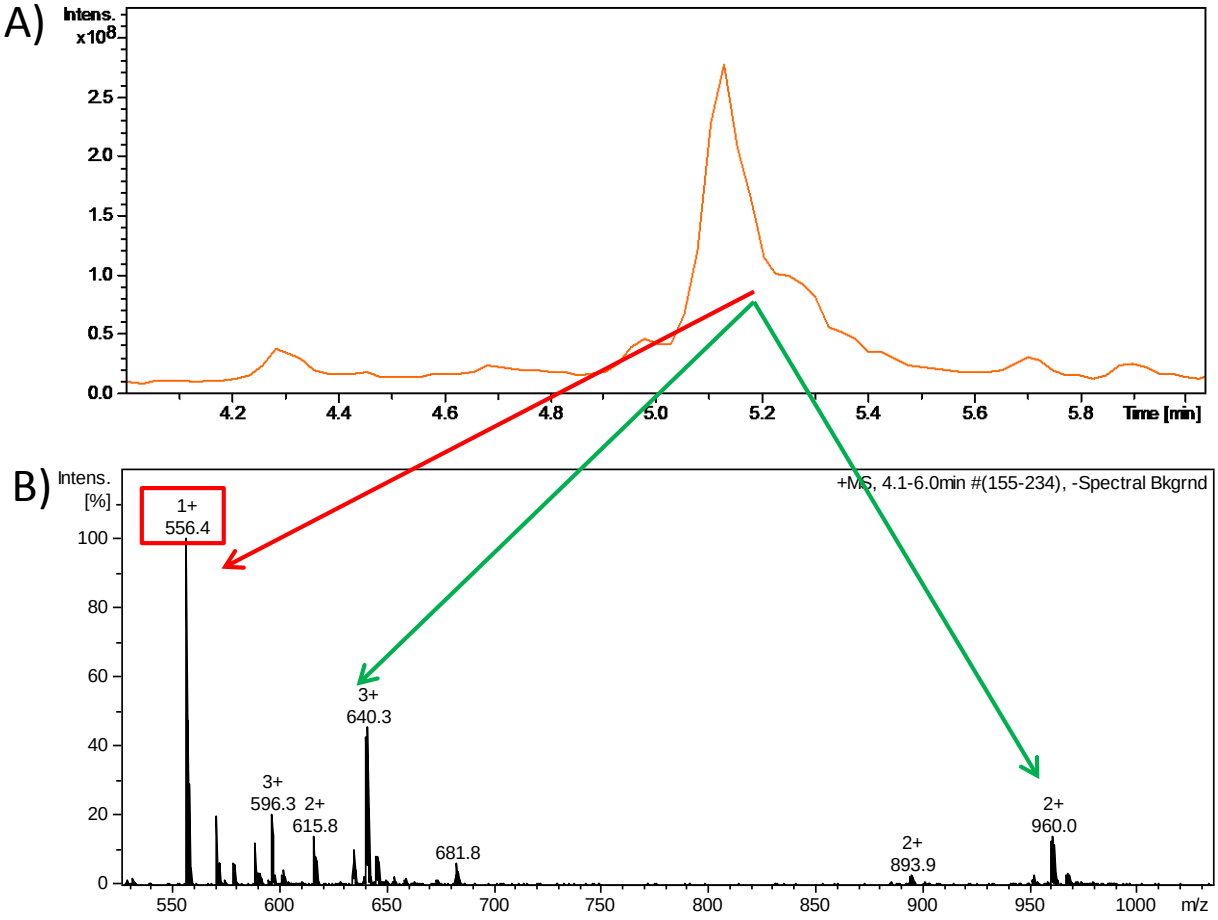

Figure S5-3. LCMS analysis of the gausemycin B, purified with HILIC HPLC: (A) total ion current chromatogram; (B) mass spectrum of the gausemycin B peak.

This ion was supposed to be fragmentary but also it could be impurity. Since the mass of the impurity is 3 times less than mass of gausemycins A and B, gel-filtration was selected for impurity removal. After gel-filtration, ion with mass 556 Da was not in mass-spectra (Figure S5-4) and antimicrobial activity was recovered.

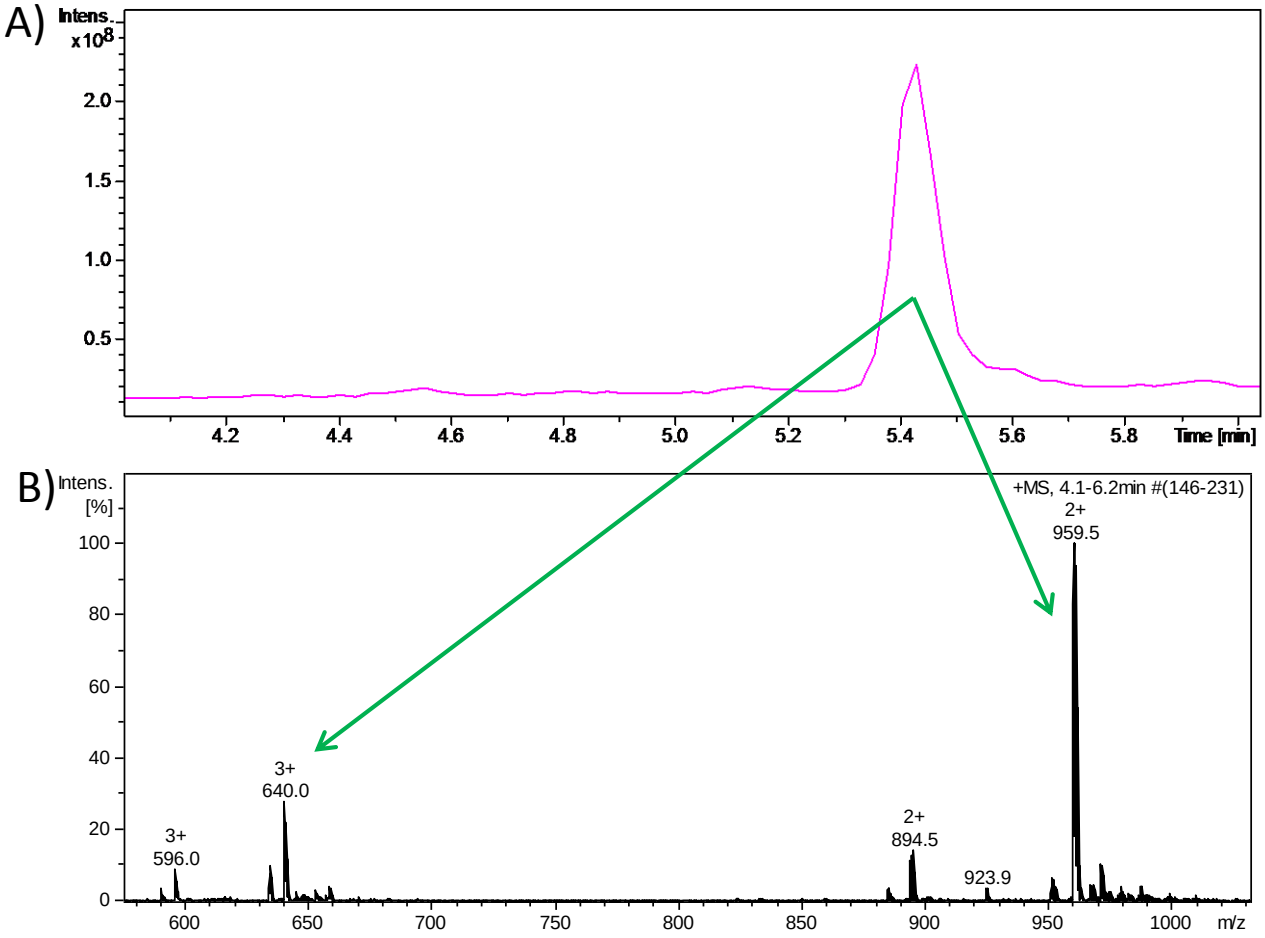

Figure S5-4. LCMS analysis of the gausemycin B, purified with HILIC HPLC and gel-filtration: (A) total ion current chromatogram; (B) mass spectrum of the gausemycin B peak.

In order to completely remove the impurity, stage of gel-filtration should be repeated several times. Therefore non-chromatographic method was required to decrease time spent on gel-filtration.

It was discovered that if antibiotic concentrate is dissolved in water with ammonia (pH 9) and then HCl is added until pH 5, dark brown precipitate is formed and solution gets pale yellow. It was found that antibiotic components were in a solution, while impurities, including the one with mass 556 Da, were in a precipitate (Figure S5-5). Substances from the solution were subjected to preparative HILIC HPLC like in previous method. This strategy (Figure S5-5) allowed to reduce the number of iterations of gel-filtration.

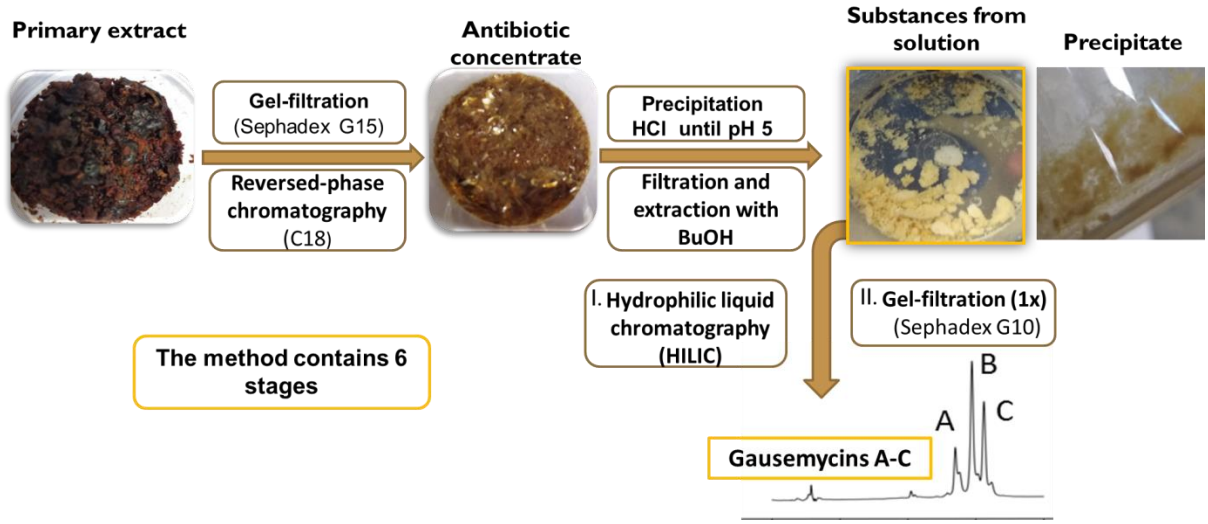

Figure S5-5. Optimized gausemycins isolation scheme

We also tried to find other techniques for individual components' isolation. It was found that sorbent LPS500-H is highly efficient in removal of most impurities with low and high molecular weight. Therefore primary extract was subjected to sorbent LPS500-H and after that, additional stage preparative reversed-phase C18 HPLC was applied, yielding mixture of gausemycins A and B fraction without hydrophobic impurities. These two stages are more effective than the stage with Sephadex G15 since they allow to remove all impurities from mixture and do not require any additional stages (Figure S5-6).

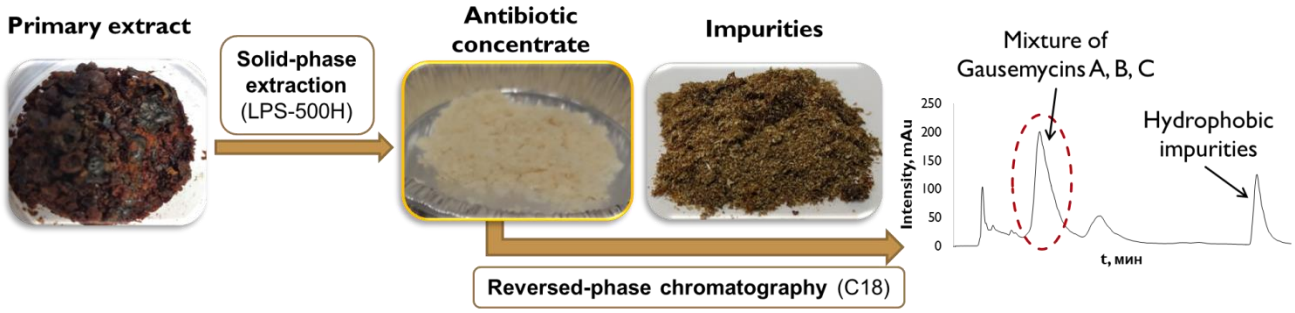

Figure S5-6. Solid-phase extraction for the gausemycin concentrate production.

It is also worth noting that the best separation quality, in case of hydrophilic interaction chromatography, was achieved with 25% of 1-propanol in liquid phase under isocratic elution (Figure S5-7). The main contamination of the samples of gausemycins A and B was the third component (C) of the mixture, the isolation and characterization of this compound will be reported in subsequent publication.

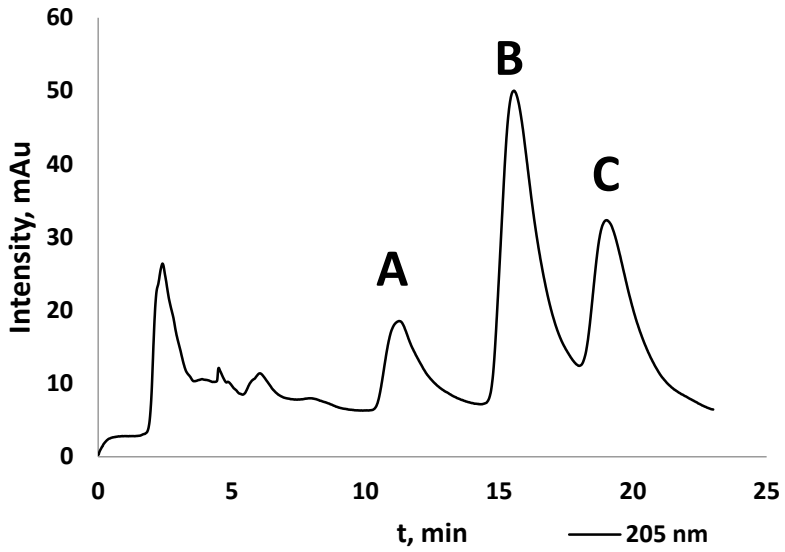

Figure S5-7. HILIC HPLC trace of the preparative separation of the main antibiotic components

Final purification scheme of gausemycins included initial liquid-liquid extraction of fermentation broth with butanol. After solvent evaporation, extract was treated with EtOAc to remove macrolide antifungal fraction. All impurities were removed with solid-phase extraction on sorbent LPS-500H and reversed phase chromatography. The resulting mixture was separated with preparative HILIC HPLC, yielding two individual components – gausemycins A and B.

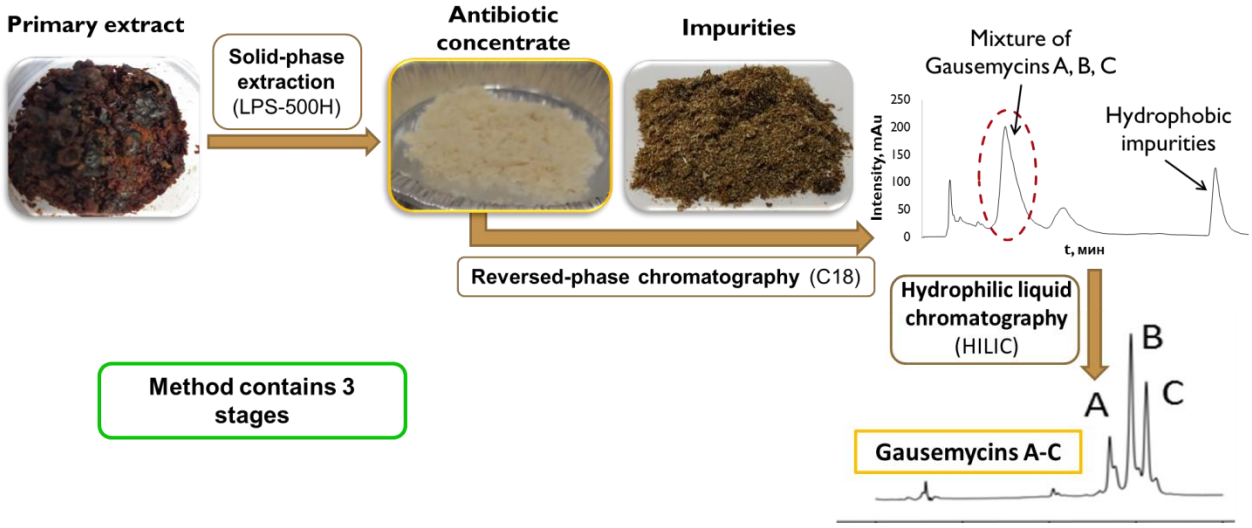

Figure S5-8. Final gausemycins isolation scheme

Back to Contents

Supplement S6. HRMS fragmentation of individual gausemycin B

Mass-spectrometry

Experiments were performed on FTICR MS Bruker Apex Ultra with harmonized cell equipped with a 7 T superconducting magnet and electrospray ion source (ESI). Prior to analysis, sample was diluted with water-methanol 1:1 mixture to 10 mg/L and then injected into the ESI source using a microliter pump at a flow rate of 90 μL/h with a nebulizer gas pressure of 138 kPa and a drying gas pressure of 103 kPa. A source heater was kept at 200ºC to ensure rapid desolvation in the ESI droplets. Broadband mass-spectra were first externally calibrated using LC MS Tunemix (Agilent) and then internally by spiking analyte with the calibration solution. Isolation and fragmentation of the ion of interest was performed by hexapole CID with the 10 m/z mass window. Narrowband mode was engaged for the analysis of isotopic fine structure if the ion of interest.

Data treatment

FTICR MS data treatment and identification of fragments and mass-differences were performed using DataAnalysis software (Bruker). Isotopic distribution was simulated using Xcalibur software (Thermo Fisher).

FTICR mass-spectrum of gausemycin B. Insets shows the assigned molecular composition and experimental mass error.

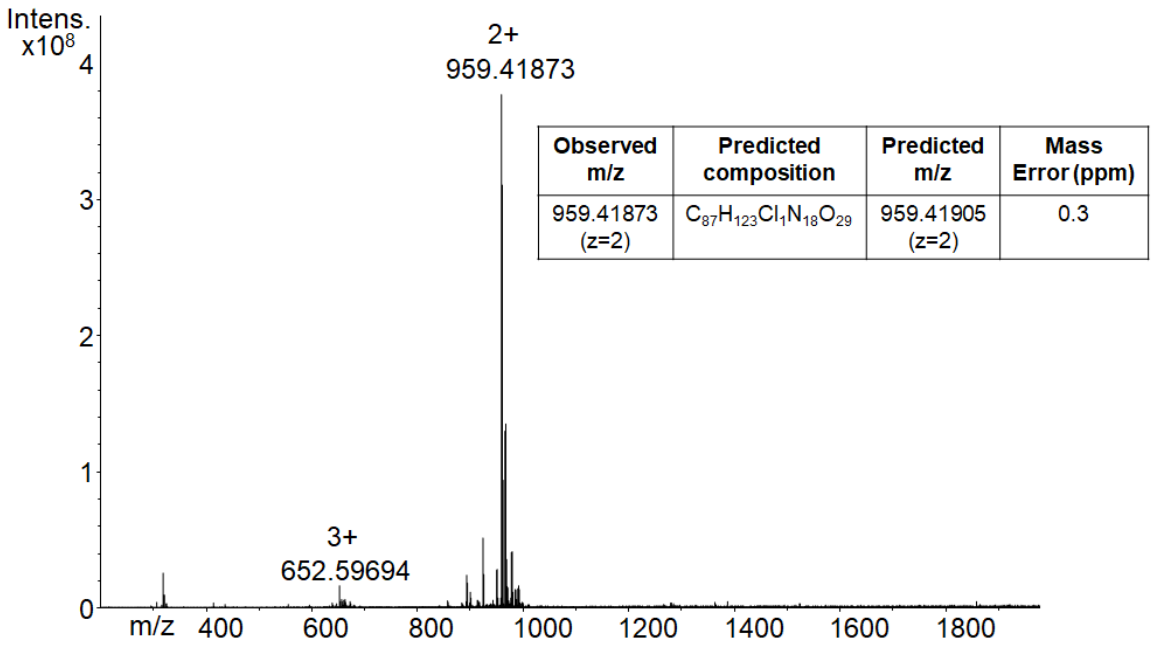

Observed m/z	Predicted composition	Predicted m/z	Mass Error (ppm)
959.41873 (z=2)	$C_{87}H_{123}Cl_1N_{18}O_{29}$	959.41905 (z=2)	0.3

The dominant peak in broadband mass-spectrum corresponded to double-charged ion with m/z=959.41873 (error 0.3 ppm). To prove the accuracy of formulae assignment, we acquired mass-spectrum in the narrow-band mode to obtain fine isotopic structure. The results are presented in Table 1. Experimental intensity distribution collaborated well with the theoretical distribution. This prove the molecular composition suggested for the gausemycin B.

Fine isotopic structure of gausemycin B ion

Composition	Mass	Minor isotope	Theor. intensity	Observed intensity
$C_{87}H_{121}ClN_{18}O_{29}$	959.41896	-	100	100
$C_{87}H_{121}Cl^{15}N_1N_{17}O_{29}$	959.91746	^{15}N	6.65	6.5
$C_{86}{}^{13}C_1H_{121}ClN_{18}O_{29}$	959.92069	^{13}C	94.10	98.8
$C_{87}H_{121}Cl^{15}N_2N_{16}O_{29}$	960.41634	$^{15}N_2$	0.21	1.4
$C_{87}H_{121}{}^{37}ClN_{18}O_{29}$	960.41753	^{37}Cl	31.96	28.5
$C_{86}{}^{13}C_1H_{121}Cl^{15}N_1N_{17}O_{29}$	960.41924	^{13}C, ^{15}N	6.26	5.4
$C_{87}H_{121}ClN_{18}O_{28}{}^{18}O_1$	960.42117	^{18}O	5.96	5.0
$C_{85}{}^{13}C_2H_{121}ClN_{18}O_{29}$	960.42240	$^{13}C_2$	43.76	41.3
$C_{87}H_{121}{}^{37}Cl^{15}N_1N_{17}O_{29}$	960.91595	^{37}Cl, ^{15}N	2.12	2.0
$C_{86}{}^{13}C_1H_{121}{}^{37}ClN_{18}O_{29}$	960.91917	^{37}Cl, ^{13}C	30.07	30.4
$C_{85}{}^{13}C_2H_{121}{}^{37}ClN_{18}O_{29}$	961.42085	^{37}Cl, $^{13}C_2$	13.99	11.9
$C_{84}{}^{13}C_3H_{121}{}^{37}ClN_{18}O_{29}$	961.92245	^{37}Cl, $^{13}C_3$	4.29	3.9

MS/MS technique of FTICR enables verification of compounds structure applying CID fragmentation of the parent ion with identification of amino-acid sequence and unusual substituents by the exact mass. Automated approach used in top-down proteomic couldn't be used due to the presence of novel structural moieties, cycle peptide in particular. The suggested fragmentation of gausemycin B is presented in figure below. Sites in peptide bonds, which undergo fragmentation by CID are highlighted by dash lines. Typical y-fragmentation pattern was expected. Fragmentation was performed in collisional-cell at different voltages as it is shown in Table 2. Almost the full structure can be verified by MS/MS experiment. At low energies separation of cyclic and linear moieties were detected. Elimination of carbohydrate fragment occurred at 10 eV. The fragmentation of cyclic moiety was observed only at high collision energy. A cleavage of the cycle may be facilitated by almost every peptide bond. We explored that majorly cycle cleaves by proline-alanine bond (y8-y1 in Fig. 2). Further identification of sequence by the exact mass of the fragment and the mass-difference enabled to prove the proposed structure.

Fragmentation of gausemycin B. A,B correspond to the molecule and its cycle fragment, respectively. c,d correspond to olefinic and carbohydrate fragment, respectively. Dash lines indicate y fragmentation sites during MS/MS.

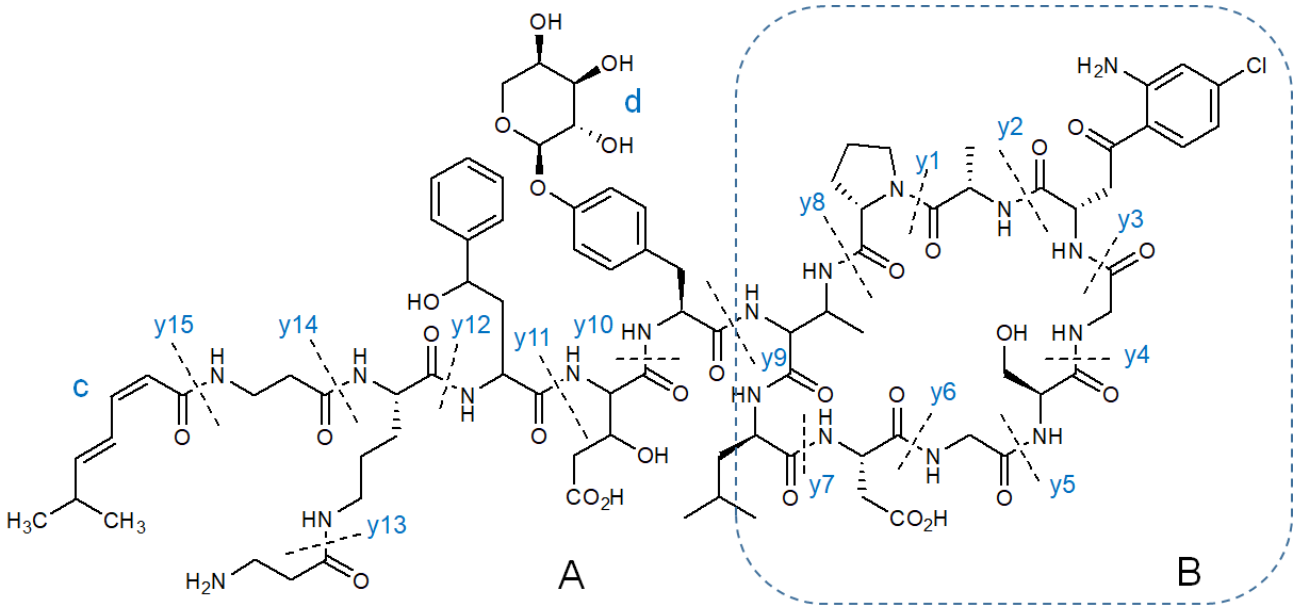

ESI-MS/MS data for compound B (m/z=959.41873 ion) fragmentation (CV = 10-40 eV) and structural assignment

Fragment ion mass, m/z	CV	Ion Formulae	Charge, z	Ion mapped, m/z	ΔM, Da	Lost fragment	Structural assignment
959.41814	0 eV	$C_{87}H_{123}Cl_1N_{18}O_{29}$	2				$A=[M+2H]^{2+}$
950.41295	10 eV		2	959.41818	18.01046	H_2O	$[A-H_2O]$

893.39710	10 eV		2	959.41818	132.04216	$C_5H_8O_4$	[A-d]
701.34925	25 eV	$C_{34}H_{49}N_6O_{10}$	1				[A-B-y10]
683.33940	25 eV	$C_{34}H_{47}N_6O_9$	1	701.34925	18.00985	H_2O	[A-B-y10-H_2O]
556.31265	25 eV	$C_{29}H_{42}N_5O_6$	1	683.33940	127.02675	$C_5H_5NO_3$	[A-B-y10-y11]
538.30171	25 eV	$C_{29}H_{40}N_5O_5$	1	556.31265	18.01094	H_2O	[A-B-y10-y11-H_2O]
379.23335	25 eV	$C_{19}H_{31}N_4O_4$	1	556.31265	177.07930	$C_{10}H_{11}NO_2$	[A-B-y10-y11-y12]
665.32861	30 eV	$C_{34}H_{45}N_6O_8$	1	683.33965	18.01104	H_2O	[A-B-y10-2H_2O]
308.19620	30 eV	$C_{16}H_{26}N_3O_3$	1	379.23339	71.03719	C_3H_5NO	[A-B-y10-y11-y12-y13]
1085.44421	30 eV	$C_{48}H_{66}Cl_1N_{12}O_{15}$	1	922.38131	163.06390	$C_9H_9NO_2$	[B+y10-d]
Fragmentation of cyclic peptide moiety							
922.38131	40 eV	$C_{39}H_{57}Cl_1N_{11}O_{13}$	1				B
904.37063	40 eV	$C_{39}H_{55}Cl_1N_{11}O_{12}$	1	922.38131	18.01068	H_2O	B-H_2O
851.34448	40 eV	$C_{36}H_{52}Cl_1N_{10}O_{12}$	1	922.38131	71.03683	C_3H_5NO	B-y1
627.30942	40 eV	$C_{26}H_{43}N_8O_{10}$	1	851.3448	224.07548	$C_{10}H_9ClN_2O_2$	B-y1-y2
570.28766	40 eV	$C_{24}H_{40}N_7O_9$	1	627.30942	57.02176	C_2H_3NO	B-y1-y2-y3
483.25553	40 eV	$C_{21}H_{35}N_6O_7$	1	570.28766	87.03213	$C_3H_5NO_2$	B-y1-y2-y3-y4
426.23418	40 eV	$C_{19}H_{32}N_5O_6$	1	483.25553	57.02135	C_2H_3NO	B-y1-y2-y3-y4-y5
382.24483	40 eV	$C_{18}H_{32}N_5O_4$		426.23418	43.98935	CO_2	B-y1-y2-y3-y4-y5-CO_2
311.20666	40 eV	$C_{15}H_{27}N_4O_3$	1	426.23418	115.02752	$C_4H_5NO_3$	B-y1-y2-y3-y4-y5-y6

Table S7. Marfey's derivatization of gausemycins hydrolysate

Amino acid	L isomer RT, min	D isomer RT, min	RT observed in gausemycin samples (averaged, corrected to internal standard), min
Ser	27.87	30.53	27.70
Asp	30.15	34.39	30.21
Gly	36.69		36.43
Ala	37.85	46.62	37.93
Pro	41.49	46.26	41.49
βAla	46.01		45.91
Orn	59.88	56.05	59.69
ClKyn	71.54	78.88	71.44
Leu	63.25	73.56	73.31
Tyr	76.53	81.62	76.93

In case of close retention times, additionally to LCMS analysis, experiments with addition of corresponding standard amino acid derivatives were performed to confirm the identity of the compounds.

Figure S8. 1D ^{1}H spectrum of gausemycin A

1D ^{1}H spectrum of gausemycin A (top). 45^{o}C, DMSO, 700MHz. Enlarged fragments with signal assignments are shown below. Signals of minor form are marked by red labels.

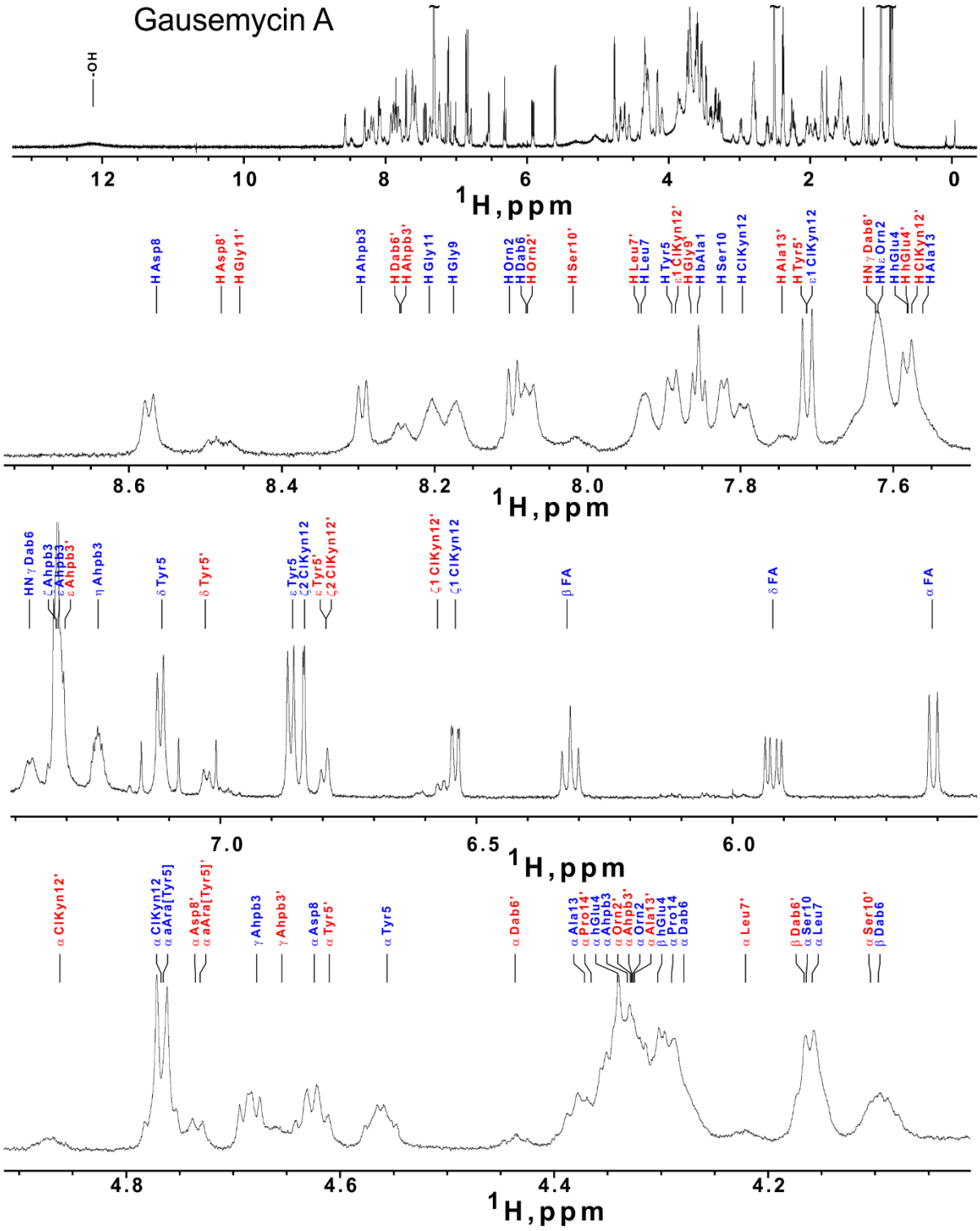

Gausemycin A

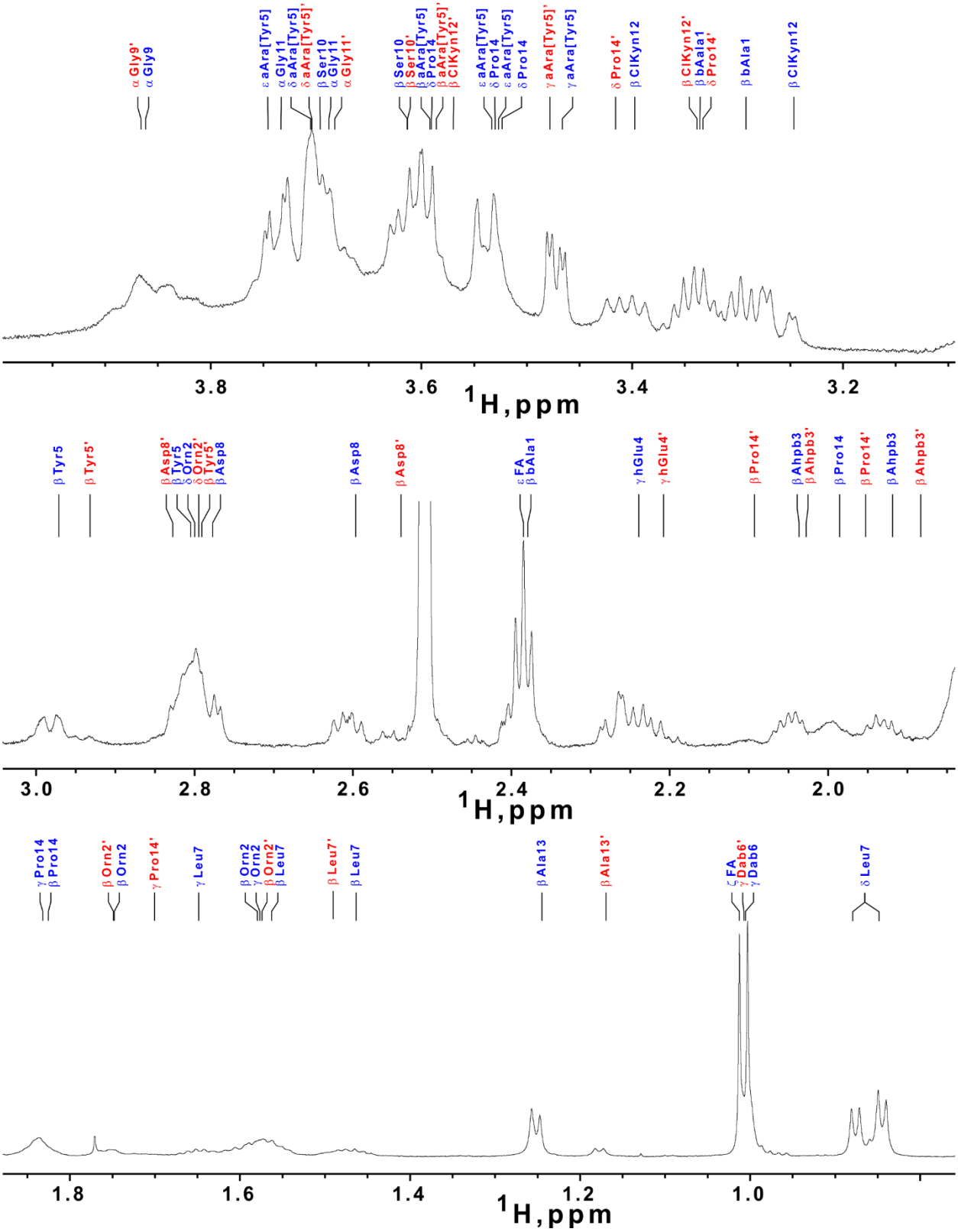

Back to Contents

Figure S9. 1D ^{1}H spectrum of gausemycin B

1D ^{1}H spectrum of gausemycin B (top). 45°C, DMSO, 700MHz. Enlarged fragments with signal assignments are shown below. Signals of minor form are marked by red labels.

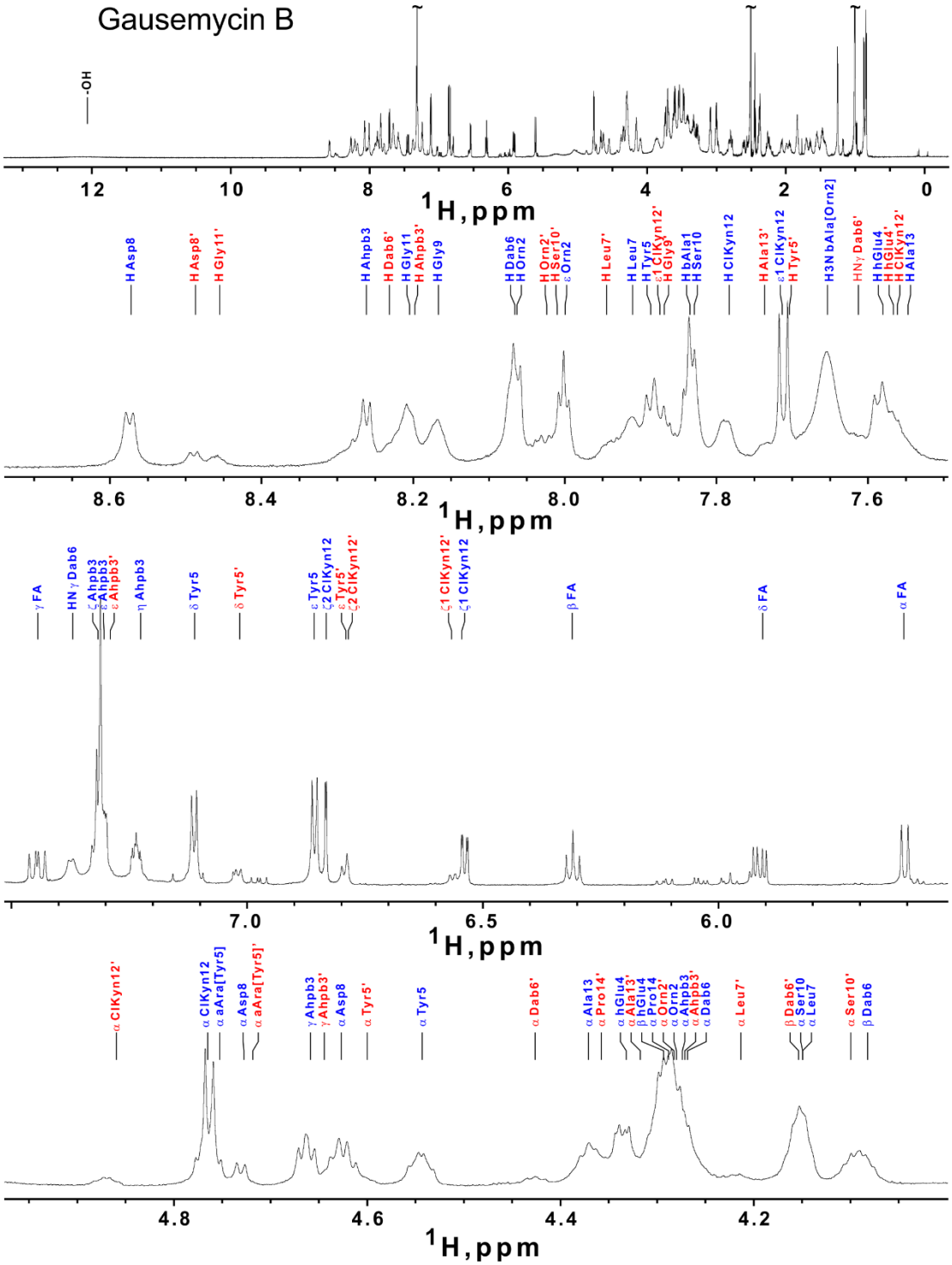

Back to Contents

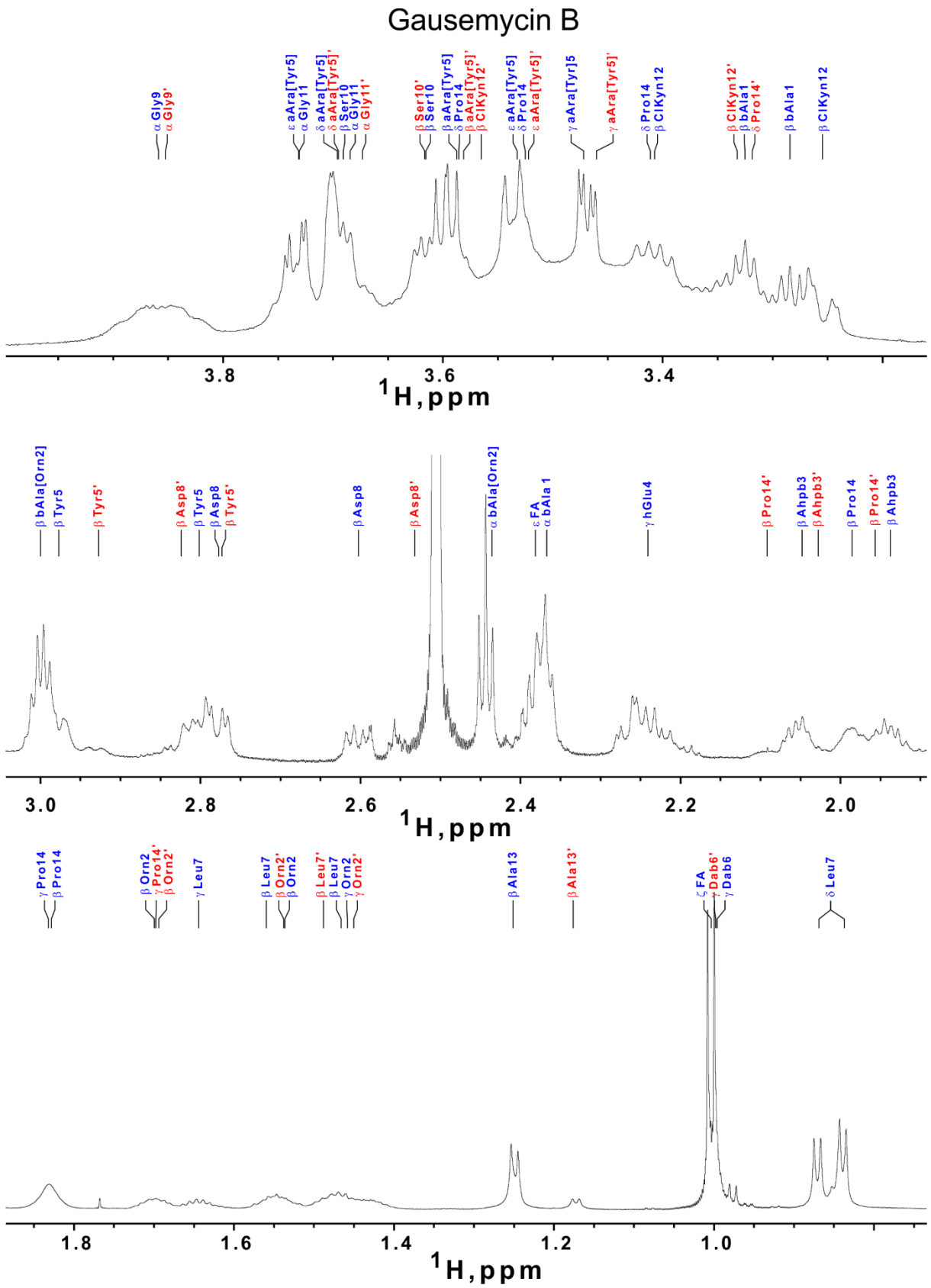

Back to Contents

Figure S10. 1D ^{13}C spectrum of gausemycin B

1D 13C spectrum of gausemycin B (top). 45°C, DMSO, 800MHz. Enlarged fragments with signal assignments are shown below. Signals of minor form are marked by red labels.

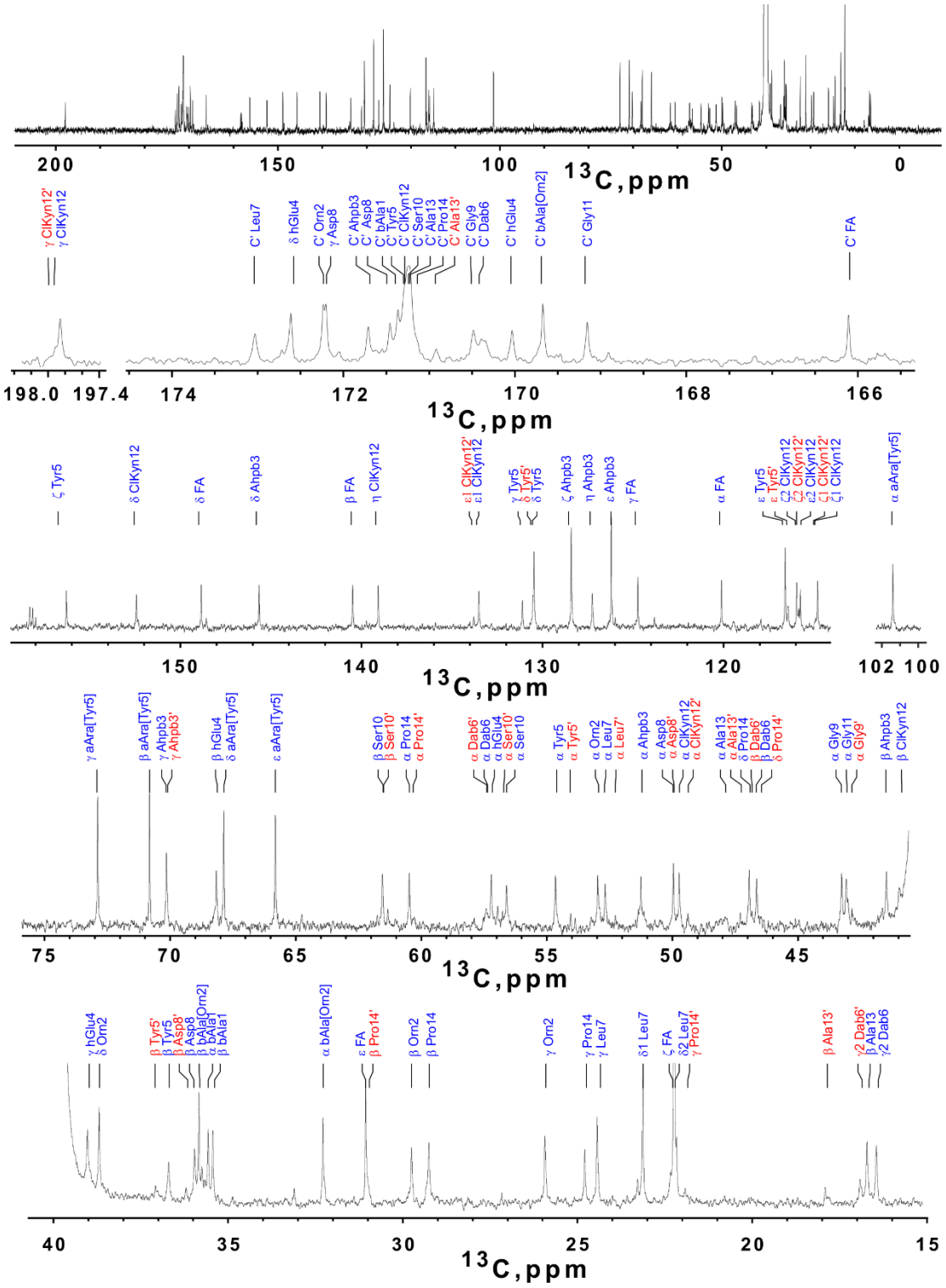

Back to Contents

Figure S11. 2D ^{13}C-HSQC spectrum of gausemycin B

2D ^{13}C-HSQC spectrum of gausemycin B (top). 45°C, DMSO, 800MHz. (1-3) Enlarged fragments with signal assignments. Signals of minor form are highlighted by red labels.

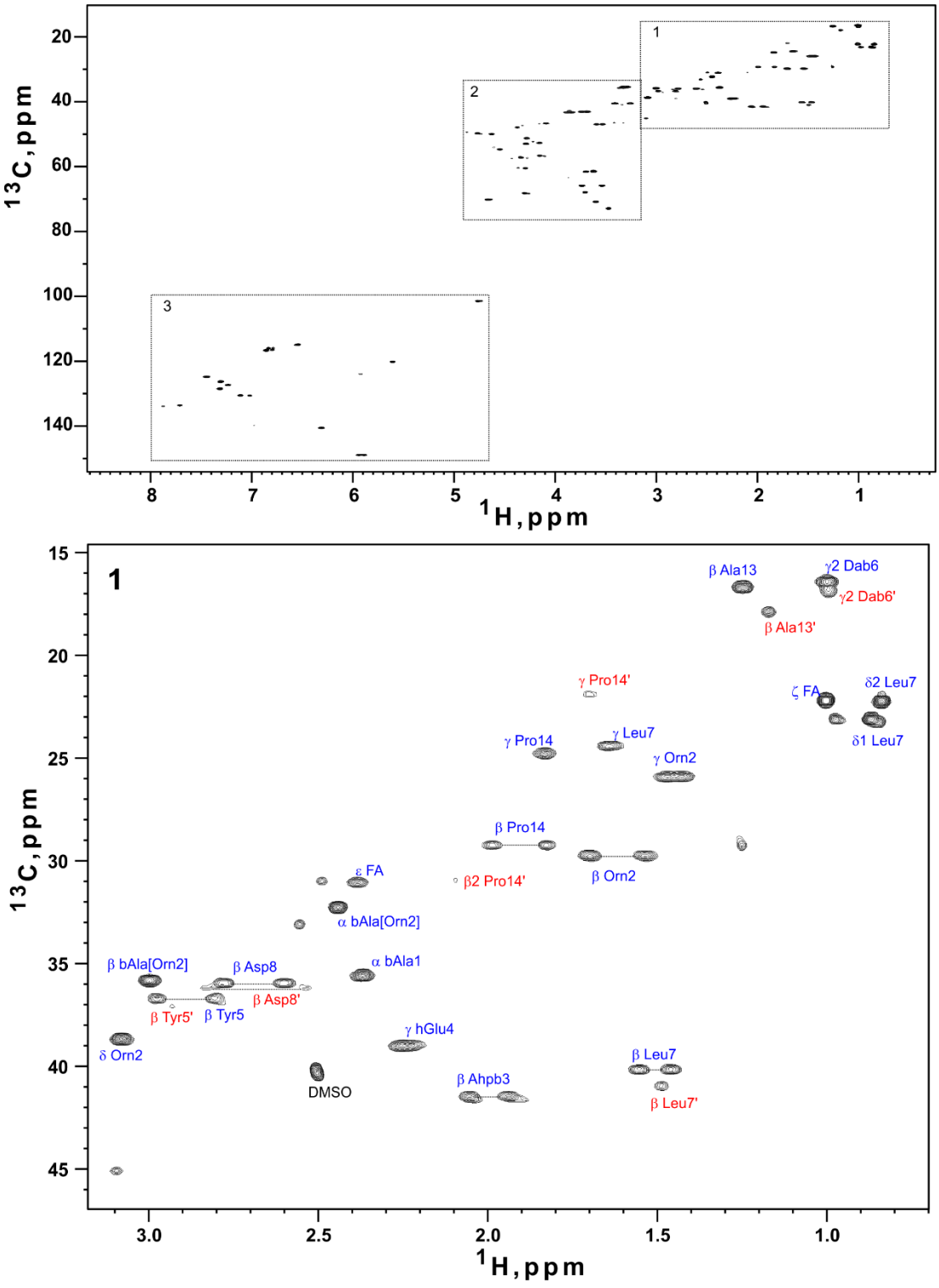

Back to Contents

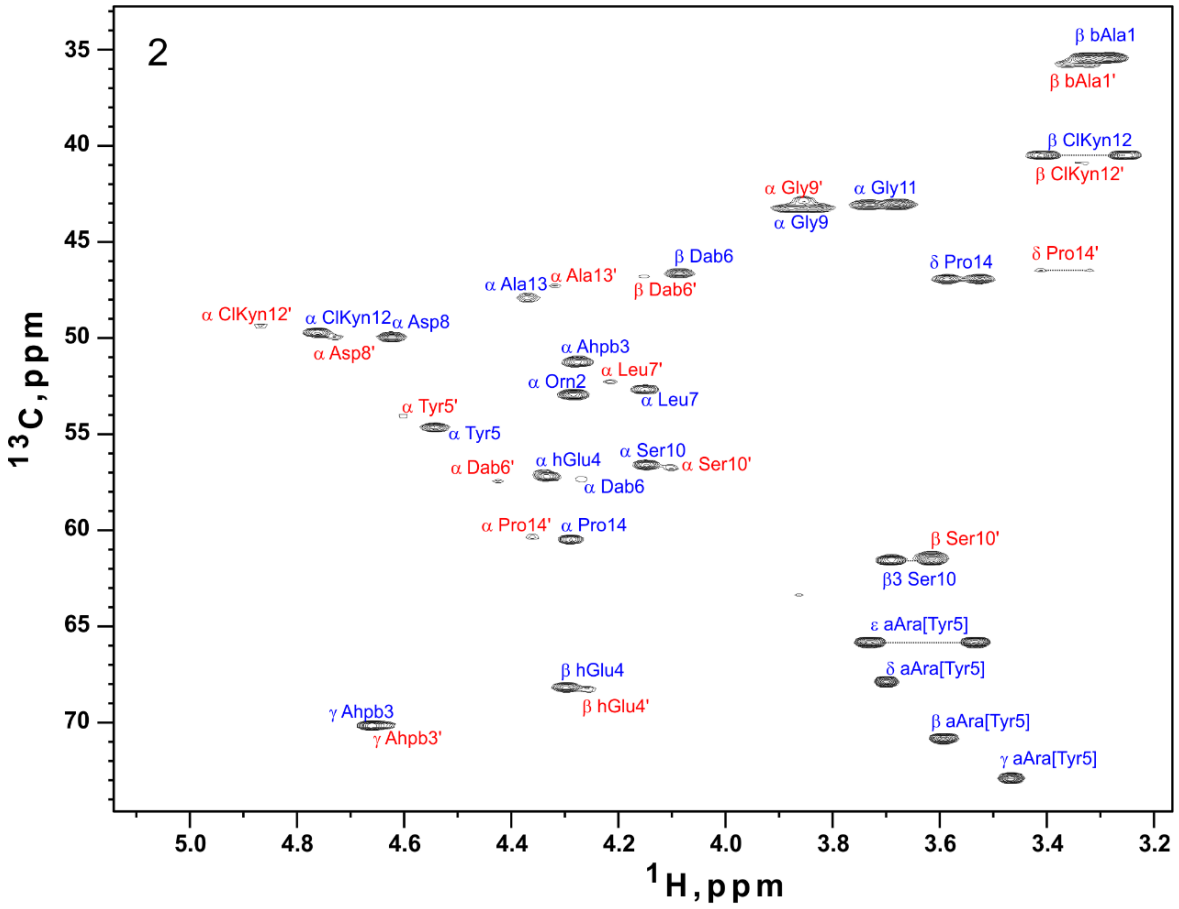

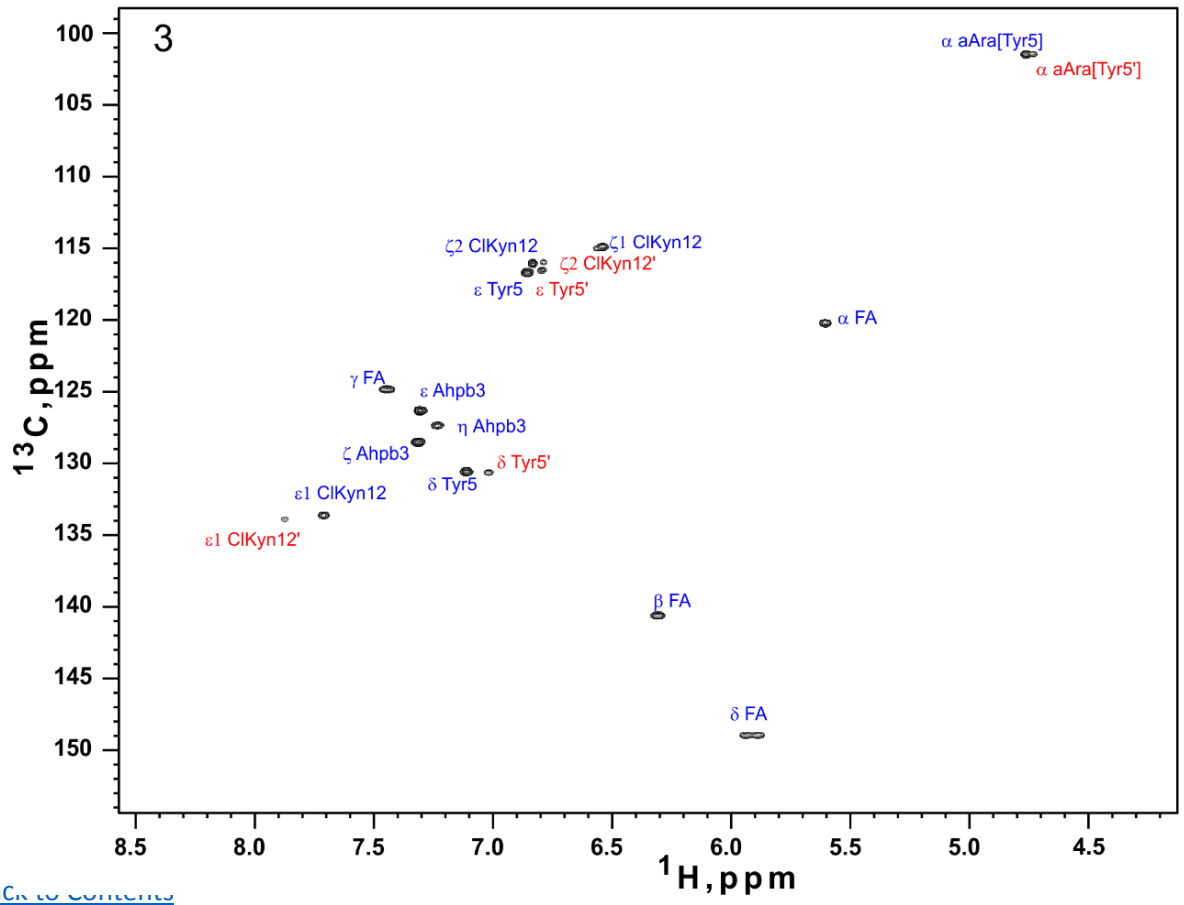

Back to contents

Table S12. Chemical shifts of gausemycin A and B observed in d_6-DMSO, 45℃

		gausemycin A				gausemycin B			
		major form ("trans")		minor form ("cis")		major form ("trans")		minor form ("cis")	
		δ_H	$\delta_C(\delta_N)$	δ_H	$\delta_C(\delta_N)$	δ_H	$\delta_C(\delta_N)$	δ_H	$\delta_C(\delta_N)$
bAla1	H^N	7.84	120.0	7.82	119.9	7.84	119.9	7.86	119.9
	α	2.37	35.6	—	—	2.37	35.6	2.37	—
	β	3.29/3.33	35.5	—	—	3.28/3.32	35.4	3.31/3.35	—
	C'		171.2		—		171.5		—
Orn2	H^N	8.09	121.9	8.07	121.8	8.06	122.8	8.03	122.6
	α	4.32	52.4	4.32	—	4.28	52.9	4.32	—
	β	1.57/1.74	29.3	1.57/1.74	—	1.53/1.70	29.7	1.54/1.69	—
	γ	1.57	24.0	—	—	1.42/1.47	25.9	1.45	—
	δ	2.80	39.0	2.79	—	3.08	38.7	3.08	—
	ε					8.00	118.7	—	—
	C'		171.7		—		172.3		—
Ahpb3	H^N	8.28	119.5	8.23	119.4	8.26	119.3	8.20	119.2
	α	4.32	51.3	4.32	—	4.27	51.2	4.27	—
	β	1.92/2.04	41.6	1.88/2.03	—	1.94/2.05	41.5	1.88/2.03	—
	γ	4.67	70.1	4.64	70.1	4.66	70.2	4.64	70.1
	δ		145.6		—		145.8		—
	ε	7.30	126.3	7.29	—	7.30	126.3	7.29	—
	ζ	7.31	128.5	—	—	7.32	128.5	—	—
	η	7.23	127.3	—	—	7.23	127.3	—	—
	C'		171.5		—		171.8		—
hGlu4	H^N	7.57	109.3	7.57	109.7	7.58	109.3	7.57	109.8
	α	4.33	57.1	—	—	4.33	57.2	—	—
	β	4.30	68.1	4.26	68.2	4.29	68.2	4.26	68.3
	γ	2.25	39.0	2.22	39.0	2.24	39.0	—	—
	δ		172.5		—		172.7		—
	C'		169.9				170.1		
Tyr5	H^N	7.88	117.9	7.70	116.7	7.89	118.0	7.70	116.7
	α	4.55	54.6	4.60	54.1	4.54	54.6	4.60	54.1
	β	2.80/2.97	36.8	2.79/2.93	37.0	2.80/2.98	36.7	2.77/2.93	37.1
	γ		131.0		—		131.2		—
	δ	7.10	130.5	7.02	130.6	7.11	130.5	7.02	130.6
	ε	6.85	116.6	6.78	116.4	6.86	116.7	6.79	116.5
	ζ		156.2		156.2		156.4		156.2
	C'		171.1		—		171.4		—
Dab6	H^N	8.07	113.4	8.23	114.2	8.07	113.4	8.23	114.2
	α	4.27	57.3	4.43	57.4	4.27	57.4	4.43	57.4
	β	4.09	46.7	4.15	46.8	4.08	46.7	4.15	46.8
	γ	0.99	16.5	1.00	16.9	0.99	16.4	0.99	16.8

	HN^{γ}	7.36	120.0	7.61	123.2	7.37	120.0	7.61	123.2
	C’		170.9		—		170.5		—
Leu7	H^N	7.92	121.8	7.92	121.0	7.91	121.8	7.94	121.0
	α	4.15	52.7	4.21	52.3	4.15	52.7	4.21	52.3
	β	1.46/1.56	40.2	1.49	40.9	1.46/1.56	40.2	1.49	40.9
	γ	1.64	24.5	—	—	1.64	24.3	—	—
	δ	0.84/0.87	22.3/23.3	—	—	0.84/0.87	22.1/23.1	—	—
	C’		172.9		—		173.1		—
Asp8	H^N	8.56	119.6	8.48	118.7	8.57	119.6	8.49	118.7
	α	4.61	50.0	4.73	49.9	4.63	50.0	4.73	49.9
	β	2.60/2.77	35.9	2.53/2.82	36.2	2.60/2.78	36.0	2.53/2.82	36.2
	γ		172.1		—		172.3		—
	C’		171.4		—		171.6		—
Gly9	H^N	8.16	106.6	7.85	104.6	8.17	106.6	7.87	104.6
	α	3.85	43.3	3.86	42.7	3.86	43.2	3.85	42.9
	C’		170.4		—		170.6		—
Ser10	H^N	7.81	113.3	8.01	113.9	7.83	113.3	8.01	113.9
	α	4.15	56.5	4.10	56.7	4.15	56.6	4.10	56.7
	β	3.61/3.69	61.5	3.61	61.5	3.61/3.69	61.5	3.61	61.5
	C’		171.1		—		171.3		—
Gly11	H^N	8.19	107.5	8.46	109.1	8.21	107.5	8.46	109.1
	α	3.68/3.72	43.1	3.67	—	3.68/3.73	43.0	3.67	—
	C’		169.0		—		169.3		—
ClKyn12	H^N	7.78	115.6	7.56	115.3	7.78	115.6	7.56	115.3
	α	4.76	49.7	4.86	49.4	4.77	49.7	4.86	49.4
	β	3.25/3.39	40.5	3.33/3.56	40.9	3.25/3.41	40.5	3.33/3.56	40.9
	γ		197.6		197.6		197.9		198.0
	δ		152.2		—		152.5		—
	ε_1	7.70	133.5	7.87	133.8	7.71	133.6	7.88	133.9
	ε_2		115.7		—		115.7		—
	ζ_1	6.53	114.8	6.56	114.9	6.54	114.9	6.55	115.0
	ζ_2	6.82	116.0	6.78	115.9	6.83	116.0	6.79	116.0
	η		139.1		—		139.2		—
	C’		171.1		—		171.4		—
Ala13	H^N	7.55	119.7	7.73	122.4	7.55	119.7	7.74	122.4
	α	4.36	47.9	4.32	47.3	4.37	47.9	4.32	47.3
	β	1.24	16.6	1.16	17.8	1.25	16.7	1.17	17.8
	C’		171.0		170.8		171.3		171.0
Pro14	α	4.28	60.5	4.36	60.3	4.29	60.5	4.36	60.3
	β	1.82/1.99	29.3	1.95/2.09	30.9	1.83/1.99	29.2	1.96/2.09	30.9
	γ	1.83	24.8	1.69	21.8	1.83	24.7	1.69	21.8
	δ	3.52/3.58	46.9	3.33/3.41	46.5	3.52/3.58	46.9	3.32/3.41	46.5
	C’		171.5				171.2		
FA	α	5.60	120.1			5.61	120.2		
	β	6.30	140.5			6.30	140.5		
	γ	7.44	124.8			7.44	124.9		

	δ	5.91	149.0			5.91	149.0		
	ε	2.38	31.1			2.38	31.0		
	ζ	1.00	22.2			1.00	22.2		
	C’		166.0				166.2		
αAra[Tyr5]	α	4.75	101.4	4.72	101.4	4.75	101.4	4.72	101.4
	β	3.59	70.8	3.58	—	3.59	70.8	3.58	—
	γ	3.46	72.9	3.46	—	3.47	72.9	3.46	—
	δ	3.69	67.9	3.69	—	3.69	67.9	3.69	—
	ε	3.53/3.73	65.8	3.52	—	3.53/3.73	65.8	3.52	—
bAla[Orn2]	α					2.44	32.3	—	—
	β					3.00	35.8	—	—
	C’						169.8		

Figure S13. 2D NOESY NMR spectrum of gausemycin A (Asp8 region)

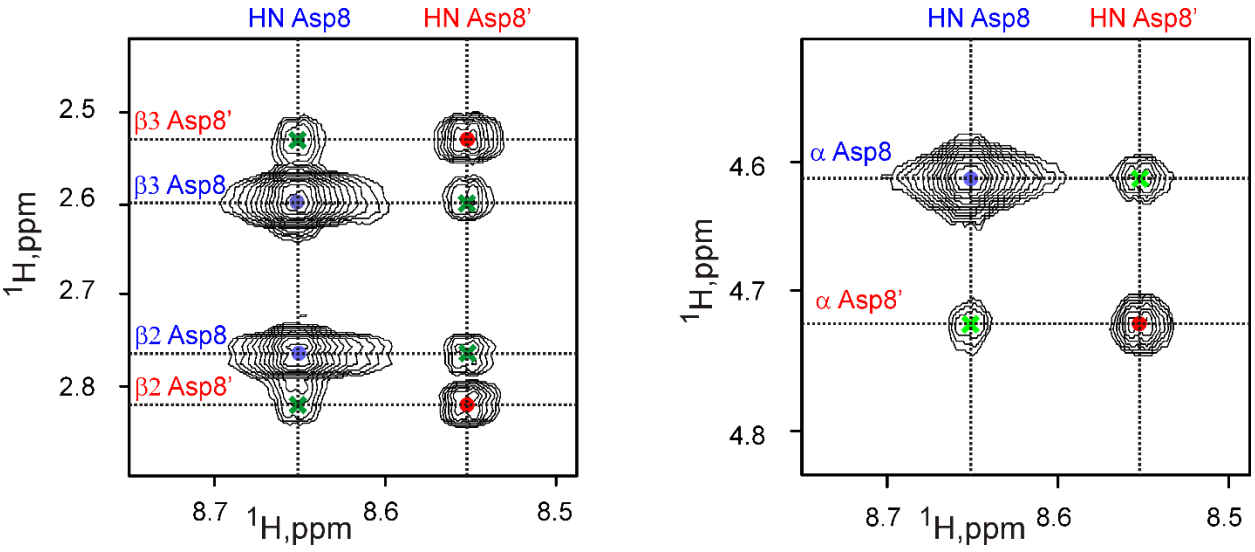

Exchange cross-peaks between two forms of gausemycin A in solution (NOESY 400 ms, DMSO-*d6*, 45°C). NOE contacts are shown by blue (major form) and red (minor form) dots. Green crosses denote exchange cross-peaks.

Figure S14. 2D NOESY NMR spectrum of gausemycin A (Dab6-Pro14 region)

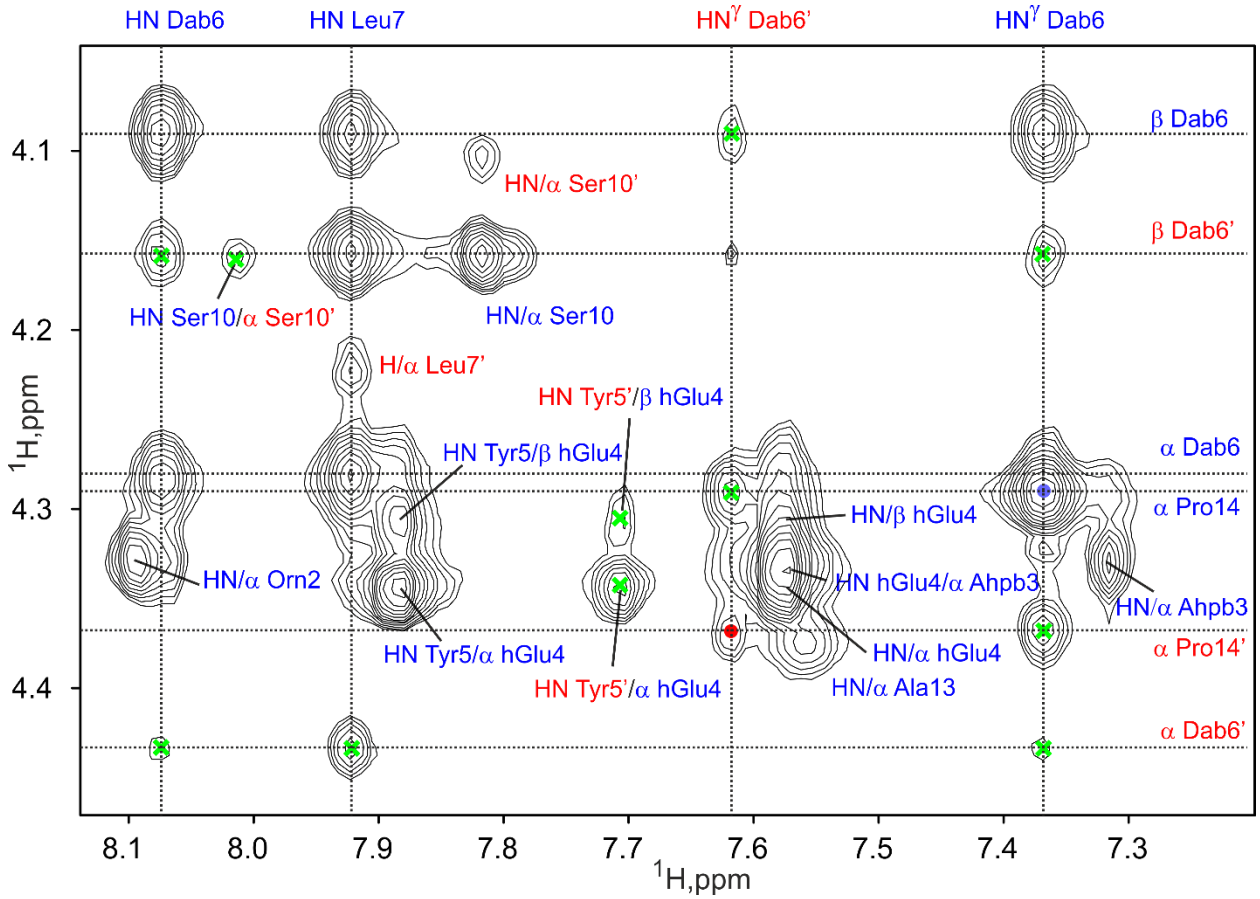

Fragments of 2D NOESY spectrum (τ_m = 400 ms, DMSO-*d6*, 45°C) of gausemycin A revealed cyclic nature of Dab6-Pro14 fragment. Contacts between Dab6 and Pro14 atoms are shown by blue (major form) and red (minor form) dots. Green crosses denote exchange cross-peaks between the major and minor forms. The signals of the major and minor forms (Ala13-Pro14 – *trans* and *cis*) are labeled by blue and red, respectively.

Figure S15. Identification of hGlu4 spin system

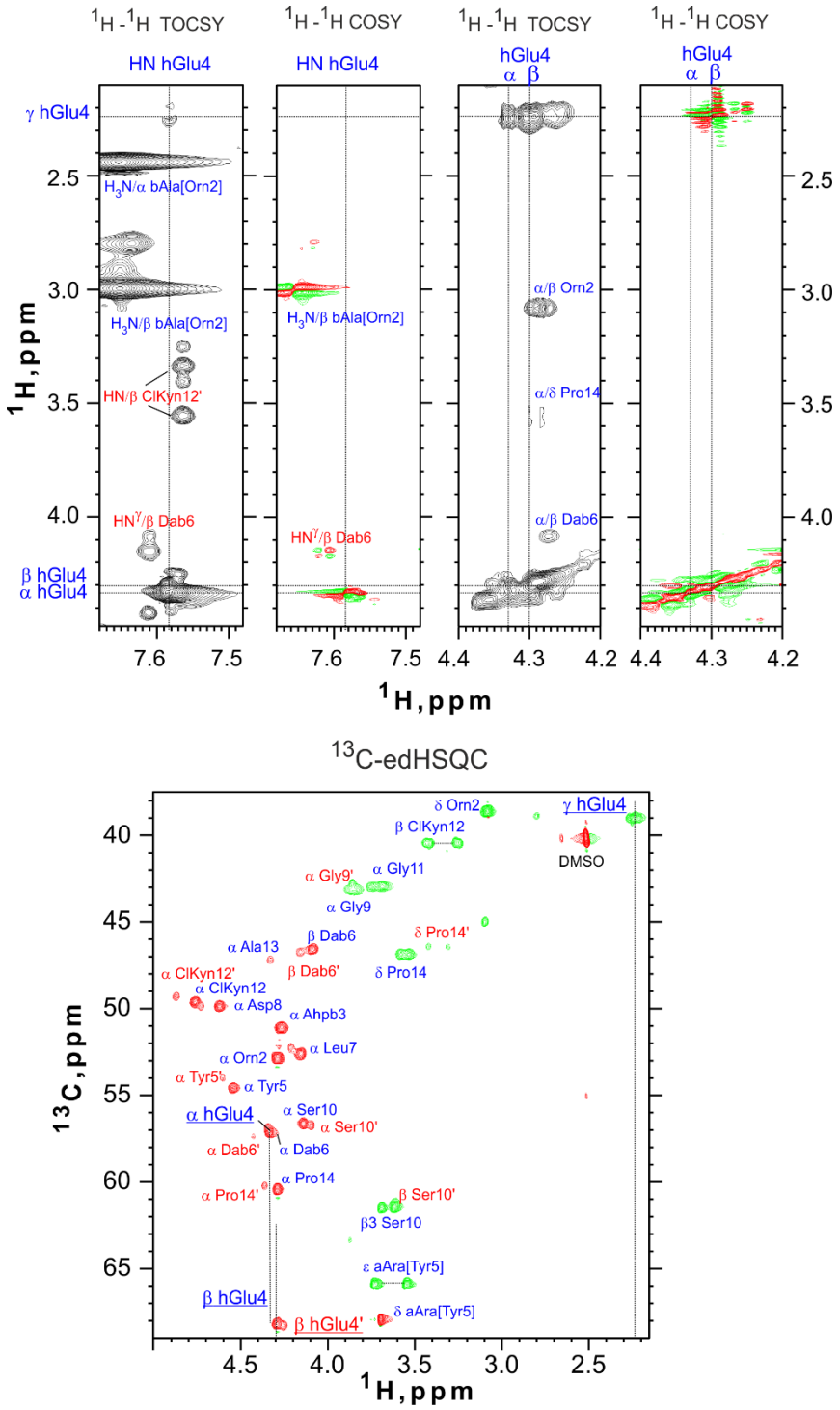

Fragments of 2D TOCSY, COSY and ^{13}C-edHSQC spectra (45°C, DMSO, 800MHz) of gausemycin B confirmed attachment of hydroxyl group to the β-position of the hydroxy-Glu4 residue. Signals with different signs are showed by red and green, respectively. In ^{13}C-edHSQC the signals of CH_2- groups are green, and the signals of CH- and CH_3- groups are red.

Back to Contents

Figure S16. The ^{1}H vicinal coupling constants of arabinose, ^{13}C-NMBC and NOESY cross-peaks between arabinose and Tyr5 signals in gausemycin A

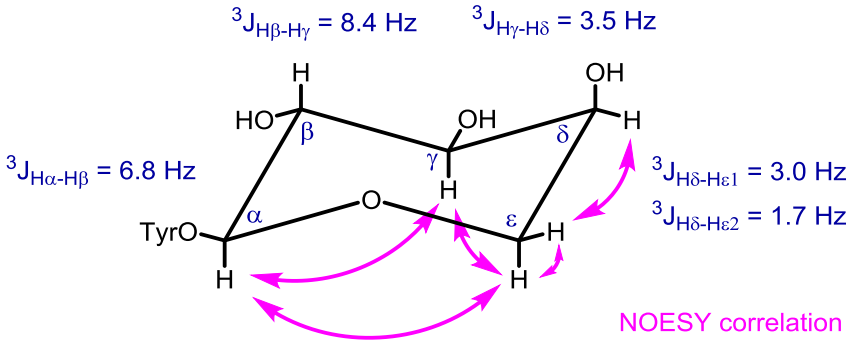

NOESY correlations and vicinal coupling constants of the sugar moiety allowed to identify this sugar as α-arabinopyranose.

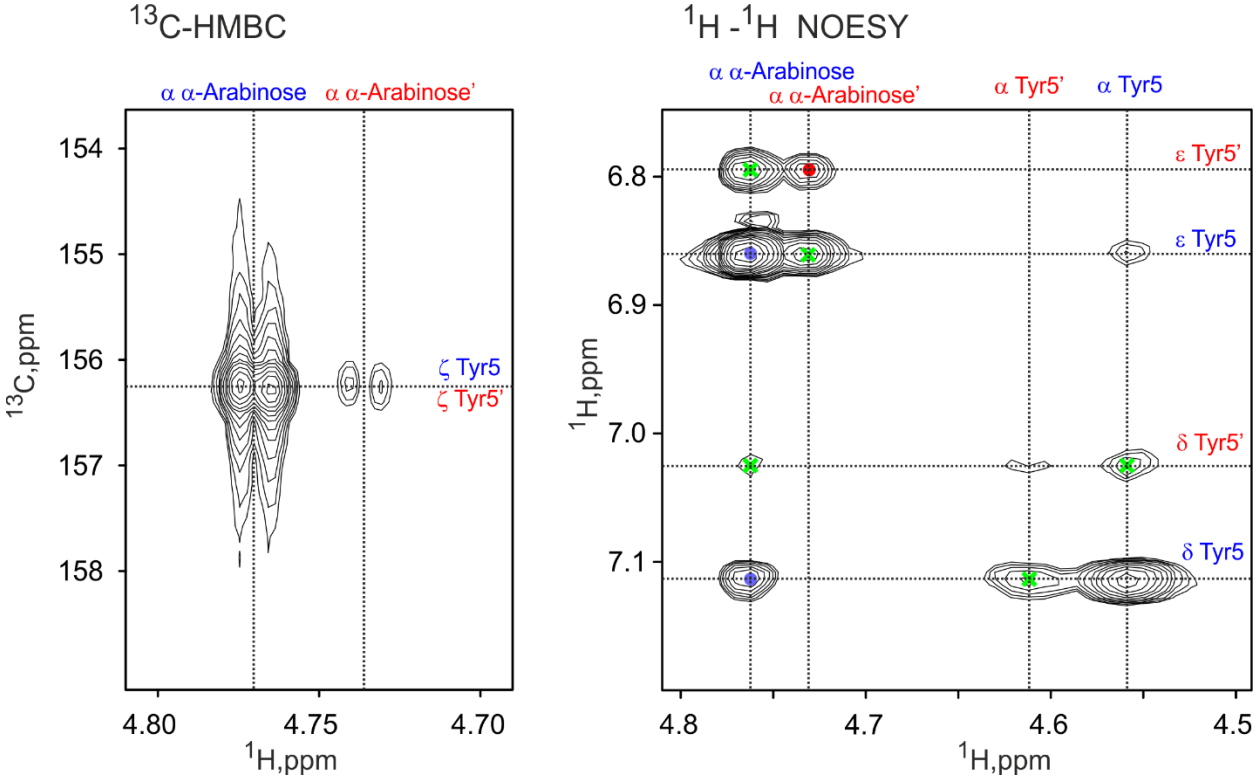

The cross-peaks in 2D ^{13}C-HMBC and NOESY (400 ms) spectra of gausemycin A revealed linkage between α -arabinose group and Tyr5 side chain.

Figure S17. The ^{13}C-HMBC, TOCSY and NOESY cross-peaks between Orn2 and side chain bAla in gausemycin B

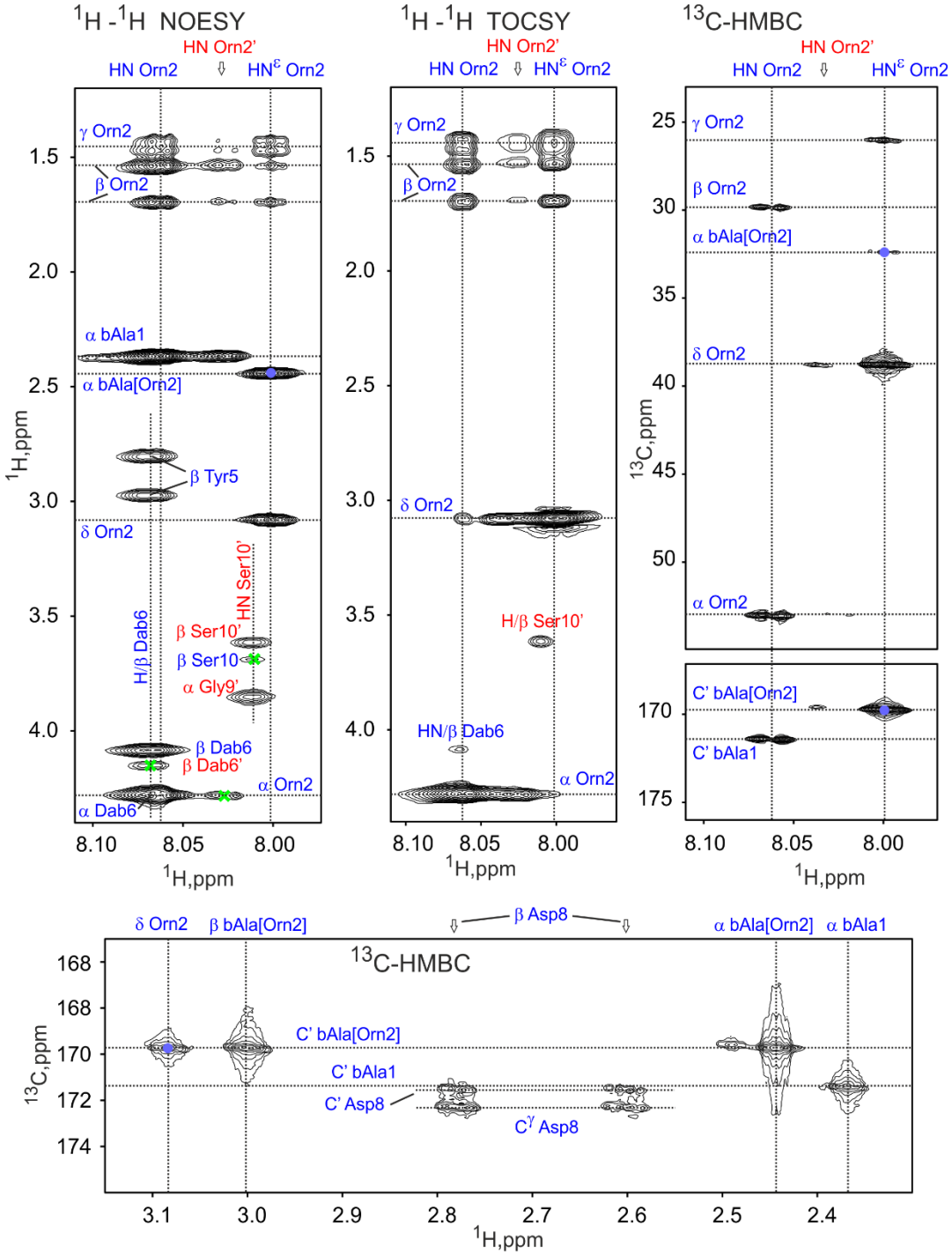

The fragments of NOESY (400 ms), TOCSY and ^{13}C HMBC spectra of gausemycin B revealed the additional β-alanine residue linked to amide group in Orn2 side chain. The contacts between Orn2 and bAla[Orn2] are shown by blue dots.

Table S18. Statistics of input data used for CYANA structure calculation of cyclic fragment (Tyr5-Pro14) and full-length peptide unit of gausemycin A

Distance and Angle restraints	**Tyr5-Pro14**	**Full-length**
Total NOE contacts	88	106
intraresidual	23	33
sequential (|i-j|=1)	29	41
medium-range (1<|i-j|≤4)	14	12
long-range (|i-j|>4)	22	23
Torsion angle restraints	11	16
Angle φ	8	9
Angle χ1	2	4
Angle ψ	1	3
Total restraints/per residue:	99/9.9	122/8.7

Table S19. Statistics for the best CYANA structures of the cyclic (Tyr5-Pro14) fragment of gausemycin A with different absolute configurations of asymmetric centers (Cα and Cβ) in Dab6 residue

Statistics for calculated structures	C^{α} – L(S) C^{β} – D(R)	C^{α} – L(S) C^{β} – L(S)	C^{α} – D(R) C^{β} – L(S)	C^{α} – D(R) C^{β} – D(R)
Structures calculated/selected	100/10			
Mean CYANA target function ($Å^2$)	0.70±0.02	1.82±0.17	1.61±0.10	1.45±0.03
Violations of restraints				
Distance (>0.2 Å)	6	13	11	10
Distance (>0.5 Å)	0	4	2	2
Dihedral angles (>5 °)	0	0	1	1
RMSD (Å)				
Backbone	0.16±0.12	0.41±0.06	1.14±0.29	0.81±0.09
Heavy atoms	0.85±0.24	1.17±0.42	2.09±0.62	1.60±0.24

Table S20. CYANA target function values (mean ± s.d., Å^2) in the sets of full-length gausemycin A structures with different absolute configurations of asymmetric centers in Ahpb3 (Cα and Cγ) and hGlu4 (Cα and Cβ) residues.

In each case, 100 structures were calculated and best 10 of them were selected for analysis.

Configuration Ahpb3 \ hGlu4	LS	LR	DS	DR
LS	1.82±0.57	1.76±0.61	1.46±0.57	1.67±0.37
LR	1.93±0.60	1.98±0.69	2.06±0.73	1.99±0.46
DS	2.08±0.68	2.61±0.53	2.58±0.42	2.26±0.76
DR	2.23±0.61	2.36±0.72	2.52±0.81	2.64±0.41

Table S21. RMSD of backbone atoms (mean ± s.d., Å) in the sets of full-length gausemycin A structures with different absolute configurations of asymmetric centers in Ahpb3 (Cα and Cγ) and hGlu4 (Cα and Cβ) residues

In each case, 100 structures were calculated and best 10 of them were selected for analysis.

Configuration Ahpb3 \ hGlu4	LS	LR	DS	DR
LS	0.87±0.24	0.86±0.14	0.87±0.06	0.88±0.18
LR	0.96±0.31	1.01±0.12	1.00±0.18	1.07±0.19
DS	0.98±0.12	0.92±0.17	1.02±0.19	0.80±0.19
DR	0.93±0.21	0.92±0.08	0.97±0.25	1.13±0.14

Table S22. Homologous NRPS clusters

Homologous clusters from the MiBiG, compared with MultiGeneBlast with putative gausemycin BGC

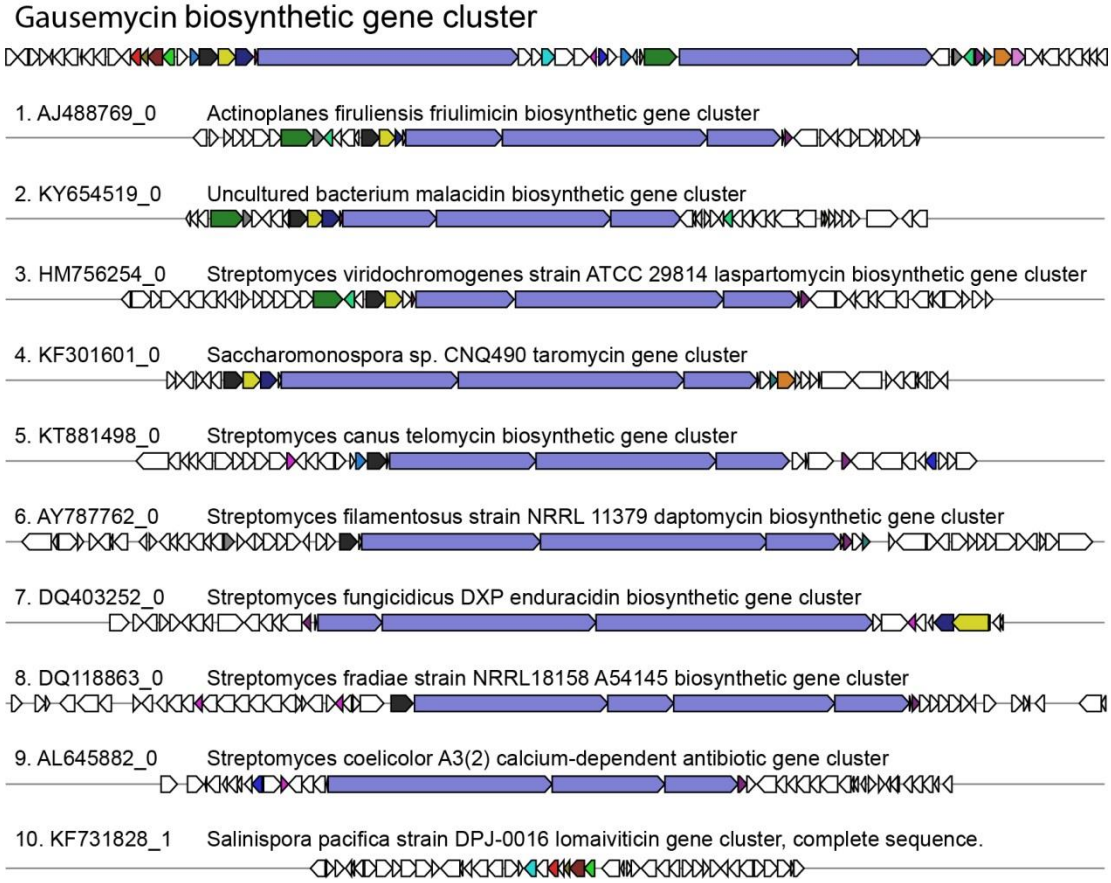

Table S23. Gausemycin biosynthetic gene cluster analysis

ORF	Gene size (bp)	Gene Name	Proposed Function	Protein [Organism], Corresponding to Gene with Sequence Similarity	NCBI Gene Bank Accession Number	E-value	Protein ID%
1	1215	orf1		calcineurin [Streptomyces sp. NRRL S-920]	**WP_051820272.1**	0.0	88.89
2	1050	orf2	UDP-Ara biosynthesis	alcohol dehydrogenase catalytic domain-containing protein [Streptomyces sp. NRRL S-920]	WP_030793214.1	0.0	88.22
3	921	orf3		hypothetical protein [Streptomyces sp. HST28]	WP_127909017.1	3,00E-89	75.16
4	933	orf4		Ku protein [Streptomyces sp. HST28]	WP_127909018.1	0.0	91.14
5	327	orf5		hypothetical protein [Streptomyces]	WP_030793208.1	9,00E-66	94.44
6	1014	orf6	Ahpb biosynthesis	SDR family oxidoreductase [Streptomyces sp. WAC 01529]	WP_125518190.1	3,00E-171	84.47
7	1185	orf7	UDP-Ara biosynthesis	Zn-dependent alcohol dehydrogenase [Streptomyces sp. NRRL S-920]	WP_030793202.1	0.0	97.46
8	174	orf8		CsbD family protein [Streptomyces sp. HmicA12]	WP_018532571.1	5,00E-26	91.23
9	984	orf9		hypothetical protein [Streptomyces sp. HST28]	WP_127910615.1	0.0	82.01
10	972	orf10	UDP-Ara biosynthesis	SDR family oxidoreductase [Streptomyces sp. SPMA113]	WP_069869837.1	0.0	90.09
11	1164	orf11		acyl-CoA dehydrogenase [Streptomyces]	WP_069869838.1	0.0	90.44
12	927	orf12		hypothetical protein [Streptomyces malaysiensis]	WP_142881337.1	6,00E-173	84.23

13	1035	orf13	Ahpb biosynthesis	MULTISPECIES: isocitrate/isopropylmalate dehydrogenase family protein [Streptomyces]	WP_103537994.1	0.0	96.77
				3-isopropylmalate dehydrogenase [Nostoc punctiforme]	WP_012409012.1	3,00E-39	33.63
14	606	orf14	Ahpb biosynthesis	MULTISPECIES: 3-isopropylmalate dehydratase small subunit [Streptomyces]	WP_103537993.1	2,00E-134	95.00
				homoaconitate hydratase family protein [Nostoc punctiforme]	WP_012409013.1	5,00E-09	35.45
15	1395	orf15	Ahpb biosynthesis	MULTISPECIES: 3-isopropylmalate dehydratase large subunit [Streptomyces]	WP_103537992.1	0.0	96.55
				homoaconitate hydratase family protein [Nostoc punctiforme]	WP_012409013.1	3,00E-65	32.77
16	1185	orf16	Ahpb biosynthesis	MULTISPECIES: pyruvate carboxyltransferase [Streptomyces]	WP_103537991.1	0.0	95.43
				2-benzylmalate synthase HphA [Nostoc punctiforme]	WP_012409019.1	5,00E-19	26.29
17	1056	orf17	glycosylation	MULTISPECIES: glycosyltransferase family 2 protein [Streptomyces]	WP_103537990.1	0.0	94.87
18	903	orf18	regulatory	winged helix-turn-helix transcriptional regulator [Streptomyces sp. SPMA113]	WP_107474662.1	0.0	88.67
19	1815	orf19	Precursor biosynthesis	MULTISPECIES: fatty acyl-AMP ligase [Streptomyces]	WP_103538012.1	0.0	94.83
20	1707	orf20	Precursor biosynthesis	MULTISPECIES: acyl-CoA dehydrogenase [Streptomyces]	WP_103537988.1	0.0	93.82

21	1746	orf21	Precursor biosynthesis	MULTISPECIES: acyl-CoA dehydrogenase [Streptomyces]	WP_103537987.1	0.0	94.85
22	264	orf22	Precursor biosynthesis	MULTISPECIES: hypothetical protein [Streptomyces]	WP_103537986.1	9,00E-47	87.36
23	25344	GauA	Scaffold biosynthesis, X - hydrophilic - X - X - tyr - X	non-ribosomal peptide synthetase [Streptomyces malaysiensis]	WP_099015585.1	0.0	85.75
24	1287	orf24	Pro hydroxylation (monooxygenation)?	MULTISPECIES: cytochrome P450 [Streptomyces]	WP_103537799.1	0.0	97.20
25	957	orf25	Hydroxylation of Glu	TauD/TfdA family dioxygenase [Streptomyces malaysiensis]	WP_099015587.1	0.0	89.31
26	1182	orf26	tyrosine aminotransferase	pyridoxal phosphate-dependent aminotransferase [Streptomyces malaysiensis]	WP_099015588.1	0.0	89.82
27	1923	orf27	transport	MULTISPECIES: ABC transporter ATP-binding protein [Streptomyces]	WP_103537802.1	0.0	96.72
28	1455	GauE	Scaffold biosynthesis, X	hypothetical protein [Streptomyces sp. SPMA113]	WP_069869853.1	0.0	87.92
29	660	orf29	regulatory	MULTISPECIES: response regulator transcription factor [Streptomyces]	WP_079153535.1	6,00E-136	93.12
30	960	orf30	transport	MULTISPECIES: ABC transporter ATP-binding protein [Streptomyces]	WP_103537806.1	0.0	98.75
31	804	orf31	transport	MULTISPECIES: ABC transporter permease [Streptomyces]	WP_103537807.1	2,00E-178	95.51
32	1002	orf32	regulatory	MULTISPECIES: winged helix-turn-helix transcriptional regulator [Streptomyces]	WP_069869855.1	0.0	86.75

33	510	orf33	aromatic halogenation	flavin reductase family protein [Streptomyces sp. B226SN101]	WP_103546903.1	9,00E-96	91.39
34	213	orf34	NRPS functioning	MULTISPECIES: MbtH family protein [Streptomyces]	WP_103538195.1	1,00E-43	98.57
35	3153	GauB	Scaffold biosynthesis, X	MULTISPECIES: amino acid adenylation domain-containing protein [Streptomyces]	WP_103538194.1	0.0	94.00
36	17436	GauC	Scaffold biosynthesis, asp - gly - ser - gly - hydrophobic-aliphatic	putative non-ribosomal peptide synthetase [Streptomyces malaysiensis]	ATL86844.1	0.0	78.97
37	7227	GauD	Scaffold biosynthesis, X - pro	non-ribosomal peptide synthetase [Streptomyces malaysiensis]	WP_099015593.1	0.0	85.14
38	1641	orf38	regulatory	MULTISPECIES: histidine kinase [Streptomyces]	WP_103538992.1	0.0	92.31
39	216	orf39	2,3-Diaminobutyric acid biosynthesis	MULTISPECIES: argininosuccinate lyase [Streptomyces]	WP_103538995.1	2,00E-10	44.64
40	912	orf40	Regulation/resistance?	MULTISPECIES: kinase [Streptomyces]	WP_103538994.1	0.0	96.19
41	987	orf41	Hydroxylation of Glu	MULTISPECIES: hypothetical protein [Streptomyces]	WP_103538990.1	0.0	93.29
42	849	orf42		MULTISPECIES: alpha/beta hydrolase [Streptomyces]	WP_103538989.1	2,00E-179	91.13
43	729	orf43		MULTISPECIES: tryptophan 2,3-dioxygenase [Streptomyces]	WP_103538988.1	3,00E-155	94.14
44	1599	orf44	aromatic halogenation	MULTISPECIES: tryptophan 7-halogenase [Streptomyces]	WP_103538987.1	0.0	97.73
45	1290	orf45	transport	cation/H(+) antiporter [Streptomyces malaysiensis]	WP_099015597.1	0.0	85.51
46	1254	orf46		decarboxylase [Streptomyces malaysiensis]	WP_099015598.1	0.0	83.89

47	462	orf47		NUDIX domain-containing protein [Streptomyces sp. SPMA113]	WP_069867525.1	4,00E-97	90.20
48	1524	orf48	Scaffold biosynthesis, X	MULTISPECIES: long-chain fatty acid--CoA ligase [Streptomyces]	WP_069867524.1	0.0	84.80
49	1053	orf49	resistance	MULTISPECIES: aminoglycoside phosphotransferase family protein [Streptomyces]	WP_069867523.1	0.0	82.95
50	1194	orf50		hypothetical protein [Streptomyces malaysiensis]	WP_099015600.1	0.0	82.41
51	642	orf51		hypothetical protein [Streptomyces sp. SPMA113]	WP_069867521.1	7,00E-139	88.73
52	804	orf52		class I SAM-dependent methyltransferase [Streptomyces sp. SPMA113]	WP_079153219.1	3,00E-152	82.64 %
53	1005	orf53		hypothetical protein SMALA_6641 [Streptomyces malaysiensis]	ATL86862.1	3,00E-179	77.78 %
54	987	orf54		aldo/keto reductase [Streptomyces sp. SPMA113]	WP_069867518.1	0.0	92.68 %
55	771	orf55		MULTISPECIES: glucose 1-dehydrogenase [Streptomyces]	WP_069867517.1	2,00E-171	94.92 %
56	1077	orf56		myo-inositol-1-phosphate synthase [Streptomyces sp. SPMA113]	WP_069867516.1	0.0	89.94 %
57	804	orf57		histidinol-phosphatase [Streptomyces malaysiensis]	WP_099015605.1	4,00E-179	91.76 %
58	1218	orf58		MULTISPECIES: S-adenosylmethionine synthetase [Streptomyces]	WP_079153218.1	0.0	92.10 %
59	1023	orf59		hypothetical protein [Streptomyces malaysiensis]	WP_069867514.1	0.0	84.71 %

60	567	orf60		MULTISPECIES: hypothetical protein [Streptomyces]	WP_141765311.1	2,00E-96	82.58 %
61	1278	orf61		DegT/DnrJ/EryC1/StrS family aminotransferase [Streptomyces malaysiensis]	WP_099015606.1	0.0	89.65 %
62	492	orf62		NUDIX domain-containing protein [Streptomyces sp. SPMA113]	WP_141765310.1	6,00E-95	87.65 %
63	735	orf63		class I SAM-dependent methyltransferase [Streptomyces malaysiensis]	WP_069867510.1	1,00E-154	83.61 %
64	324	orf64		MULTISPECIES: hypothetical protein [Streptomyces]	WP_069867509.1	2,00E-45	88.24 %
65	750	orf65		HAD hydrolase family protein [Streptomyces malaysiensis]	WP_107528536.1	2,00E-114	78.71 %
66	1023	orf66	UDP-Ara biosynthesis	UDP-glucose 4-epimerase [Streptomyces malaysiensis]	ATL86874.1	0.0	87.28 %
67	912	orf67		MULTISPECIES: hypothetical protein [Streptomyces]	WP_069867507.1	0.0	92.74 %
68	1131	orf68		hypothetical protein [Streptomyces sp. SPMA113]	WP_069867506.1	0.0	81.38 %

Table S24. Adenylation domains in gausemycin BGC

Predicted selectivity and Stachelhaus code[5] of adenylation domains in GauA-GauD NRPSs.

Gene	Adenylation domain	Stachelhaus sequence	Nearest Stachelhaus code	Stachelhaus code match	Type of amino acid
GauA	1	IDTtvSlGDK	ala-b	70% (weak)	N/A
	2	DtwDLGlVDK	gln	70% (weak)	hydrophilic
	3	DtWAttgVgK	phe	50% (weak)	N/A
	4	DAWQaGLvDK	gln	80% (moderate)	hydrophilic
	5	DASTtAAVCK	tyr	90% (moderate)	hydrophobic-aromatic
	6	DALlvGAVMK	phe	80% (moderate)	hydrophobic-aliphatic
GauB	1	DiWQstadDK	gln	50% (weak)	N/A
GauC	1	DLTKvGAVNK	asp	90% (moderate)	hydrophilic
	2	DILQLGvVWK	gly	90% (moderate)	hydrophobic-aliphatic
	3	DVWHlSLVDK	ser	90% (moderate)	hydrophobic-aliphatic
	4	DILQLGvVWK	gly	90% (moderate)	hydrophobic-aliphatic
	5	DAWTttgIaK	phe	60% (weak)	hydrophobic-aliphatic
GauD	1	DILQmGgVyK	gly	70% (weak)	N/A
	2	DVQlAAHVVK	pro	90% (moderate)	hydrophobic-aliphatic

Table S25. Comparison of putative Dab-encoding proteins

Putative diaminobutyric acid synthases sequences were acquired from the MIBiG database: BGC0000354 (friulimicin A),[6] BGC0000379 (laspartomycin),[7] BGC0001448 (malacidin)[8].

Query protein	Analogues genes	Cluster	BLAST score	E value	Per. Ident
ctg1_6207	MlcT	BGC0001448 BGC0000354 BGC0000379	469 150 178	6e-165 2e-43 7e-54	49.69% 63% 60%
ctg1_6208	MlcB	BGC0001448	233	4e-79	47.37%
ctg1_6209	MlcS DabA DabA	BGC0001448 BGC0000354 BGC0000379	750 231 248	0 2e-67 2e-61	52.76% 42.72% 44.13%

Figure S26. Feeding/chemical complementation experiment

Streptomyces sp. INA-Ac-5812 cultures were grown as described above for gausemycin production. After 18 and 40 h of cultivation, fluorinated phenylalanine analogues in the form of water suspension were added to the producing strain to a final concentration 2 mM. The cultures were futher incubated for 4 days before extraction and further analysis by LC-MS and MS^n experiments. All experiments were repeated independently with three replicates for each compound. In parallel, culture of *Streptomyces* sp. INA-Ac-5812 was grown as control.

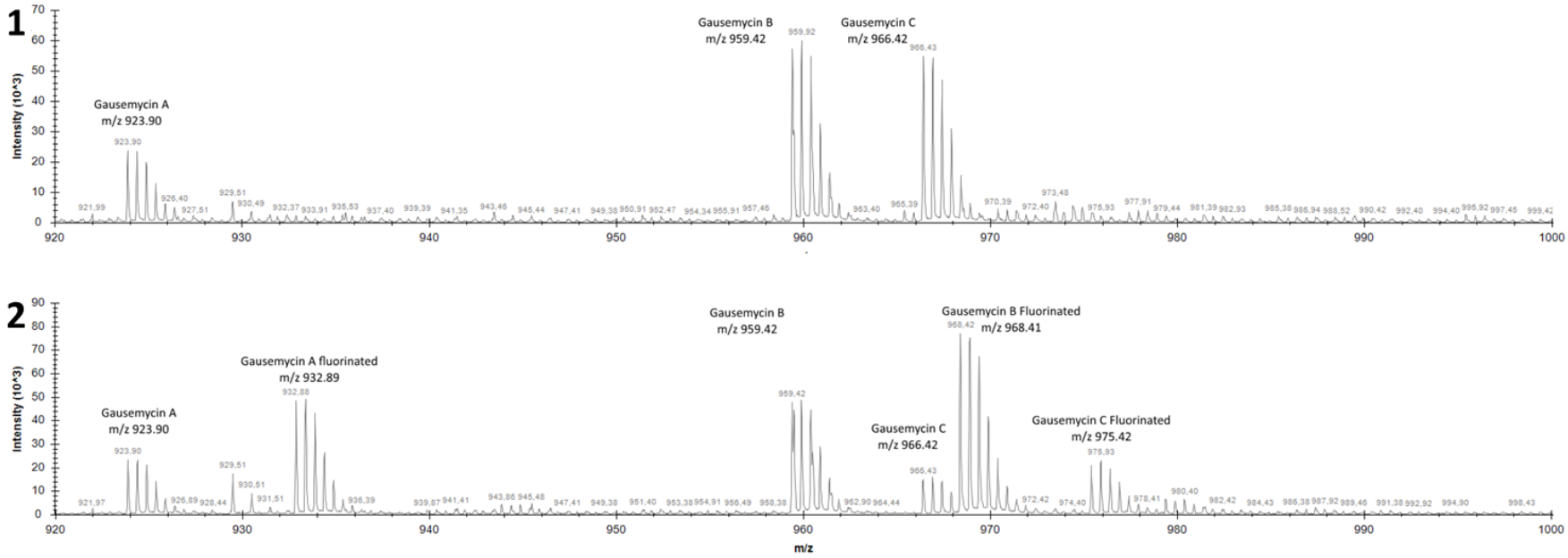

1) LC-MS spectrum of gausemycin extracts without chemical supplementation; 2) Example of LCMS spectrum of gausemycin extract after *o*-fluorophenylalanine chemical supplementation, indicating the emergence of mono-fluorinated species.

Back to Contents

Figure S27. Fragmentation of fluorinated gausemycins analogues

Fragmentation data provides possibility to conclude, that fluorine atom is incorporated into Ahpb moiety:

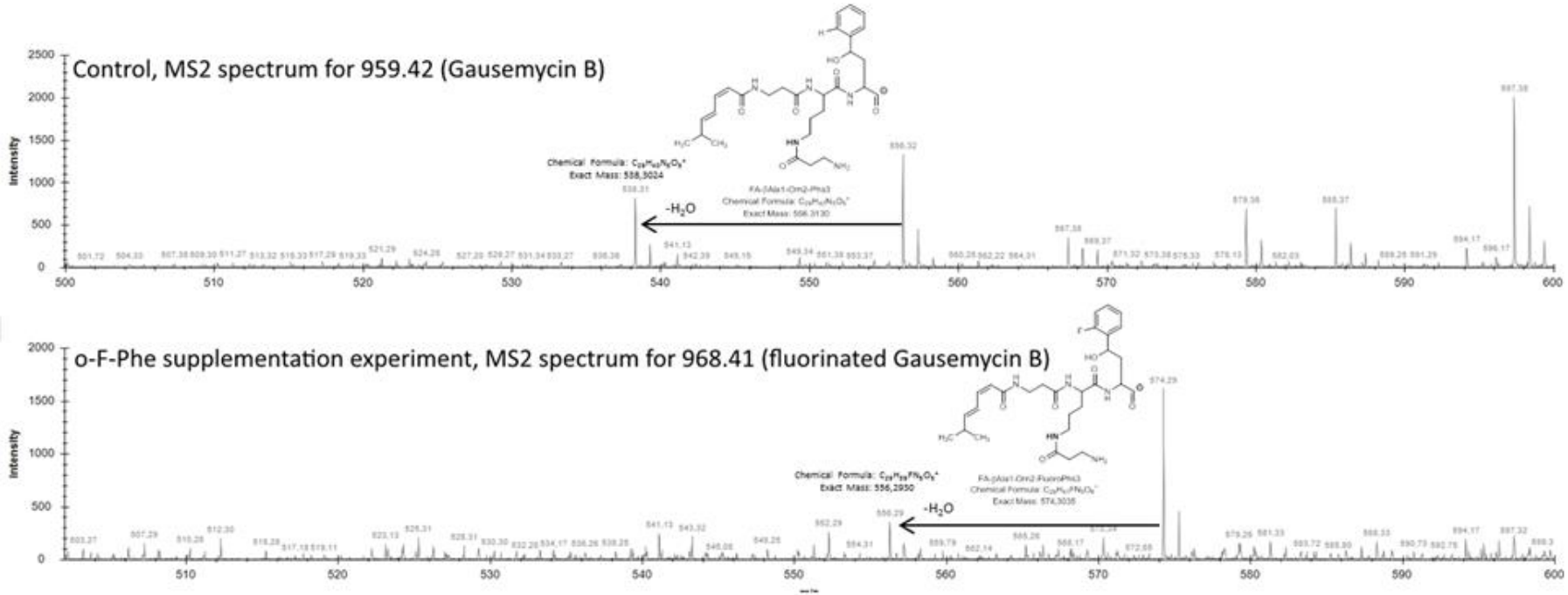

Back to Contents

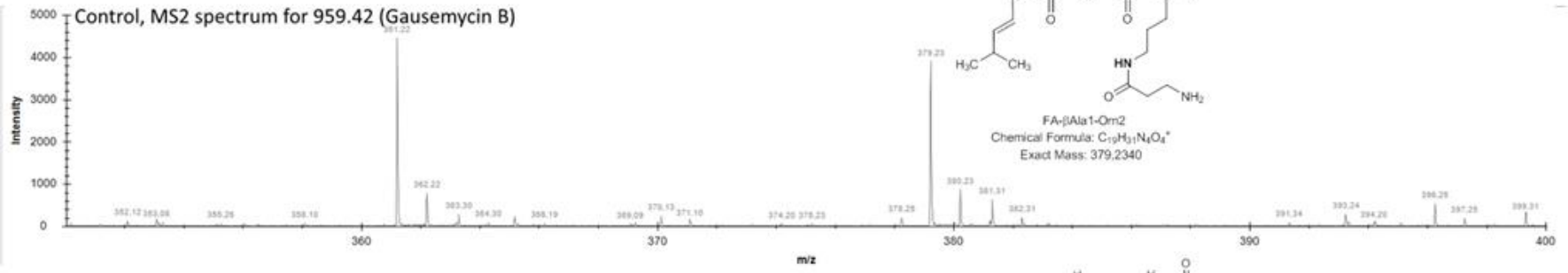
Control, MS2 spectrum for 959.42 (Gausemycin B)
Intensity
m/z
FA-βAla1-Orn2
Chemical Formula: C19H31N4O4+
Exact Mass: 379.2340

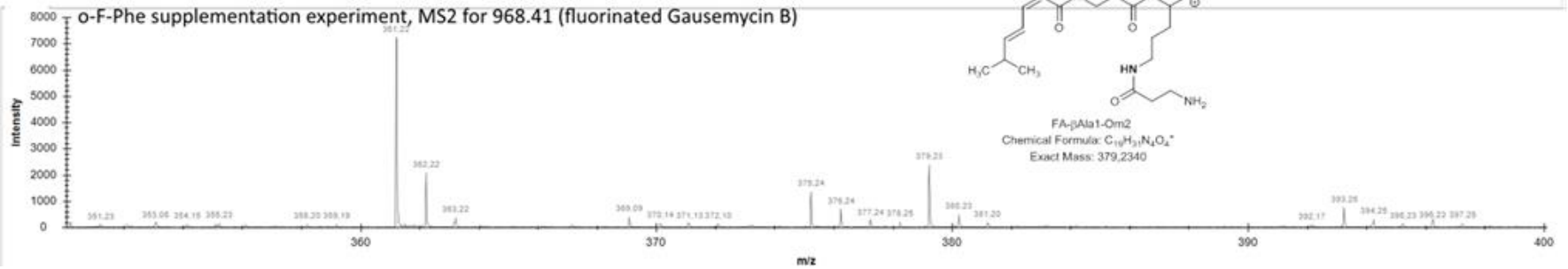
o-F-Phe supplementation experiment, MS2 for 968.41 (fluorinated Gausemycin B)
Intensity
m/z
FA-βAla1-Orn2
Chemical Formula: C19H31N4O4+
Exact Mass: 379.2340

Table S28. Ca^{2+} dependence of the gausemycins activity

Strain	MIC (µg/mL)					
	Gausemycin A		Gausemycin B		Ramoplanin	
	no Ca^{2+}	0.45 mM Ca^{2+}	no Ca^{2+}	0.45 mM Ca^{2+}	no Ca^{2+}	0.45 mM Ca^{2+}
Staphylococcus aureus ATCC 29213	0.5	0.5	1	1	4	4
Staphylococcus aureus ATCC 33592 (MRSA)	0.5	0.5	1	0.5	4	4
Staphylococcus epidermidis ATCC 14990	0.25	0.25	0.5	0.5	4	4
Enterococcus faecalis ATCC 29212	>64	64*	>64	>64	2*	2*
Enterococcus faecium 3576 (VanR)	64*	64*	>64	>64	2*	2*
Enterococcus gallinarum 1308 (VanR)	>64	>64	>64	>64	2*	2*
Escherichia coli ATCC 25922	>64	>64	>64	>64	>64	>64

*visible growth density decrease

Table S29. Spectrum of the gausemycins activity

Strain	MIC (µg/mL)				
	Gausemycin A	Gausemycin B	Ramoplanin	Daptomycin (+Ca^{2+})	Vancomycin
Staphylococcus aureus ATCC 29213	0.5	1	4	n/a	n/a
Staphylococcus aureus ATCC 33592 (MRSA)	0.5	1	4	n/a	n/a
Staphylococcus epidermidis ATCC 14990	0.25	0.5	4	n/a	n/a
Enterococcus faecalis ATCC 29212	>64	>64	2	n/a	n/a
Enterococcus faecium 3576 (VanR)	64	>64	2	n/a	>64
Enterococcus gallinarum 1308 (VanR)	>64	>64	2	n/a	>64
Escherichia coli ATCC 25922	>64	>64	>64	n/a	>64
Streptococcus pneumoniae ATCC 49619	32	>32	n/a	0.06	0.25
Streptococcus pneumoniae ATCC 6305	>32	32	n/a	0.25	0.5
Streptococcus pyogenes 7004	16	32	n/a	0.06	0.25
Streptococcus pyogenes P6	16	32	n/a	0.06–0.125	0.25
Streptococcus pyogenes P26	16	32	n/a	0.06	0.25
Streptococcus agalactiae S 17	>32	>32	n/a	0.5	0.5
Streptococcus anginosus Cp 16	>32	>32	n/a	0.5	0.25
Mycobacterium tuberculosis H37Rv	>40	>40	n/a	n/a	n/a

n/a – not tested

Table S30. Activity of the gausemycin against clinical isolates of *Staphylococcus* sp.

MIC (μg/mL)									
Strain	N	Gausemycin				Daptomycin		Vancomycin	
		A		B					
		median	interval	median	interval	median	interval	median	interval
Coagulase-positive *Staphylococcus* (CPS)									
S. aureus (MSSA)	11	0.125	0.125–0.5	0.5	0.125–0.5	0.5	0.25–0.5	1	0.5–1
S. aureus (MRSA)	12	0.125	0.125–0.5	0.5	0.125–1	0.5	0.25–1	1	0.5–1
S.intermedius (MSS)	1	0.25	-	0.5	-	0.25	-	1	-
S.intermedius (MRS)	1	0.125	-	0.25	-	0.125	-	1	-
All CPS (MSS+MRS)	25	0.125	0.125–0.5	0.5	0.125–0.5	0.25	0.125-1	1	0.5–1
Coagulase-negative Staphylococcus (CNS)									
S.epidermidis (MSSE)	10	0.25	0.125–0.25	0.5	0.25–0.5	0.375	0.25–0.5	1	0.5–1
S.epidermidis (MRSE)	7	0.25	0.125–0.25	0.375	0.25–0.5	0.5	0.25–1	1.5	0.5–2
Other CNS MSS*	5	0.25	0.125–0.25	0.5	0.5–1	0.25	0.125–0.5	0.5	0.5–1
Other CNS MRS**	13	0.25	0.125–0.25	0.5	0.5–1	0.25	0.25–0.5	0.5	0.5–1
All CNS (MSS+MRS)	35	0.25	0.125–0.25	0.5	0.5–1	0.25	0.125–0.5	0.5	0.25–2

N – number of tested strains; MSS – methicillin susceptible *Staphylococcus* sp. strains; MRS – Methicillin-resistant *Staphylococcus* sp. strains

* *S.haemolyticus (2), S. cohnii (1), S. simulans (1), S. warneri (1)*

** *S.haemolyticus* (6), *S. cohnii* (1), *S. simulans* (1), *S.sciuri* (2), *S. klosii* (1), *S. capitis* (1), *S. warneri* (1)

Table S31. Antiproliferative activity of gausemycins

Cell line	Type	IC_{50} (μg/mL)		
		Gausemycin A	Gausemycin B	Doxorubicin
COLO357	carcinoma	10	10	0.1
J774	pseudonormal	5	10	0.02
EL-4	thymoma	5	10	0.1
Colon26	carcinoma	5	10	0.5
HT-29	carcinoma	10	10	0.5

Table S32. Bacterial cytological profiling

Bacillus subtilis was treated with 2.5 MICs of various antibiotics, including DNA replication inhibitors (rifampicin and ciprofloxacin), cell wall biosynthesis inhibitors (vancomycin, benzylpenicillin), protein synthesis inhibitor (chloramphenicol). Morphological changes were visualized using fluorescent dyes (FM4-63, red, stains membranes and DAPI, blue, stains nucleic acids).

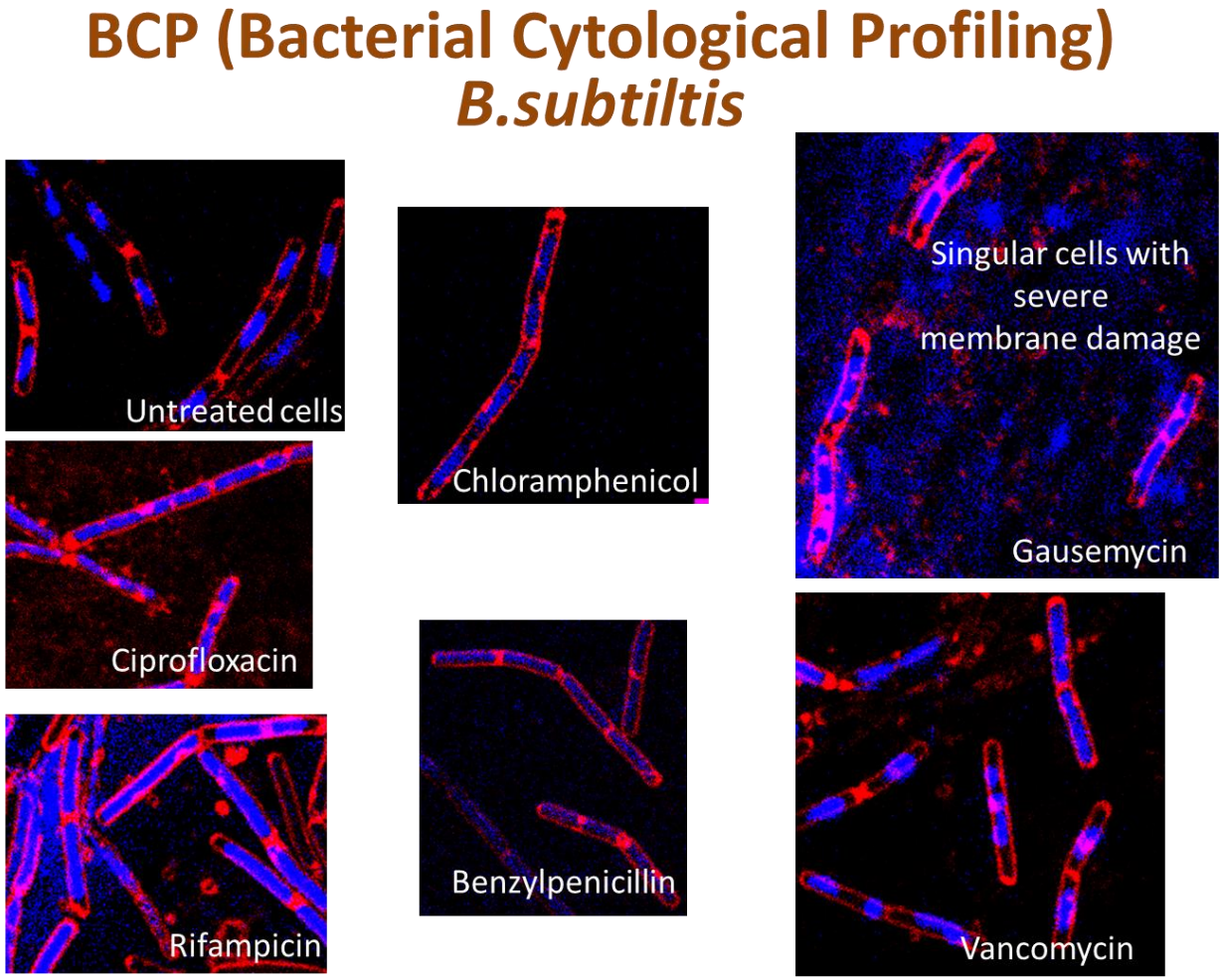

Figure S33. *In vitro* cell-free translation inhibition by gausemycins

In vitro translation reactions were made in PURExpress system (NEB), each reaction in 5 µl, supplied with 200 ng of Fluc mRNA and 0.1 mM of d-luciferin.[9]

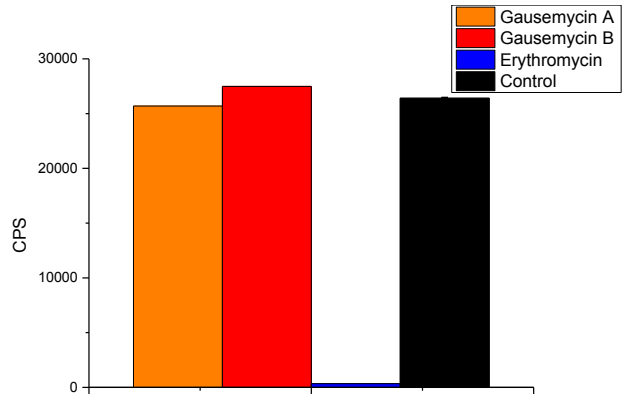

Supplement S34. Model membranes conductance experiments

Figure 1a presents the typical tracks demonstrating the step-like current fluctuations corresponding to openings and closures of single pores formed by one-sided addition of gausemycin into the membrane bathing solution of 0.1 M KCl (pH 7.4) at transmembrane voltage 150 mV. The antibiotic threshold concentration required to observe single channels in bilayers composed of DOPE/DOPG (50/50 mol%) was equal to 50 ± 11 μg/mL. Figure 2 shows *I–V* diagrams of ion-permeable single pores produced by gausemycin in DOPE/DOPG bilayers. Table 1 summarizes the threshold concentration provoked the appearance of single pores, the mean pore conductance at $V \rightarrow 0$ and the dwell time of the gausemycin B channels.

The lipid mixture used contains neutral (DOPE) and negatively charged (DOPG) lipid components. To assess the selectivity of gausemycin B interaction with the neutral lipids we have replaced DOPE for DOPC (Figure 6, discussion section). Gausemycin demonstrated the ability to produce ion-permeable pores in DOPC/DOPG (50/50 mol%) membranes similar to DOPE/DOPG bilayers (Fig.6, discussion section, Table 1). The threshold concentrations, the pore conductance and their lifetime coincided within the measurement error for DOPE/DOPG and DOPC/DOPG bilayers.

Table 1. Characteristic parameters of the membrane activity of gausemycin in lipid bilayers of different composition

membrane lipid composition	*C,* μg/mL	$G_{V\rightarrow 0}$, *pS*	*τ, s*
DOPE/DOPG (50/50 mol%)	50 ± 11	15 ± 5	13 ± 4
DOPC/DOPG (50/50 mol%)	40 ± 9	16 ± 4	8 ± 2

C – the antibiotic threshold concentration required to observe single pores;
$G_{V\rightarrow 0}$ – the mean conductance of single channels at $V \rightarrow 0$;
τ – the mean dwell time of gausemycin pores.

Supplemental Literature

(1) Saitou, N.; Nei, M. The Neighbor-Joining Method: A New Method for Reconstructing Phylogenetic Trees. *Mol. Biol. Evolut.* **1987**, *4* (4), 406–425. https://doi.org/10.1093/oxfordjournals.molbev.a040454.

(2) Felsenstein, J. Confidence Limits on Phylogenies: An Approach Using the Bootstrap. *Evolution* **1985**, *39* (4), 783. https://doi.org/10.2307/2408678.

(3) Tamura, K.; Nei, M.; Kumar, S. Prospects for Inferring Very Large Phylogenies by Using the Neighbor-Joining Method. *Proc. Natl. Acad. Sci. USA* **2004**, *101* (30), 11030. https://doi.org/10.1073/pnas.0404206101.

(4) Kumar, S.; Stecher, G.; Li, M.; Knyaz, C.; Tamura, K. MEGA X: Molecular Evolutionary Genetics Analysis across Computing Platforms. *Mol. Biol. Evolut.* **2018**, *35* (6), 1547–1549. https://doi.org/10.1093/molbev/msy096.

(5) Stachelhaus, T.; Mootz, H. D.; Marahiel, M. A. The Specificity-Conferring Code of Adenylation Domains in Nonribosomal Peptide Synthetases. *Chem. Biol.* **1999**, *6* (8), 493–505. https://doi.org/10.1016/S1074-5521(99)80082-9.

(6) Müller, C.; Nolden, S.; Gebhardt, P.; Heinzelmann, E.; Lange, C.; Puk, O.; Welzel, K.; Wohlleben, W.; Schwartz, D. Sequencing and Analysis of the Biosynthetic Gene Cluster of the Lipopeptide Antibiotic Friulimicin in *Actinoplanes Friuliensis*. *Antimicrob. Agents Chemother.* **2007**, *51* (3), 1028–1037. https://doi.org/10.1128/AAC.00942-06.

(7) Wang, Y.; Chen, Y.; Shen, Q.; Yin, X. Molecular Cloning and Identification of the Laspartomycin Biosynthetic Gene Cluster from *Streptomyces Viridochromogenes*. *Gene* **2011**, *483* (1), 11–21. https://doi.org/10.1016/j.gene.2011.05.005.

(8) Hover, B. M.; Kim, S.-H.; Katz, M.; Charlop-Powers, Z.; Owen, J. G.; Ternei, M. A.; Maniko, J.; Estrela, A. B.; Molina, H.; Park, S.; Perlin, D. S.; Brady, S. F. Culture-Independent Discovery of the Malacidins as Calcium-Dependent Antibiotics with Activity against Multidrug-Resistant Gram-Positive Pathogens. *Nat. Microbiol.* **2018**, *3* (4), 415–422. https://doi.org/10.1038/s41564-018-0110-1.

(9) Osterman, I. A.; Wieland, M.; Maviza, T. P.; Lashkevich, K. A.; Lukianov, D. A.; Komarova, E. S.; Zakalyukina, Y. V.; Buschauer, R.; Shiriaev, D. I.; Leyn, S. A.; Zlamal, J. E.; Biryukov, M. V.; Skvortsov, D. A.; Tashlitsky, V. N.; Polshakov, V. I.; Cheng, J.; Polikanov, Y. S.; Bogdanov, A. A.; Osterman, A. L.; Dmitriev, S. E.; Beckmann, R.; Dontsova, O. A.; Wilson, D. N.; Sergiev, P. V. Tetracenomycin X Inhibits Translation by Binding within the Ribosomal Exit Tunnel. *Nature Chemical Biology* **2020**, *16* (10), 1071–1077. https://doi.org/10.1038/s41589-020-0578-x.

[Back to Contents]